

MEDEDELINGEN EN VERHANDELINGEN

No. 98

L. C. HEIJBOER

**DESIGN OF A BAROCLINIC THREE-LEVEL
QUASI-GEOSTROPHIC MODEL WITH SPECIAL
EMPHASIS ON DEVELOPING SHORT
FRONTAL WAVES**

1977

Prijs f 49,—

DESIGN OF A BAROCLINIC THREE-LEVEL
QUASI-GEOSTROPHIC MODEL WITH SPECIAL
EMPHASIS ON DEVELOPING SHORT
FRONTAL WAVES

KONINKLIJK NEDERLANDS METEOROLOGISCH INSTITUUT
MEDEDELINGEN EN VERHANDELINGEN

No. 98

L. C. HEIJBOER

DESIGN OF A BAROCLINIC THREE-LEVEL
QUASI-GEOSTROPHIC MODEL WITH SPECIAL
EMPHASIS ON DEVELOPING SHORT
FRONTAL WAVES

1977

STAATSDRUKKERIJ/'S-GRAVENHAGE

PUBLIKATIENUMMER K.N.M.I. 102-98

U.D.C.: 551.509.313 :
551.511.3 :
551.515.11 :

VOORWOORD

In 1967 zijn op het K.N.M.I. de eerste activiteiten ontplooid die tot doel hadden het stromingspatroon in de atmosfeer met numerieke methodes één tot anderhalf etmaal vooruit te berekenen. Deze eerste pogingen waren nog uiterst primitief en gebaseerd op de veronderstelling dat de atmosferische ontwikkelingen kunnen worden beschreven met behulp van processen die op één niveau, ongeveer ter halve hoogte van de atmosfeer, plaatsvinden (barotroop model).

Geleidelijk is het model verbeterd en in zoverre realistischer gemaakt (baroklien model) dat er rekening mee werd gehouden dat de stroming in de atmosfeer niet op ieder niveau hetzelfde beeld vertoont en derhalve niet correct kan worden beschreven met behulp van processen in een enkele luchtlaag. Bovendien bleek dat een adequaat inzicht in de ontwikkeling van de stroming in een gebied, dat vrijwel het gehele Noordelijke Halfrond omvat, niet kan worden verkregen indien geen rekening wordt gehouden met de vrijkomende condensatiewarmte die met name bij de verstoringen van het stromingspatroon, die afmetingen bezitten van de orde van de depressies van gematigde breedte, een belangrijke bijdrage tot de ontwikkeling geeft.

Drs. L. C. Heijboer heeft bij de uitbouw van het oorspronkelijke barotrope model tot een drie-lagen baroklien model de hoofdrol vervuld. Hij heeft daarmee een zeer waardevolle nederlandse bijdrage geleverd tot de toepassing van de dynamische meteorologie op de weersvoorspelling.

De Hoofddirecteur van het

Koninklijk Nederlands Meteorologisch Instituut

H. C. BIJVOET

PREFACE

In 1967 the first attempts were initiated at the Royal Netherlands Meteorological Institute to calculate the flow patterns of the atmosphere for periods up to thirty-six hours ahead.

These calculations were based on the assumption that atmospheric developments could be described taking into account processes taking place on a level about halfway up in the atmosphere (barotropic model). In the succeeding years the model was improved upon and made to resemble reality in so far that different layers in the atmosphere were taken into account.

It became evident that it was impossible to gain adequate knowledge of the nature of the flow patterns over the Northern Hemisphere, without also taking into account the latent heat released in extra-tropical frontal disturbances.

This latent heat has a major influence on the development of these disturbances.

Drs. L. C. Heijboer was the leader in the transformation of the original barotropic model into the present baroclinic model. With his work the Netherlands have made an appreciable contribution in the field of the application of dynamic meteorology to numerical weather prediction.

*The Director in Chief of the
Royal Netherlands Meteorological Institute*

H. C. BIJVOET

CONTENTS

page		
1		CHAPTER I: Introduction
5		CHAPTER II: Basic equations
11		CHAPTER III: Theoretical investigations with special emphasis on developing short frontal waves
11	1	Definition of a reference atmosphere
12	2	Specification of the reference atmosphere for 25-3-'71, 00 GMT
12	2.1	Divergence profiles and ω -profiles
23	2.2	Specification of the advection of relative vorticity at 500 mbar (RVA)
27	2.3	Some numerical values of D and ω
28	3	The relation between the real atmosphere and the reference atmosphere
28	3.1	Height and thermal fields of isobaric levels of the reference atmosphere compared with those of the real atmosphere
32	3.2	Static stability computations for 500 mbar for 25-3-'71, 00 GMT
34	3.3	Some considerations with respect to the formulation of the thermodynamic equation and the choice of the static stability
43	3.4	Relation between the advection of relative vorticity at 500 mbar and the frontal waves at sea level
48	3.5	Divergence D and ω of young developing frontal waves and a comparison with those of the reference atmosphere
57	4	Stability analysis of the quasi-geostrophic equations
57	4.1	General theory
61	4.2	The case of a young developing frontal wave
63	4.3	Spatial structure of stable waves
67	4.4	Spatial structure of unstable waves
73	5	Conclusions with regard to the construction of a baroclinic model
76		CHAPTER IV: Design of the baroclinic model
76	1	Outline of the design
77	2	Prognostic equations

81	3	The dry model
81	3.1	Vertical profile of the horizontal divergence D
83	3.2	Integrations of the prognostic equations
86	3.3	Equations of the dry BK3-model in β -plane approximation
88	3.4	Computation of the coefficients
91	4	The inclusion of the release of latent heat
91	4.1	Description of the method
96	4.2	Comparison of the method with the results of section III 3.5
101	4.3	Further discussion on the assumptions
103	5	Final prognostic equations for polar stereographic projection
103	5.1	The equations of the dry model
106	5.2	The corrections due to the inclusion of release of latent heat
107	6	Description of the computational procedures
107	6.1	Computational grid
107	6.2	Finite difference approximations
109	6.3	Lateral boundary conditions and smoothing procedures
111	6.4	Computational scheme
113		CHAPTER V: A survey of the performance of the dry and moist versions of the BK3-model
113	1	Some remarks on the performance of the dry versions of the BK3-model with and without the correction terms in the integrated forms of the thermodynamic equation
115	2	The performance of the moist version of the BK3-model
122	3	Some further theoretical considerations with respect to the correction terms in the BK3-model
135		LIST OF SYMBOLS
143		SUMMARY
148		REFERENCES

CHAPTER I

INTRODUCTION

In this treatise a description is given of the design of a baroclinic model. This model is suitable for short range weather predictions up to 36 hours ahead.

In numerical forecasting, the physical laws governing the atmospheric flow are applied. These laws are expressed by the equation of motion, the continuity equation, the equation of state and the first law of thermodynamics.

The time-dependent properties of the air particles, which can be predicted by these equations, are the velocity V , the absolute temperature T and the pressure p . If the differential equations are replaced by their difference forms, it is possible to carry out the time integrations if the boundary conditions are formulated and the initial values of V , p and T are known. In doing so one has to reckon with several demands, the most important of which are the computational speed and the memory capacity of the available computer. For the EL-X8 computer of the Royal Netherlands Meteorological Institute, which was in use from 1968 till September 1975, the general unsimplified equations were too complicated for a baroclinic model suitable for operational purposes, because the numerical forecasts had to be available to the meteorological service within a limited period of time to be useful for weather predictions.

To carry out the necessary simplifications of the equations it is important that the resulting equations still enable a description of behaviour of the systems responsible for the day-to-day weather fluctuations. These systems have length-scales varying from ~ 1000 km to ~ 7000 km and consist of so-called short frontal waves as well as long waves. With the aid of a scale analysis it is possible to simplify the equations in a suitable manner, resulting in the quasi-geostrophic equations in β -plane approximation. A review is given in chapter II. The quasi-geostrophic equations are used for the construction of the baroclinic model.

In this treatise special emphasis is given to the developing short frontal waves. In doing so, a theoretical investigation is carried out in chapter III. It indicates that long waves show an equivalent barotropic behaviour and that short frontal waves are really baroclinic, showing a phase shift between height and thermal fields. The experience, that the equivalent barotropic vorticity equation applied at 500 mbar gives relatively good predictions at least up to 36 hours ahead, agrees with the equivalent barotropic behaviour of long waves. Moreover, these predictions also show that the speeds of the short waves at 500 mbar can be predicted as can be seen by investigating the areas of advection of relative vorticity at that level. These two results form a guide for the theoretical investigations and for the construction of a baroclinic model. For that purpose an equivalent barotropic reference atmosphere is designed

in chapter III. Substitution of the equations of this model atmosphere into the integrated forms of the thermodynamic equations results in a relation between the wavelengths of the waves and the static stability. This relation will be further investigated and it will be shown that it holds for both short and long waves. The values of the static stability for the short waves are in accordance with those belonging to saturated adiabatic lapse rates, and the values for the long waves agree with those following from the lapse rate of the ICAO standard atmosphere.

Therefore, in a model suitable to describe the development of short frontal waves one has to take the 'saturated adiabatic' values. However, for such values the integrated forms of the thermodynamic equation are no longer consistent with the requirements of the equivalent barotropic reference atmosphere because a long wave, which is equivalent barotropic at $t = t_0$, will not remain so during the integration of the equations.

In chapter III, correction terms are introduced in the integrated thermodynamic equation from 300 to 500 mbar and from 500 to 850 mbar, which make it possible to overcome that difficulty. These terms offer the possibility of using the required low 'saturated adiabatic' values of the static stability in the integrated thermodynamic equations, which are consistent with the requirements of the equivalent barotropic reference atmosphere. These correction terms are zero for the short waves, so for these frontal waves the original form of the thermodynamic equation remains unchanged.

For the baroclinic model, which is described in chapter IV, the thermodynamic equation is integrated from 300 to 500 mbar and from 500 to 850 mbar. To carry out these integrations knowledge of the profile in the vertical of the horizontal divergence is necessary. For the reference atmosphere this profile is known. To hold the integrations consistent with the properties of the reference atmosphere this profile is also taken for the baroclinic model. For the long waves this divergence profile will be a good approximation, but for the short frontal waves this is not necessarily true. Therefore in chapter III an investigation is carried out with a simple two-parameter model taking into account the release of latent heat. The calculations of this investigation give for the centre of the perturbation at sea level a divergence profile, which consists of two parts, namely that of the reference atmosphere and a linear part due to the incorporation of the release of latent heat. The horizontal divergence of this simple model can be expressed as a function of the advection of relative vorticity at 500 mbar (RVA). The divergence- and ω -computations have been compared with three case studies and agreement has been confirmed.

The results of the two-parameter model show that for developing short frontal waves the release of latent heat is very important and has to be incorporated in a baroclinic model.

For the integrations of the thermodynamic equations of a baroclinic model it is

possible to split D and ω into a dry and a moist part, due to the linearity of D and ω in the equations. Now it follows from the results of the two-parameter model that the divergence profile of the reference atmosphere is a good approximation for the dry part of D and that a linear profile is suitable for the moist part of D .

To give the investigations a firmer theoretical basis, a stability analysis of the linear quasi-geostrophic equations is carried out. From this analysis two kinds of wave solutions can be found, namely unstable waves with a phase shift in the vertical and stable waves with a structure like that of the reference atmosphere. Two special cases are investigated, namely the most unstable wave and a stable wave, which has a level of non-divergence at 500 mbar. The divergence D and ω in the centre at sea level of the most unstable wave are expressed as functions of the advection of relative vorticity at 500 mbar and are compared with the results of the two-parameter model. There appears to be agreement.

Experimental investigations by DODDS (1971) show that most of the depressions at sea level have wavelengths between 1600-2000 km. According to the stability analysis, such waves can only be unstable if release of latent heat is taken into account.

The stability analysis also gives insight into the choice of the number of levels for the baroclinic model, because it appears that the most unstable wave can be described by three parameters, namely two parameters describing the baroclinic disturbance and one describing the basic flow. So the number of parameters and also the number of levels must be three at least.

Taking into account the results of the investigations in chapter III the following will be required in designing the baroclinic model:

1. Three levels.
2. The values of the static stability in accordance with those of saturated adiabatic lapse rates.
3. *Inclusion of correction terms in the integrated forms of the thermodynamic equation to preserve the equivalent barotropic character of long waves.*
4. *Inclusion of release of latent heat to make the short frontal waves unstable in the model.*
5. A profile of the dry part of the horizontal divergence in accordance with that of the reference atmosphere and a linear profile for the moist part of the divergence.

The above-mentioned requirements are applied to the baroclinic BK3-model, which is described in chapter IV.

In chapter V a survey is given of the performance of the dry and moist versions of the model. It will appear that the experimental results confirm the results of the theoretical investigations.

Finally, it should be remarked that, in the author's opinion, a theoretical investigation like the one carried out in this treatise is absolutely necessary for the design of numerical models. Otherwise it is not quite possible to understand the behaviour of the model and to introduce changes, which may lead to significant improvements.

CHAPTER II

BASIC EQUATIONS

It is supposed in the present treatise that in the atmosphere each physical quantity is continuous and can be differentiated with respect to space and time. Though it seems that discontinuities such as fronts occur in the atmosphere, these can be considered to be continuous if both space and time scales are taken sufficiently small. For the purpose of numerical weather prediction, the important properties of an air particle are the velocity V , the pressure p , the density ρ , the absolute temperature T and the specific humidity q .

The behaviour of these quantities can be described with the aid of the equation of motion, the equation of state, the continuity equation, the first law of thermodynamics and the equation describing the amount of water vapour as a function of space and time.

Since the above-mentioned general equations have no general analytic solutions, it is necessary to replace them by difference equations to be able to solve them by numerical methods. For the computations one has to choose a suitable coordinate system. After that it is possible to carry out the computations if the boundary conditions are formulated and the initial values of V , p , T and q are known.

For the computations it is most convenient to choose a coordinate system in which the atmosphere motions can be described in a suitable way. Because the atmosphere moves on a spherical earth and the large-scale motions of the atmosphere are quasi-horizontal with respect to the earth's surface, spherical curvilinear coordinates are most suitable.

With the aid of scale analysis it is possible to estimate the magnitudes of the various terms in the equations, because these are defined by the length and time scales of the atmospheric systems. These length and time scales can be deduced from pressure and horizontal wind analyses. For mid-latitudes these scales are respectively ~ 1000 km to ~ 7000 km and one to about five days. Examples of scale analyses are given by CHARNEY (1948) and BURGER (1958). The scale analysis proves to be a useful tool to simplify the equations. For the theoretical considerations, which are carried out in chapter III, the quasi-geostrophic equations in β -plane approximation are used. These relatively simple equations have been formulated in a Cartesian coordinate system with the x -axis along the latitude circle of 45°N from west to east and the y -axis from south to north. The coordinates are formulated as

$$x = a \cdot \cos(\varphi_0) \cdot (\lambda - \lambda_0) \quad \text{and} \quad y = a \cdot (\varphi - \varphi_0) \quad (2.1)$$

with a as mean earth's radius, $\varphi_0 = 45^\circ$ and λ_0 the longitude of the origin of the coordinate system.

The pressure p has been used as independent variable for the vertical coordinate.

The relevant equations in β -plane approximation are given below.

Equations of motion:

$$\frac{\partial u_0}{\partial t} + u_0 \frac{\partial u_0}{\partial x} + v_0 \frac{\partial u_0}{\partial y} - f_0 \cdot v = - \frac{\partial \Phi}{\partial x} \quad (2.2)$$

$$\frac{\partial v_0}{\partial t} + u_0 \frac{\partial v_0}{\partial x} + v_0 \frac{\partial v_0}{\partial y} + f_0 \cdot u = - \frac{\partial \Phi}{\partial y} \quad (2.3)$$

where $\Phi \equiv g \cdot z$ is the geopotential,

g is the absolute value of gravity g ,

z is the geopotential height,

$f_0 \equiv 2\Omega \sin 45^\circ$ is the value of the horizontal component of the coriolis acceleration at 45°N ,

Ω is the value of the angular velocity of the earth,

u_0 and v_0 are the components of the horizontal quasi-geostrophic wind components with

$$u_0 \equiv - \frac{1}{f_0} \frac{\partial \Phi}{\partial y} \quad \text{and} \quad v_0 \equiv \frac{1}{f_0} \frac{\partial \Phi}{\partial x} \quad (2.4)$$

Continuity equation:

$$\frac{\partial \omega}{\partial p} + \frac{\partial u}{\partial x} + \frac{\partial v}{\partial y} - \frac{\beta}{f_0} \omega = 0 \quad (2.5)$$

where $\beta \equiv \left(\frac{df}{dy} \right)_{\varphi = 45^\circ}$ is supposed to be constant. $\omega \equiv \frac{dp}{dt}$ is the total time derivative of the pressure p of an air particle.

First law of thermodynamics:

$$\frac{\partial}{\partial t} \left(\frac{\partial \Phi}{\partial p} \right) + u_0 \frac{\partial}{\partial x} \left(\frac{\partial \Phi}{\partial p} \right) + v_0 \frac{\partial}{\partial y} \left(\frac{\partial \Phi}{\partial p} \right) + \sigma \cdot \omega = - \frac{R \cdot Q}{c_p \cdot p} \quad (2.6)$$

where R is the gas constant for dry air,

c_p is the specific heat at constant pressure.

Q is the rate of heat addition or subtraction per unit time and mass,

σ is the static stability parameter, which only depends on p and is defined by

$$\sigma \equiv \frac{\partial^2 \bar{\Phi}}{\partial p^2} + \frac{c_v}{c_p \cdot p} \frac{\partial \bar{\Phi}}{\partial p} \quad (2.7)$$

with $\bar{\Phi}$ the geopotential of a standard atmosphere, which depends only on p .

Boundary conditions:

$$\omega = 0 \quad \text{for} \quad p = 0 \quad \text{and} \quad p = 1000 \text{ mbar} \quad (2.8)$$

The above-mentioned quasi-geostrophic equations in β -plane approximation have been derived by PHILLIPS (1963).

This β -plane approximation can be achieved by reformulating the general equations in spherical curvilinear coordinates into those for the Cartesian coordinate system (2.1), making them dimensionless with the aid of scale analysis, expanding the horizontal wind components, the vertical velocity and the coriolis parameter f as power series in the Rossby number Ro , and substituting these series into the dimensionless equations of motion, the continuity equation and the thermodynamic equation. After omitting all terms of order Ro^2 and higher, the quasi-geostrophic equations in β -plane approximation result. Instead of using the Cartesian coordinates (2.1), PHILLIPS used the coordinates of a Mercator projection to derive the desired equations. He came to the following conclusions:

1. For the free atmosphere the friction terms in the equations of motion are not important. However, near the earth's surface the friction terms are probably important if the surface synoptic systems have a pronounced vorticity.
2. *The release of latent heat has to be taken into account if the precipitation intensity is ≥ 1 mm/hour.* Such an intensity can be reached easily in extratropical frontal cyclones.
3. For a flat horizontal earth the boundary condition $\omega = 0$ is valid. However, if there are mountains, the induced vertical velocity w has to be taken into account by $\omega = -g \cdot \rho \cdot w$ with $w = u_0 \frac{\partial h}{\partial x} + v_0 \frac{\partial h}{\partial y}$. Application of a smoothing procedure on the height h of the earth's surface is necessary, in order to prevent too large values of w (≥ 1 cm/s).

After introducing the quasi-geostrophic streamfunction $\psi \equiv \Phi/f_0$, the vorticity ζ (the vertical component of the rotation of the wind V) and the divergence D of the horizontal wind components are given in the β -plane approximation by:

$$\zeta \equiv \frac{\partial v_0}{\partial x} - \frac{\partial u_0}{\partial y} = \nabla^2 \psi \quad \text{and} \quad D \equiv \frac{\partial u}{\partial x} + \frac{\partial v}{\partial y} - \frac{\beta}{f_0} v_0 \quad (2.9)$$

Differentiation of (2.3) with respect to x and of (2.2) with respect to y , with the use of (2.9) gives the vorticity equation in β -plane approximation:

$$\frac{\partial}{\partial t} (\nabla^2 \psi) + J(\psi, \nabla^2 \psi + f) + f_0 \cdot D = 0 \quad (2.10)$$

with the Jacobian defined as

$$J(a, b) \equiv \frac{\partial a}{\partial x} \cdot \frac{\partial b}{\partial y} - \frac{\partial a}{\partial y} \cdot \frac{\partial b}{\partial x} \quad (2.11)$$

In β -plane approximation the coriolis parameter f equals

$$f = f_0 + \beta \cdot y \quad \text{with} \quad f_0 \equiv 2\Omega \sin 45^\circ \quad \text{and} \quad \beta \equiv \left(\frac{df}{dy} \right)_{\varphi=45^\circ} \quad (2.12)$$

The continuity equation (2.5) can be written with the aid of (2.9) as

$$\frac{\partial \omega}{\partial p} + D = 0 \quad (2.13)$$

The thermodynamic equation (2.6) becomes with the quasi-geostrophic stream-function ψ :

$$\frac{\partial}{\partial t} \left(\frac{\partial \psi}{\partial p} \right) + J \left(\psi, \frac{\partial \psi}{\partial p} \right) + \frac{\sigma}{f_0} \omega = - \frac{R \cdot Q}{c_p \cdot f_0 \cdot p} \quad (2.14)$$

Equations (2.10), (2.13) and (2.14) together with the boundary conditions (2.8) form the set of basic equations, which will be used for the theoretical considerations given in chapter III. These equations are valid for the area situated roughly between 35°N and 55°N , as follows from the derivation of the equations by PHILLIPS.

However, the computational area used in the baroclinic model, which is described in chapter IV, also consists of regions south of 35°N and north of 55°N . Consequently, a coordinate system of a stereographic projection will be used instead of the Cartesian system (2.1). In the stereographic projection the earth's surface is projected from the south pole on a plane through the parallel of 60°N . If the centre of the coordinate system coincides with the projected north pole, the spherical coordinates λ and φ are related to the stereographic coordinates x_s and y_s by

$$x_s = m \cdot a \cdot \cos \varphi \cdot \cos \lambda \quad \text{and} \quad y_s = m \cdot a \cdot \cos \varphi \cdot \sin \lambda \quad (2.15)$$

$$\text{with } m \equiv \frac{1 + \sin 60^\circ}{1 + \sin \varphi}$$

Here m is the map scale factor, which equals the ratio between an infinitesimal distance on the plane and the corresponding distance on the sphere. The general equations in spherical curvilinear coordinates have to be formulated in the polar stereographic coordinates. After that, the procedure of simplifying is similar to that of obtaining the quasi-geostrophic equations in β -plane approximation. The simplified equations are given below.

Vorticity equation:

$$\frac{\partial \zeta}{\partial t} + m_1 \cdot u_1 \frac{\partial}{\partial x_s} (\zeta + f) + m_1 \cdot v_1 \frac{\partial}{\partial y_s} (\zeta + f) + f_1 \cdot D = 0 \quad (2.16)$$

This equation is valid for an area around the point where $x_s = x_{s1}$ and $y_s = y_{s1}$, for every latitude $\varphi = \varphi_1$ with $\varphi_1 > \sim 25^\circ\text{N}$. For this area the map scale factor is $m = m_1$ with $m_1 \equiv (1 + \sin 60^\circ)/(1 + \sin \varphi_1)$.

The coriolis parameter is approximated by

$$f = f_1 + \left(\frac{\partial f}{\partial x_s} \right)_{x_{s1}} \cdot (x_s - x_{s1}) + \left(\frac{\partial f}{\partial y_s} \right)_{y_{s1}} \cdot (y_s - y_{s1}) \text{ with } f_1 \equiv 2\Omega \sin \varphi_1 \quad (2.17)$$

The vorticity ζ and the divergence D are approximated by

$$\zeta = m_1^2 \left[\frac{\partial(v_1/m_1)}{\partial x_s} - \frac{\partial(u_1/m_1)}{\partial y_s} \right] \text{ and} \quad (2.18)$$

$$D = m_1^2 \left[\frac{\partial(u_1/m_1)}{\partial x_s} + \frac{\partial(v_1/m_1)}{\partial y_s} \right] - u_1 \cdot \left(\frac{\partial m}{\partial x_s} \right)_{x_{s1}} - v_1 \cdot \left(\frac{\partial m}{\partial y_s} \right)_{y_{s1}} \quad (2.19)$$

The quasi-geostrophic wind components are given by

$$u_1 = - \frac{m_1}{f_1} \frac{\partial \Phi}{\partial y_s} \quad \text{and} \quad v_1 = + \frac{m_1}{f_1} \frac{\partial \Phi}{\partial x_s} \quad (2.20)$$

The continuity equation reads:

$$\frac{\partial \omega}{\partial p} + D = 0 \quad (2.21)$$

The thermodynamic equation is given by:

$$\frac{\partial}{\partial t} \left(\frac{\partial \Phi}{\partial p} \right) + m_1 \cdot u_1 \frac{\partial}{\partial x_s} \left(\frac{\partial \Phi}{\partial p} \right) + m_1 \cdot v_1 \frac{\partial}{\partial y_s} \left(\frac{\partial \Phi}{\partial p} \right) + \sigma \cdot \omega = - \frac{R \cdot Q}{c_p \cdot p} \quad (2.22)$$

(2.16) and (2.22) can be rewritten with the use of the quasi-geostrophic streamfunction $\psi \equiv \Phi/f_0$ and become:

Vorticity equation:

$$\frac{\partial}{\partial t} (m_1^2 \nabla^2 \psi) + \frac{m_1^2 f_0}{f_1} J(\psi, m_1^2 \nabla^2 \psi) + m_1^2 J(\psi, f) + \frac{f_1^2}{f_0} D = 0 \quad (2.23)$$

Thermodynamic equation:

$$\frac{\partial}{\partial t} \left(\frac{\partial \psi}{\partial p} \right) + \frac{m_1^2 f_0}{f_1} J \left(\psi, \frac{\partial \psi}{\partial p} \right) + \frac{\sigma}{f_0} \omega = - \frac{R \cdot Q}{c_p \cdot f_0 \cdot p} \quad (2.24)$$

(2.21), (2.23), (2.24) and the boundary conditions given by (2.8) are the basic equations in polar stereographic coordinates of the baroclinic model. They are used in chapter IV.

CHAPTER III

THEORETICAL INVESTIGATIONS WITH SPECIAL
EMPHASIS ON DEVELOPING SHORT FRONTAL
WAVES

1 Definition of a reference atmosphere

It is supposed that the height z of each pressure level p satisfies

$$z = A \cdot z_5 + B \quad (3.1)$$

A and B being functions of p and $A = 0$ at $p = 0$ mbar and $A = 1$ and $B = 0$ at $p = 500$ mbar. Further it is assumed that the quasi-geostrophic vorticity equation (2.10), the continuity equation (2.13) and the boundary conditions (2.8) are valid. These are given below for convenience.

$$\nabla^2 \dot{\psi} + J(\psi, \nabla^2 \psi + f) + f_0 \cdot D = 0 \quad \text{with} \quad \psi \equiv \frac{g \cdot z}{f_0} \quad \text{and} \quad \dot{\psi} \equiv \frac{\partial \psi}{\partial t} \quad (3.2)$$

$$\frac{\partial \omega}{\partial p} + D = 0 \quad (3.3)$$

$$\omega = 0 \quad \text{at} \quad p = 0 \quad \text{and} \quad p = p_{10}, \quad p_{10} \text{ being } 1000 \text{ mbar} \quad (3.4)$$

The thermodynamic equation (2.14) is left out of consideration for the moment and will be discussed in section 3.3. From (3.1) it follows that the quasi-geostrophic streamfunction has to satisfy the equation

$$\psi = A \cdot \psi_5 + \frac{g \cdot B}{f_0}, \quad \text{where } \psi_5 \text{ refers to the } 500 \text{ mbar level} \quad (3.5)$$

After some computational work it follows from (3.2) to (3.5) that the horizontal divergence D is given by

$$D = -\frac{1}{f_0} (A \cdot K - A^2) \cdot \text{RVA} \quad (3.6)$$

with

$$K \equiv \left(\int_0^{p_{10}} A^2 dp \right) \left/ \left(\int_0^{p_{10}} A dp \right) \right. \quad (3.7)$$

and the advection of relative vorticity at the 500 mbar level

$$\text{RVA} \equiv -J(\psi_5, \nabla^2 \psi_5) \quad (3.8)$$

With the aid of the continuity equation (3.3) the 'vertical velocity' ω can be computed as

$$\omega = - \int_0^p D \, dp = \frac{1}{f_0} \int_0^p (A \cdot K - A^2) dp \cdot \text{RVA} \quad (3.9)$$

2 Specification of the reference atmosphere for 25-3-'71, 00 GMT

2.1 Divergence profiles and ω -profiles

If A is a known function of p , the D -profile and the ω -profile can be defined as functions of p . The dependence of x , y and t is given by the relative vorticity advection

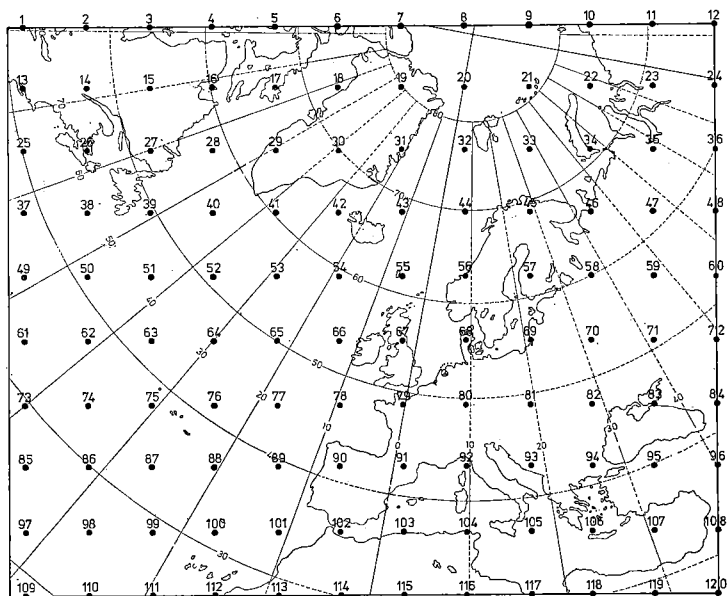


Fig. 1 Grid on which the geopotential heights (gpdam) of the standard pressure levels 100, 200, 300, 500, 700 and 850 mbar and the thickness field of 500—1000 mbar are defined for 25 March 1971, 00 GMT.

RVA. At each moment t it is possible to define A and B of the relevant reference atmosphere by correlating the heights z of each pressure level with the heights of the 500 mbar level at the same grid points. For the standard pressure levels of 100, 200, 300, 500, 700 and 850 mbar as well as for the thickness 500–1000 mbar, A and B have been specified in this way for 25-3-'71, 00 GMT. For that purpose the analyses of the standard pressure levels of the German Meteorological Service (Deutscher Wetterdienst in Offenbach) were chosen. The area of these analyses extended from the north pole to the Azores and from New Foundland to the Urals. A rectangular grid containing 120 grid points as shown in fig. 1 was defined in this area. The analyses of the standard pressure levels, the thickness 500–1000 mbar and the sea surface weather map are given in figures 2a and 2b. For each grid point the heights of the standard pressure levels were determined. For each pressure level these heights were correlated with the corresponding heights of 500 mbar. The values of A and B are defined by the straight lines given in figure 3. The relevant regression equations are given in table 1.

level	$A(p)$	$B(p)$	regression equation
mbar	—	dam	$z(\text{dam})$
100	0.85	+1140	$z_1 = 0.85 z_5 + 1140$
200	1.36	+419	$z_2 = 1.36 z_5 + 419$
300	1.33	+173	$z_3 = 1.33 z_5 + 173$
700	0.67	-72	$z_7 = 0.67 z_5 - 72$
850	0.43	-92	$z_{8.5} = 0.43 z_5 - 92$
1000	0.20	-98	$z_{10} = 0.20 z_5 - 98$

Table 1 The values of the functions A and B of the reference atmosphere for 25-3-'71, 00 GMT.

The functions A and B are also given in figures 4 and 5.

The values of the function A of 25-3-'71, 00 GMT, are used for the computations of the coefficients of the baroclinic model in chapter IV 3.4. So these coefficients are defined with the aid of A -values depending on only one date. However, it appeared from comparison with other situations that these values were fairly representative for polar jetstream conditions over the Atlantic and Western Europe. Moreover, computations of the static stability at 500 mbar in 3.2 show that the areal mean value of the static stability of the reference atmosphere as defined by (3.1) and based on the values of A and B of 500 mbar at 25-3-'71, 00 GMT, agree with the value of the static stability of the ICAO standard atmosphere. Concerning the values of B it can be remarked that probably there is a systematic annual variation. This is not serious, because knowledge of the function B is not required for the considerations of this treatise.

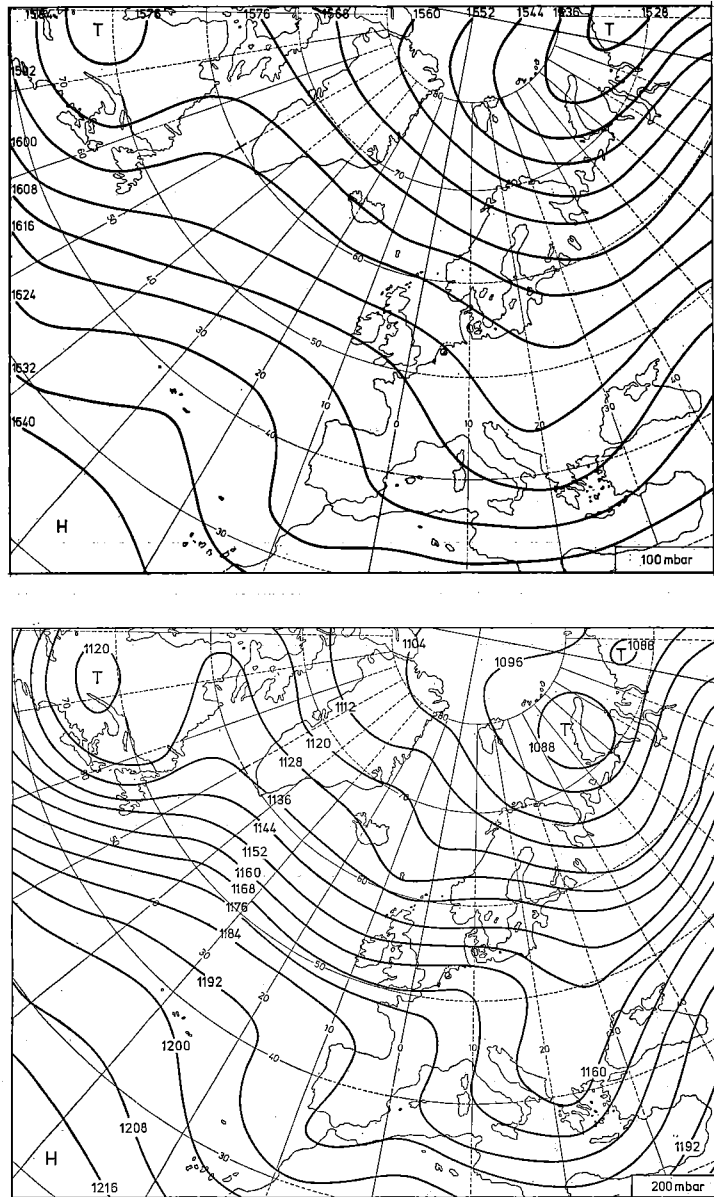
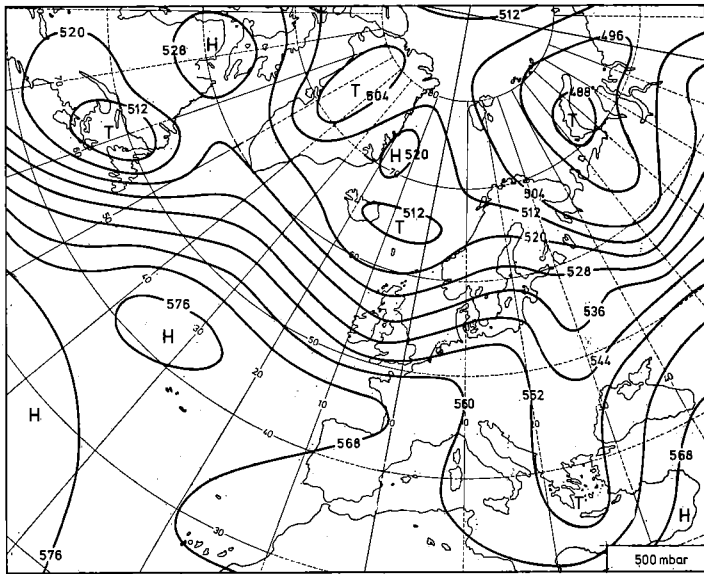
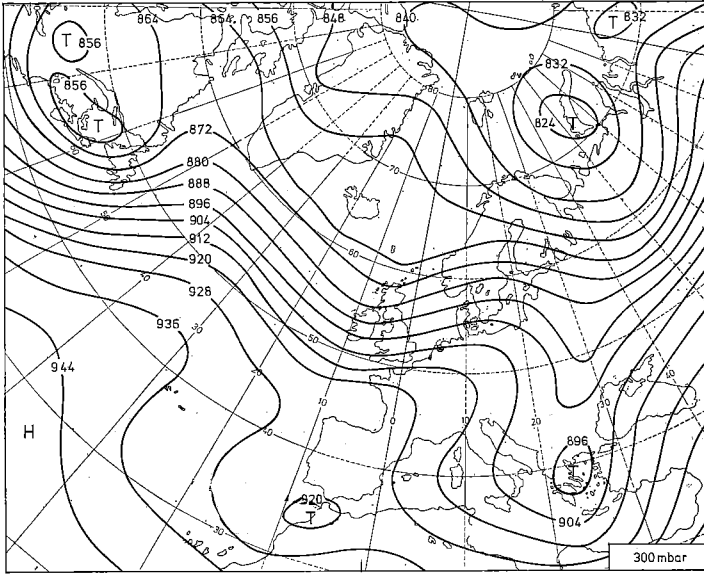


Fig. 2a Analyses of the topographies of 100, 200, 300 and 500 mbar according to the Deutscher



Wetterdienst (Offenbach) for 25 March 1971, 00 GMT. Contours are labelled in gpdam.

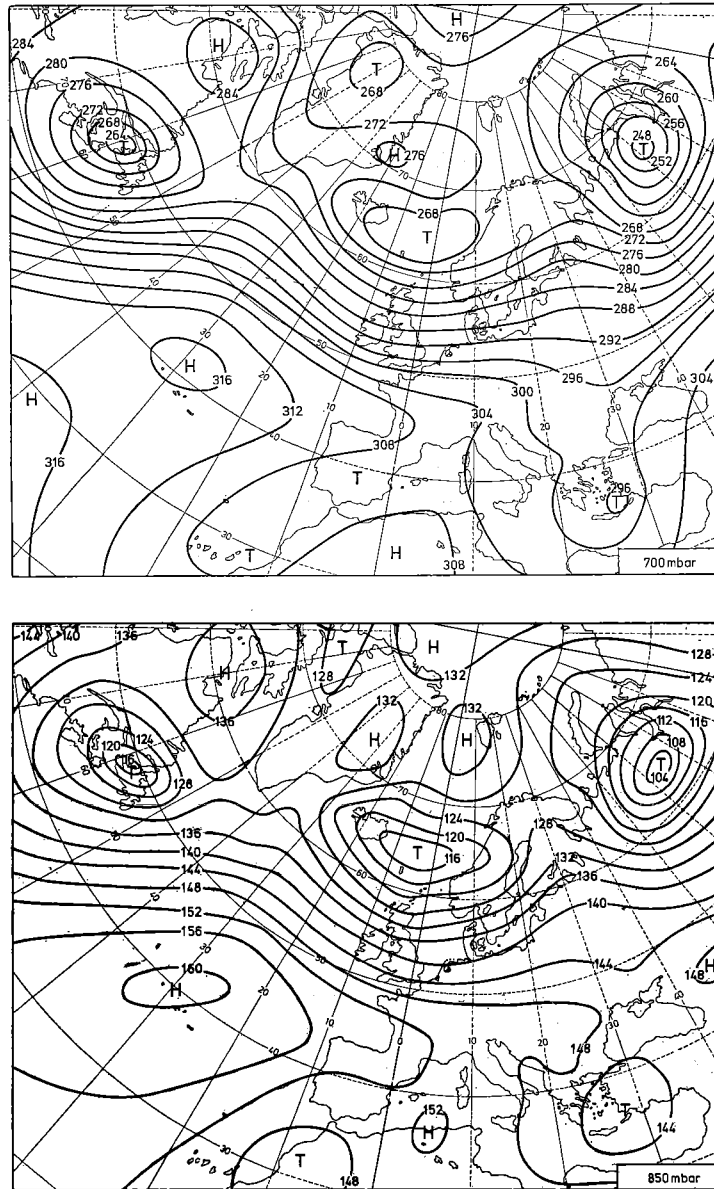
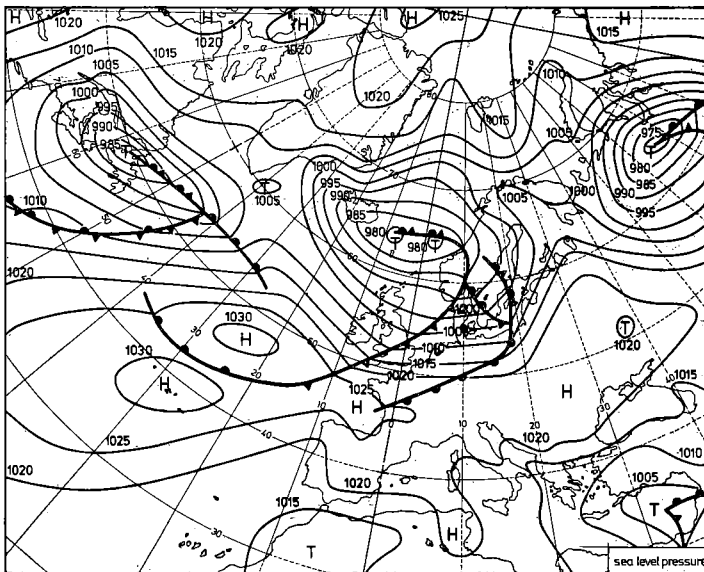
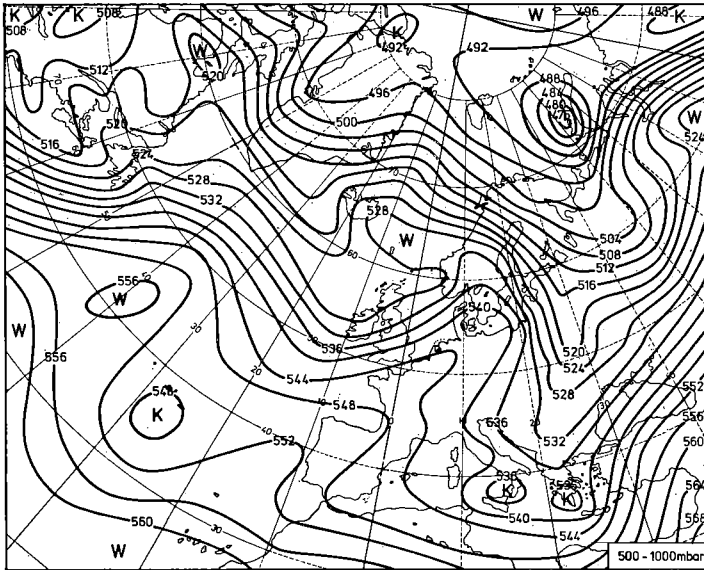


Fig. 2b Analyses of the topographies of 700 and 850 mbar, the thickness field of 500—1000 mbar and sea level pressure according to the Deutscher Wetterdienst (Offenbach) for 25 March



1971, 00 GMT. Contours are labelled in gpdam, except for those of sea level pressure, which are labelled in mbar.

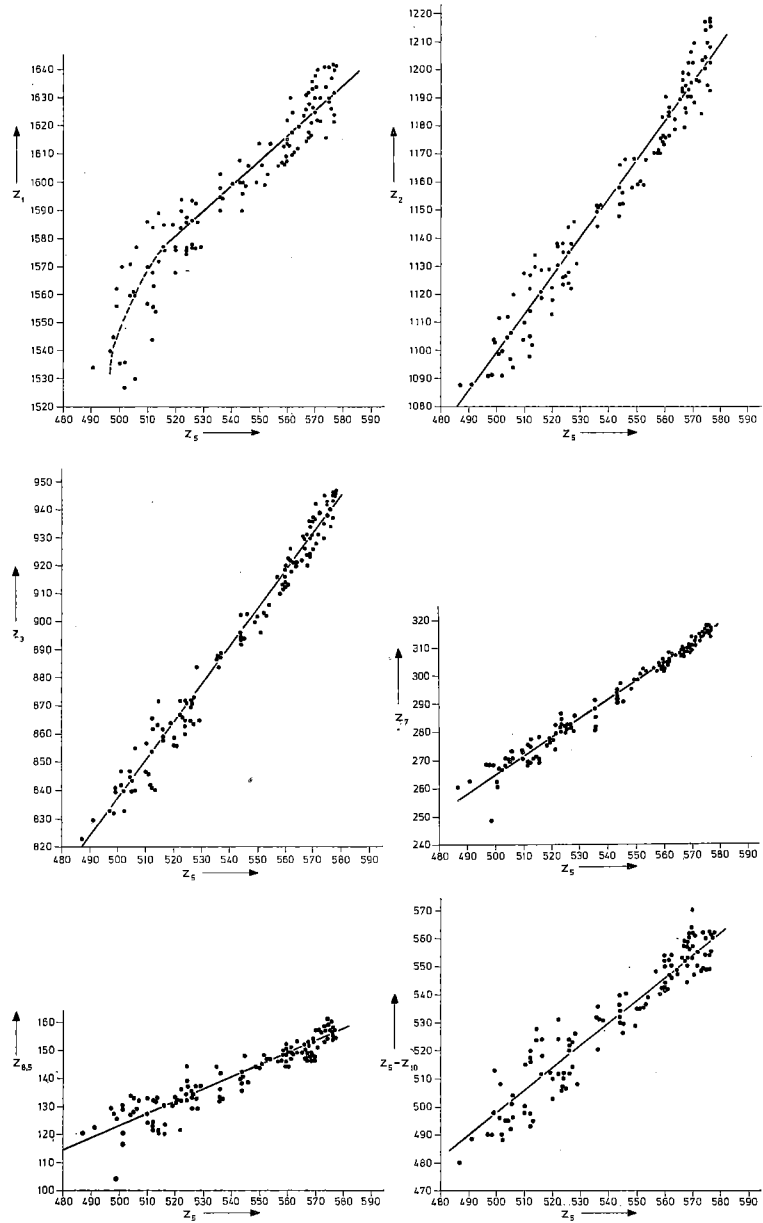


Fig. 3 Relation between the geopotential heights (gpdam) of 500 mbar and of 100, 200, 300, 700 and 850 mbar and the thickness field of 500–1000 mbar for 25 March 1971, 00 GMT. The heights are denoted by z_5 , z_1 , z_2 , z_3 , z_7 , $z_{8.5}$ and the thickness by $z_5 - z_{10}$, respectively, and are then specified using the analyses in figures 2a and 2b for the 120 gridpoints in figure 1.

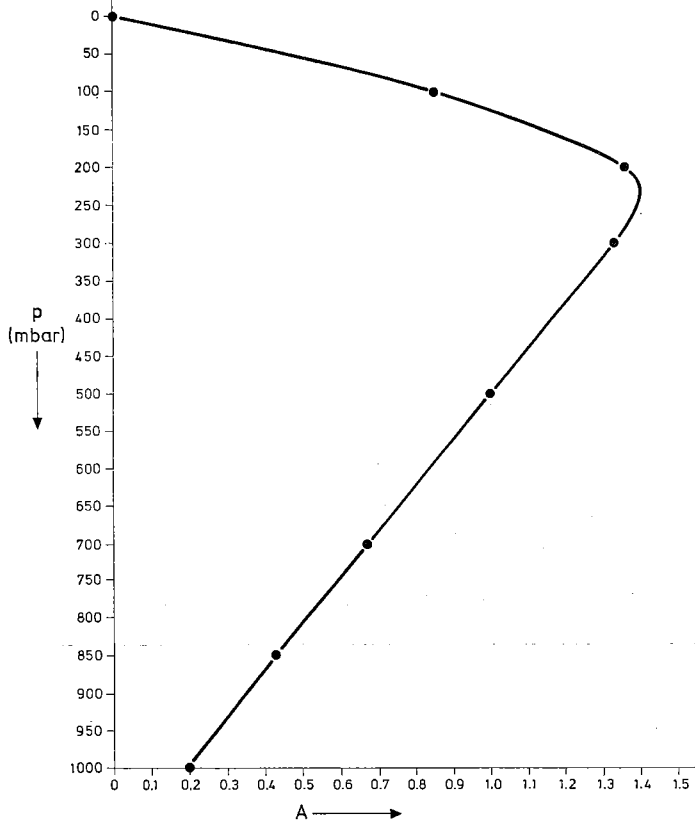


Fig. 4 The function A of the reference atmosphere for 25 March 1971, 00 GMT.

With the aid of (3.6) and (3.9), D and ω can be expressed as

$$D = \frac{D'}{f_0} RVA \quad (3.10)$$

and

$$\omega = \frac{\omega'}{f_0} RVA \quad (3.11)$$

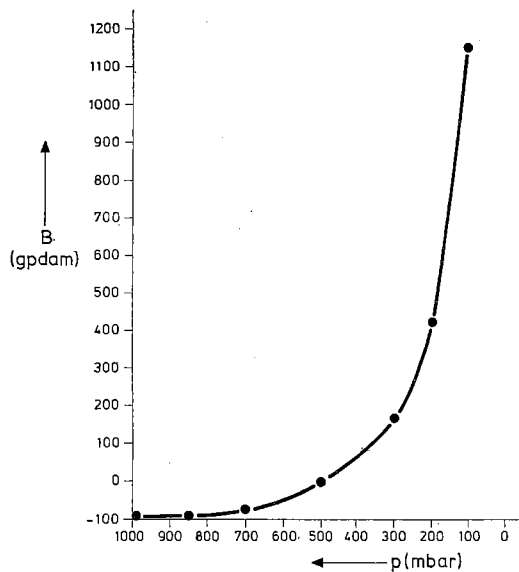


Fig. 5 The function B of the reference atmosphere for 25 March 1971, 00 GMT.

$$D' \equiv -A \cdot K + A^2 \quad (3.12)$$

and

$$\omega' \equiv - \int_0^p D' dp \quad (3.13)$$

To compute D' and ω' as functions of p , the values of A are determined from figure 4 for intervals of 25 mbar from 0 to 250 mbar and for intervals of 50 mbar from 250 to 1000 mbar. First, the quantity K is computed according to (3.7).

K appears to equal 0.99. Then, with the aid of (3.12) and (3.13), D' and ω' can be defined. The integrals in (3.7) and (3.13) have been approximated with the use of the trapezoidal rule given by (3.14) for an arbitrary function f .

$$\int_{p_0}^{p_n} f(p) dp \approx \left[\frac{1}{2} f(p_0) + f(p_1) + \dots \dots + f(p_{n-1}) + \frac{1}{2} f(p_n) \right] \cdot \Delta p \quad (3.14)$$

with $\Delta p \equiv p_i - p_{i-1}$ for $i = 1, 2, \dots \dots, n$

The computed values of D' and ω' are given in table 2.

p	A	A^2	$A \cdot K$	$D' = -A \cdot K + A^2$	$\omega' = -\int_0^p D' dp$
mbar	—	—	—	—	$10^{+4} \text{ kg m}^{-1}\text{s}^{-2}$
0	0	0	0	0	0
25	0.25	0.06	0.25	-0.19	+0.02
50	0.48	0.23	0.48	-0.25	+0.08
75	0.68	0.46	0.67	-0.21	+0.14
100	0.85	0.72	0.84	-0.12	+0.18
125	1.00	1.00	0.99	+0.01	+0.19
150	1.13	1.28	1.12	+0.16	+0.17
175	1.25	1.56	1.24	+0.32	+0.11
200	1.36	1.85	1.35	+0.50	+0.01
225	1.40	1.96	1.39	+0.57	-0.13
250	1.39	1.93	1.38	+0.55	-0.26
300	1.33	1.77	1.32	+0.45	-0.51
350	1.24	1.54	1.23	+0.31	-0.70
400	1.16	1.34	1.15	+0.19	-0.83
450	1.08	1.17	1.07	+0.10	-0.90
500	1.00	1.00	0.99	+0.01	-0.93
550	0.92	0.85	0.91	-0.06	-0.92
600	0.84	0.71	0.83	-0.12	-0.87
650	0.76	0.58	0.75	-0.17	-0.80
700	0.67	0.45	0.66	-0.21	-0.71
750	0.59	0.35	0.58	-0.23	-0.60
800	0.51	0.26	0.51	-0.25	-0.48
850	0.43	0.19	0.43	-0.24	-0.35
900	0.35	0.12	0.35	-0.23	-0.23
950	0.27	0.07	0.27	-0.20	-0.12
1000	0.20	0.04	0.20	-0.16	0.00

Table 2 Values of the functions A , D' and ω' of the reference atmosphere for 25-3-'71, 00 GMT.

The extreme values of D can be found at the pressure levels for which $\frac{\partial D}{\partial p} = 0$.

From (3.6) it follows that in that case $(K - 2A) \frac{dA}{dp} = 0$. This is true for $A = \frac{1}{2}K$ or

$\frac{dA}{dp} = 0$. From figure 4 one can see that there are two levels for which $A = \frac{1}{2}K$,

namely at 50 mbar and 810 mbar, and one level for which $\frac{dA}{dp} = 0$, namely at 230

mbar. The level for which $\frac{dA}{dp} = 0$ is also the level of a maximum value of A and as

follows from (3.5), of a maximum geostrophic wind. The extreme values of ω are found at the levels for which $\frac{\partial \omega}{\partial p} = 0$ or, as follows from the continuity equation (3.3), $D = 0$. In that case A equals $A = 0$ or $A = K = 0.99$. The relevant levels are found at 0 mbar and 510 mbar respectively, as can be seen from figure 4.

In figure 6, with the aid of table 2 and the results with respect to extreme values of D and ω , the graphs of D' and ω' are drawn for the case of advection of positive relative vorticity at 500 mbar.

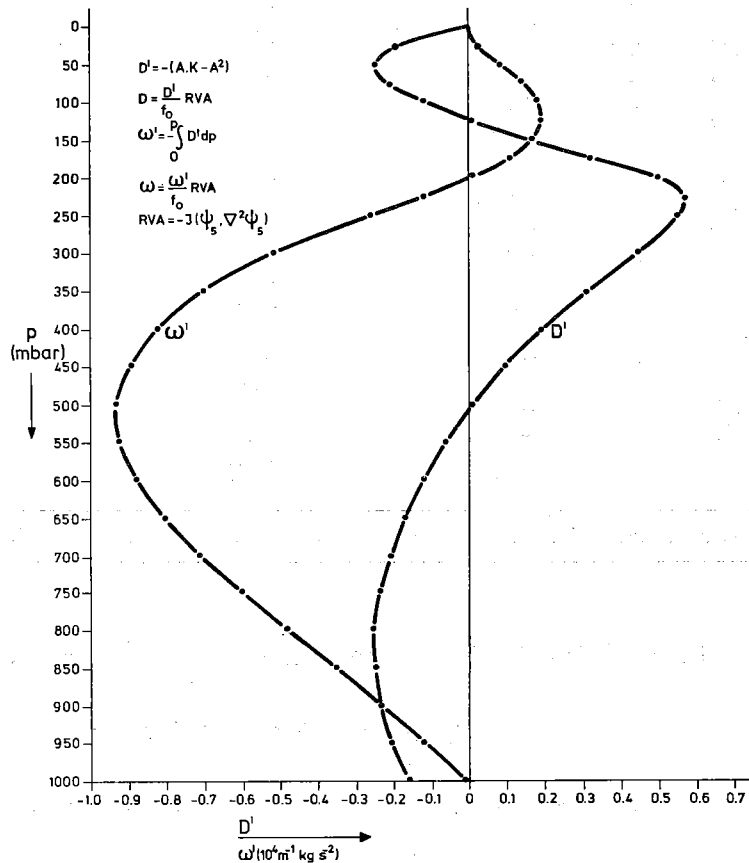


Fig. 6 The profiles of the 'vertical velocity' ω and the horizontal divergence D as functions of pressure p in the case of advection of positive relative vorticity at 500 mbar ($\text{RVA} > 0$) according to the reference atmosphere for 25 March 1971, 00 GMT.

It will be evident that it is necessary to know the values of RVA at 500 mbar, in order to be able to compute numerical values for D and ω . This is done in the next section.

2.2 *Specification of the advection of relative vorticity at 500 mbar (RVA)*

The computation of $RVA = -J(\psi_5, \nabla^2 \psi_5)$ at 500 mbar is carried out with the aid of the objective analysis of 500 mbar for 25-3-'71, 00 GMT. This analysis is given by the isolines in figure 7. The points of that figure are the points of the computational grid of the baroclinic model. This grid, which covers Western Europe, the Atlantic and North-America and differs from the one shown in figure 1, is described in detail in IV 6.1. The grid distance at 60°N is 375 km.

At each grid point the advection of relative vorticity at 500 mbar was computed with the aid of a finite difference approximation of the Jacobian. Due to the difference scheme, it was only possible to compute values of RVA at the grid points at least two grid distances away from the boundaries.

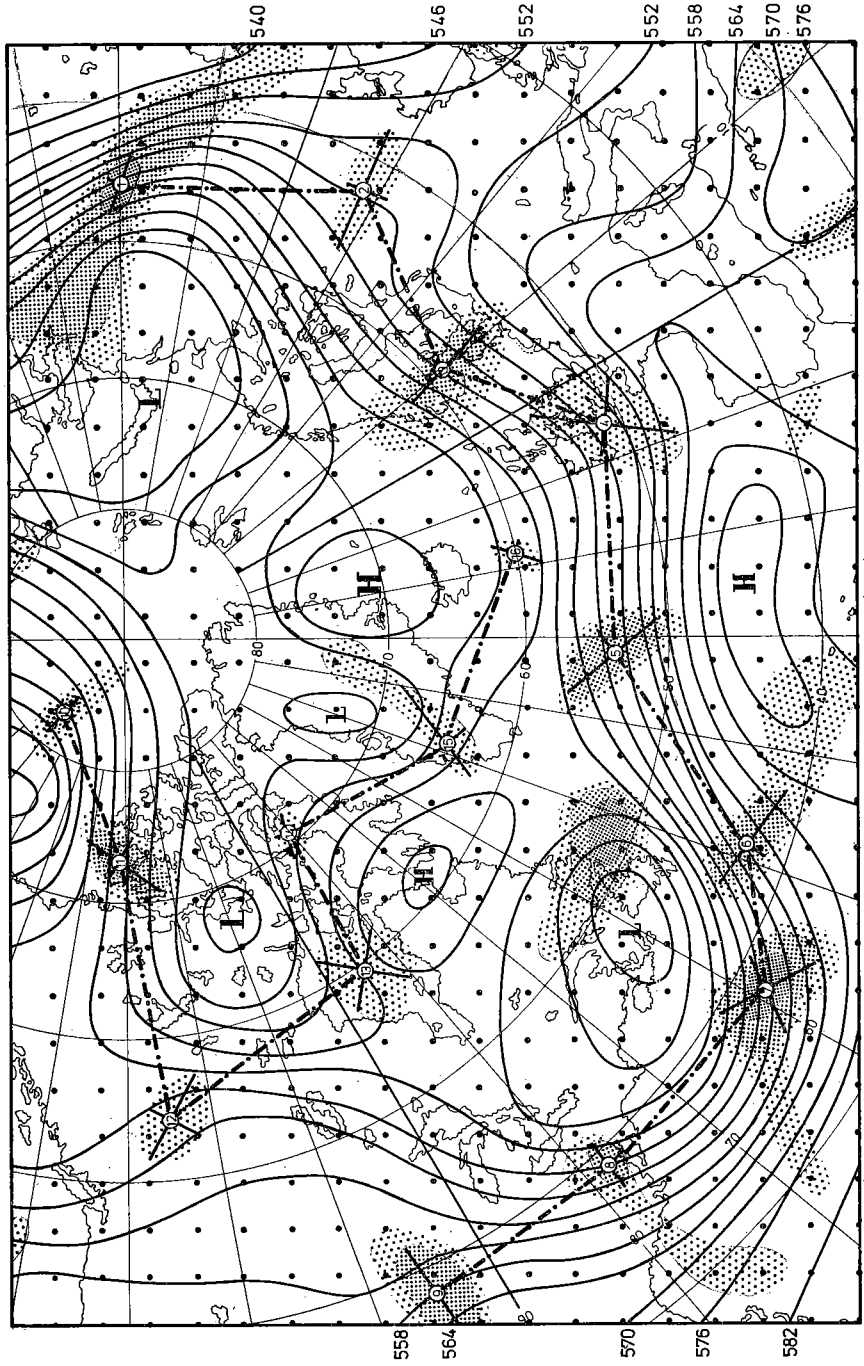
The computed mean value was $2.6 \times 10^{-11} \text{s}^{-2}$ with a standard deviation equal to $1.7 \times 10^{-9} \text{s}^{-2}$. This means that, compared with the real values of RVA, the mean value of this quantity is negligible, and assuming a normal distribution of this parameter one can conclude that 95% of its value must lie between $-3.42 \times 10^{-9} \text{s}^{-2}$ and $+3.42 \times 10^{-9} \text{s}^{-2}$.

The positive RVA-areas have been analyzed with the aid of the computed values at the grid points. These areas are shown in figure 7 by isolines, which are drawn at values of 1.2, 2.4, $4.8 \times 10^{-9} \text{s}^{-2}$, etc. The same analysis could be carried out with the negative RVA-areas. However, in this treatise only the positive RVA-areas are investigated, because these areas are related with frontal waves. This relation is outlined in section 3.4. In the rectangle of figure 7, 16 positive RVA-areas numbered 1 to 16 can be distinguished. These areas can be considered to consist of two wave trains, namely the numbers 1 to 9 belonging to the polar jetstream and the numbers 10 to 16 belonging to the arctic jetstream.




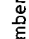
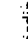

Because the RVA-areas all show a more or less elliptic shape, a local system of coordinates is fixed for every RVA-area, with the origin in the point of maximum RVA, the x -coordinate along the short axis of the ellipse and the y -coordinate along the long axis. The elliptic shape of the RVA-areas permits the approximation of the quasi-geostrophic streamfunction for each local area by

$$\psi_5 = -U_5 \cdot y + \psi_5^* \cos(\mu_y \cdot y) \sin(\mu_x \cdot x) + E \quad (3.15)$$

with ψ_5^* the amplitude, E a constant, μ_y and μ_x the wave numbers in the local y - and x -directions respectively, and U_5 the geostrophic wind of the basic flow in the



Explanation of the areas of advection of positive relative vorticity (RVA):

-  $1.2 - 2.4 \times 10^{-9} \text{ s}^{-2}$
-  $2.4 - 4.8 \times 10^{-9} \text{ s}^{-2}$
-  $> 4.8 \times 10^{-9} \text{ s}^{-2}$
-  Number
-  Coordinate system
-  Wave-train of RVA-areas

x -direction. The wave numbers μ_x and μ_y are defined by $\mu_x \equiv 2\pi/L_x$ and $\mu_y \equiv 2\pi/L_y$, with L_x the wavelength in the x -direction and L_y that in the y -direction. It follows from (3.8) and (3.15) that RVA is given by

$$\begin{aligned} \text{RVA} &= U_5 \psi_5^* \mu_x (\mu_x^2 + \mu_y^2) \cos(\mu_y \cdot y) \cos(\mu_x \cdot x) = \\ &= U_5 \psi_5^* \frac{8\pi^3}{L_x^3} [1 + (L_x/L_y)^2] \cos(\mu_y \cdot y) \cos(\mu_x \cdot x) \end{aligned} \quad (3.16)$$

(3.16) shows that the maximum value of RVA is determined by the quantities U_5 , ψ_5^* , L_x and the ratio L_x/L_y , which can be computed with the aid of figure 7.

The ratio L_x/L_y has been determined by measuring the lengths of the line segments along the local x - and y -axes between the two intersections of some arbitrarily chosen isoline. The values of L_x could be determined by measuring the length of the line segment along the x -axis between the two intersections of the zero isoline. As follows immediately from figure 7, this determination of L_x is very inaccurate, due to the uncertainty in the choice of the coordinate system for each RVA-area. Therefore, another, more accurate procedure has been carried out. After connecting the points of maximum RVA-values of each wave train by straight lines, the length of each line segment was measured. The value of L_x for the RVA-area with the number n has been computed with

$$L_x(n) = (L_1 + L_2)/2 \quad (3.17)$$

with L_1 the length of the line segment between the numbers $n - 1$ and n , and L_2 the length of the line segment between the numbers n and $n + 1$. To compute U_5 in the centre of the RVA-area, (3.15) is differentiated to y , which gives

$$\frac{\partial \psi_5}{\partial y} = -U_5 - \mu_y \cdot \psi_5^* \sin(\mu_y \cdot y) \sin(\mu_x \cdot x) \quad (3.18)$$

For the origin of the coordinate system, which coincides with the centre of the RVA-area and where the RVA has a maximum value, (3.18) reduces to

$$\frac{\partial \psi_5}{\partial y} = -U_5 \quad (3.19)$$

Fig. 7 Objective analysis of the topography of 500 mbar with areas of advection of positive relative vorticity (RVA > 0) for 25 March 1971, 00 GMT. Dots indicate the grid points used in the BK3-model. Isohyphes of 500 mbar (gpdam) are drawn.

For the centre of each RVA-area U_5 has been approximated by

$$U_5 \approx \frac{g \cdot m}{f} \frac{\Delta z}{\Delta y} \quad (3.20)$$

with $g = 9.8 \text{ ms}^{-2}$. m is the map scale factor belonging to the latitude of the origin of the coordinate system. f is the value of the coriolis parameter belonging to the same latitude. A height difference of 120 or 240 m has been taken for Δz along the y -axis. The centre of the corresponding line segment Δy is approximately coincident with the origin of the coordinate system. The values of Δz have been chosen arbitrarily and depend on the lengths of the line segments Δy , which have to lie completely in the jetstream area.

Replacing the amplitude ψ_5^* of the quasi-geostrophic streamfunction ψ_5 of (3.15) by a height amplitude z_5^* according to $z_5^* = \frac{f}{g} \psi_5^*$ and using (3.16), z_5^* can be expressed as

$$z_5^* = \frac{f \cdot L_x^3 \cdot I}{8\pi^3 g \cdot U_5 [1 + (L_x/L_y)^2]} \quad (3.21)$$

I is the maximum value of the RVA. This value has been approximated by the highest isoline value for each RVA-area. As U_5 , L_x , L_x/L_y and I are known, z_5^* can be estimated with the aid of (3.21).

The values of L_x , L_x/L_y , U_5 , I and z_5^* are given in table 3.

number of the RVA area	latitude	L_x/L_y	L_x km	U_5 ms^{-1}	I 10^{-9}s^{-2}	z_5^* dam
1	56°	0.50	—	32	4.8	—
2	53°	0.31	1725	12	1.2	2.2
3	59°	0.40	1425	25	2.4	1.3
4	51°	0.52	1525	20	2.4	1.6
5	54°	0.41	1735	30	2.4	1.8
6	43°	0.35	1390	43	2.4	0.5
7	38°	0.67	1330	51	4.8	0.5
8	39°	0.64	1560	40	2.4	0.7
9	39°	0.53	—	25	2.4	—
10	83°	0.42	—	21	2.4	—
11	73°	0.48	1730	21	4.8	5.6
12	54°	0.58	2005	13	1.2	2.8
13	60°	0.85	1590	18	1.2	0.8
14	71°	0.56	1390	8	1.2	1.8
15	65°	0.37	1565	20	1.2	1.1
16	60°	0.57	—	20	1.2	—

Table 3 Quantities of the positive RVA-areas for 25-3-'71, 00 GMT.

With the aid of table 3 the mean values of the given quantities can be computed. These values are given in table 4 for the polar and arctic jetstream separately.

mean values	latitude	L_x km	L_x/L_y	U_5 ms ⁻¹	z_5 dam
polar jetstream	48 °N	1527	0.48	31	1.2
arctic jetstream	67 °N	1656	0.55	17	2.4

Table 4 Mean values of several quantities belonging to the positive RVA-areas of the polar jetstream and the arctic jetstream for 25-3-'71, 00 GMT.

These mean values have a certain inaccuracy. For instance the mean value of L_x is somewhat underestimated, because the distance between two successive RVA-areas has been measured along straight lines, whereas the streamlines of the basic streamfunction are curved. Nevertheless the value of L_x of about 1600 km reasonably agrees with the results of DODDS (1971), who found that depressions at sea level with wavelengths between 1600 and 2000 km occur most frequently. The mean values of L_x/L_y and U_5 depend on the determination of the directions of the coordinate axes for each RVA-area. These directions are not well defined. However, in spite of that uncertainty the value of about 0.5 for the mean value of L_x/L_y is fairly characteristic for RVA-areas, as can be seen from maps of RVA-patterns, which are drawn at the Royal Netherlands Meteorological Institute on a routine basis. The mean value of U_5 is not characteristic, as is indicated by table 4, giving a difference of a factor 2 between the wind velocity in the polar jetstream and that in the arctic jetstream. This fact is not serious for the computations given in the next sections, as U_5 is used exclusively in the formulas for the relation between the wavelength of the waves and the static stability in section 3.3 and, as is shown in this section, the computed wavelengths of the short and the long waves ($< \sim 5000$ km) are fairly insensitive to variations of U_5 .

The low values of z_5^* in table 4, only a few decameters, are striking. But inspection of figure 7 shows indeed that the waves, which form the RVA-pattern, must be regarded as small perturbations on the large-scale flow pattern.

2.3 *Some numerical values of D and ω*

From the absolute values of RVA given in 2.2 the values of D and ω at several levels

can be computed with the aid of (3.10) and (3.11). The extreme values of D have been found at the levels of 50, 230 and 810 mbar respectively, and the extreme value of ω at 510 mbar. In section 2.2 it has been shown that 95% of the RVA-values are between $-3.42 \times 10^{-9} \text{s}^{-2}$ and $+3.42 \times 10^{-9} \text{s}^{-2}$. These extreme values of RVA can be used to compute the extreme values of D and ω for the reference atmosphere, which are given below for a value of $f_0 = 10^{-4} \text{s}^{-1}$. The value of D at 1000 mbar is also included.

$$\begin{aligned}
 p = 230 \text{ mbar: } & -1.96 \times 10^{-5} \text{s}^{-1} \leq D \leq +1.96 \times 10^{-5} \text{s}^{-1} \\
 p = 810 \text{ mbar: } & -0.84 \times 10^{-5} \text{s}^{-1} \leq D \leq +0.84 \times 10^{-5} \text{s}^{-1} \\
 p = 1000 \text{ mbar: } & -0.54 \times 10^{-5} \text{s}^{-1} \leq D \leq +0.54 \times 10^{-5} \text{s}^{-1} \\
 p = 510 \text{ mbar: } & -275 \text{ mbar/24 hrs} \leq \omega \leq +275 \text{ mbar/24 hrs}
 \end{aligned} \tag{3.22}$$

The vertical velocity w in the reference atmosphere can be estimated with the aid of $\omega \approx -g \cdot \rho \cdot w$. According to the ICAO standard atmosphere $\rho = 0.69 \text{ kg m}^{-3}$ at 500 mbar. With $g = 9.8 \text{ ms}^{-2}$ the possible values of w become:

$$-4.7 \text{ cm s}^{-1} \leq w \leq +4.7 \text{ cm s}^{-1} \tag{3.23}$$

3 The relation between the real atmosphere and the reference atmosphere

3.1 *Height and thermal fields of isobaric levels of the reference atmosphere compared with those of the real atmosphere*

From formula (3.1) one can easily see that the contour lines of the height fields of each pressure level must always be parallel to those of the 500 mbar level. This should also hold for the real atmosphere, if this atmosphere would be equivalent barotropic. In general, the contour lines of isobaric levels of the real atmosphere are not parallel to each other. Figures 2a and 2b show that the greatest deviation is found at sea level and that in the troposphere above the 500 mbar level the contours are fairly parallel. These figures also clearly show that the departures at sea level are caused by the frontal waves.

PALMÉN and NEWTON (1969) discussed the relation between the long waves and the short waves in the upper troposphere and the disturbances at sea level. They found that the short waves are related to the sea level disturbances. The isotherm patterns of these short waves are not in phase with the streamlines. For such waves the real atmosphere obviously differs from the constructed reference atmosphere. The long waves, however, consist of cold troughs and warm ridges with isotherm patterns that are nearly in phase with the streamlines. Therefore, the real atmosphere agrees fairly

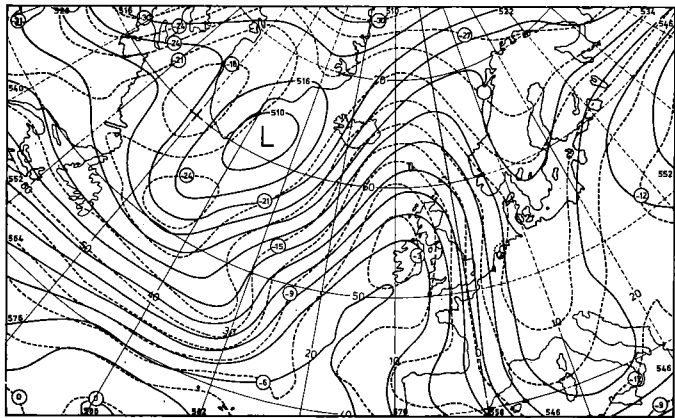
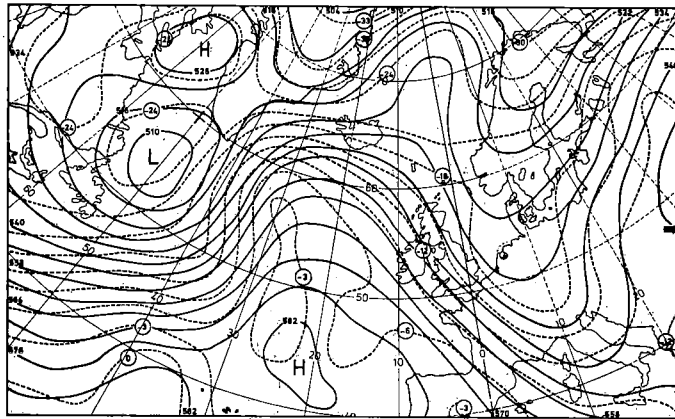
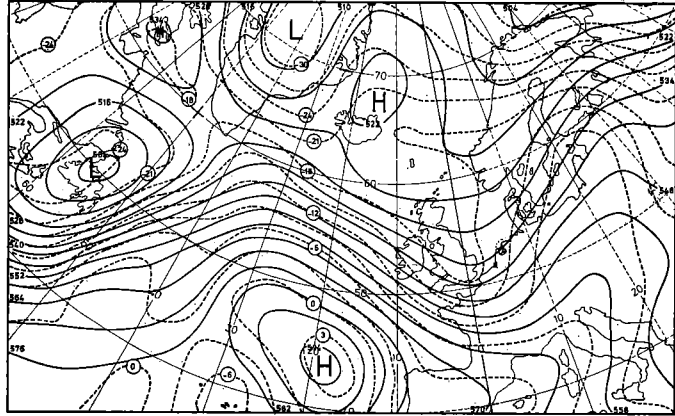
well with the reference atmosphere as far as only these long waves are considered. The short waves generally act as small perturbations on the long waves in the upper troposphere. That explains the fairly good agreement of the upper troposphere with the reference atmosphere. In the lower troposphere, however, the short waves do not form small perturbations on the long waves, as the long waves have their most pronounced development in the upper troposphere. So, the behaviour of the lower part of the troposphere differs from the behaviour of the reference atmosphere. This difference is manifested by phase shifts between the patterns of the isotherms and the streamlines. Therefore, a further investigation into the relation between the height field of 500 mbar and the thickness pattern of 500–850 mbar must be considered necessary.

For the construction of a baroclinic model it is also important to know that relation, because a good prediction of the 500 mbar height and a wrong prediction of the thickness pattern of 500–850 mbar will inevitably lead to a poor forecast of the 1000 mbar height. (It should be noted here that the thickness pattern of 500–1000 mbar can be related in a relatively easy way to the thickness pattern of 500–850 mbar. This is elucidated in V.1). Such a wrong prediction can be caused for instance by an incorrect phase shift between the waves in the thickness pattern and those in the 500 mbar surface. It is a well-known fact that the 1000 mbar forecasts of baroclinic models based on filtered equations are rather poor compared with those of the 500 mbar level. It is not very unrealistic to suppose that a possible cause of the relatively unsuccessful prediction for sea level by some baroclinic models is due to a false prediction of the phase shift of the thickness field. For one may assume that nearly all models give good predictions of the movements of the waves at 500 mbar for at least 24–36 hours ahead, as even the use of the simplest barotropic vorticity equation at that level results into good forecasts for such periods.

It was possible to investigate the relation between the thickness patterns of 500–850 mbar and the heights of the 500 mbar level during the year 1971. This investigation was carried out with the aid of the maps of the Royal Netherlands Meteorological Institute, which were drawn for 00 and 12 GMT every day. The relationship thus found for the real atmosphere can be summarized as follows:

- 1° The waves of the two patterns move with nearly the same speed.
- 2° The two patterns show the same development (decreasing or increasing amplitudes, appearance or disappearance of cut-off systems).
- 3° The phase shift between the two patterns is nearly constant with respect to time (little or no phase lag for the long waves and a phase lag between 0° and 90° for the short waves).

These features are illustrated by an example given in figures 8a, 8b and 8c for the dates 25-3-'71, 12 GMT, 26-3-'71, 12 GMT and 27-3-'71, 12 GMT. Dashed lines are isolines of the 500–850 mbar thickness pattern, and continuous lines represent the



heights of the 500 mbar level. Of special interest here is the long wave with the top of the 552 dam isopleth at 30°W, 56°N in figure 8a.

During the following 48 hours this wave moved to the east with an increasing amplitude. The positions of the 552 dam top in figures 8b and 8c are 22°W, 61°N and 7°W, 63°N respectively. These figures clearly show that the dashed lines of the thickness field, marked by the circled numbers (mean temperatures), followed the movement and the development of the long wave in the 500 mbar pattern. For this wave the phase shift between the thickness pattern and the 500 mbar pattern was small. The short waves, which are superposed on the long wave pattern, are most easily recognized in the thickness pattern. See for instance figure 8a, where the -15°C isotherm shows three tops at 48°W, 51°N, 38°W, 59°N and 13°W, 56°N respectively.

The relation between the height of the 500 mbar surface and the thickness of 500–850 mbar of the reference atmosphere follows from (3.1), namely

$$z_5 - z_{8.5} = (1 - A_{8.5}) z_5 - B_{8.5} \quad (3.24)$$

This formula shows that for the reference atmosphere the two patterns must have the same speeds, the same developments and no phase shifts. The behaviour of the height of the 500 mbar surface is described by the barotropic vorticity equation, because the level of non-divergence was found at about 500 mbar. See also figure 6.

The good results achieved with the barotropic vorticity equation, used at the 500 mbar level for forecast periods till about 36 hours ahead, which are especially obtained for the long waves, indicate that *the defined reference atmosphere of section 1 is a good first order approximation for the behaviour of the long waves in the atmosphere*. The short waves, however, are baroclinic and therefore a further investigation of the agreements and differences between the short waves and the reference atmosphere is necessary. In the next sections more quantitative comparisons are given. The static stability at 500 mbar, the horizontal divergence and the vertical velocity of the real atmosphere are compared with the same parameters for the reference atmosphere. Moreover, some considerations are held about the formulation of the thermodynamic equation and the choice of the value of static stability occurring in that equation.

Fig. 8 Analyses of topographies of 500 mbar and thickness fields of 500–850 mbar.
 — Isophyses of 500 mbar (gpdam).
 --- Contours of mean temperature (°C) of the layer of 500–850 mbar.
 a. Valid for 25 March 1971, 12 GMT.
 b. Valid for 26 March 1971, 12 GMT.
 c. Valid for 27 March 1971, 12 GMT.

3.2 *Static stability computations for 500 mbar for 25-3-'71, 00 GMT*

The static stability is defined as

$$\sigma \equiv \frac{\partial^2 \Phi}{\partial p^2} + \frac{c_v}{c_p \cdot p} \frac{\partial \Phi}{\partial p} \quad (3.25)$$

With the aid of (3.1) and the above formula the static stability $\sigma_{r.a.}$ of the reference atmosphere becomes

$$\sigma_{r.a.} = g \left[\left(\frac{d^2 A}{dp^2} + \frac{c_v}{c_p \cdot p} \frac{dA}{dp} \right) z_5 + \left(\frac{d^2 B}{dp^2} + \frac{c_v}{c_p \cdot p} \frac{dB}{dp} \right) \right] \quad (3.26)$$

So $\sigma_{r.a.}$ is a linear function of the height of the 500 mbar level. The static stabilities at 500 mbar of both the reference atmosphere and the real atmosphere will now be compared for the date 25-3-'71, 00 GMT, as this is the time for which the reference atmosphere has been specified in 2. For the computation a difference approximation of (3.25) is used, namely:

$$\sigma = g \frac{z_3 + z_7 - 2z_5}{(\Delta p)^2} - \frac{c_v \cdot g}{c_p \cdot p_5} \frac{z_3 - z_7}{2\Delta p}, \quad (3.27)$$

where $\Delta p = p_5 - p_3 = p_7 - p_5$ and the indices 3, 5, 7 refer to respectively 300, 500 and 700 mbar. Using this difference approximation, the σ -value of the real atmosphere can be computed at the 120 grid points of figure 1. Noticing that the heights of the reference atmosphere at 300 mbar and 700 mbar are given by $z_3 = A_3 \cdot z_5 + B_3$ and $z_7 = A_7 \cdot z_5 + B_7$, the $\sigma_{r.a.}$ -values can also be computed with (3.27) for two arbitrary values of z_5 . Then $\sigma_{r.a.}$ is known for every value of z_5 , because of the linear dependency of $\sigma_{r.a.}$ on z_5 . The computed values of σ (points) and $\sigma_{r.a.}$ (straight line) are given in figure 9. In this figure the σ -values of the real atmosphere are plotted as a function of the heights of 500 mbar for the corresponding grid points. Though the computed σ -values vary considerably there is no inconsistency between these values and the straight line of the reference atmosphere.

For the 120 grid points the mean values of σ and $\sigma_{r.a.}$ were computed and compared with σ at 500 mbar of the ICAO standard atmosphere, which was also computed with the aid of (3.27). The value of $\sigma_{r.a.}$ for the polar jetstream in figure 7 was obtained by taking the mean of the heights z at all RVA-centres 1 to 9, which is 544 dam, and by reading the corresponding value of $\sigma_{r.a.}$ in figure 9. The computed values are given below and agree mutually.

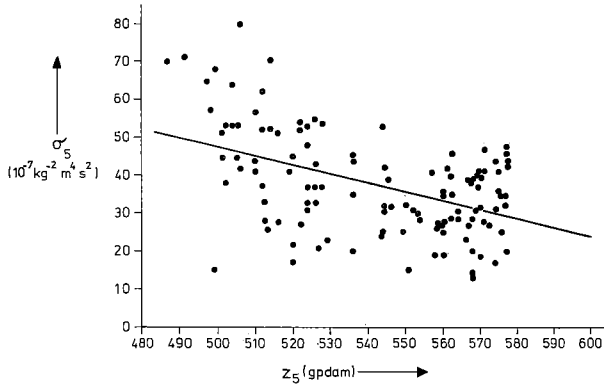


Fig. 9 Relation between the values of the static stability for 25 March 1971, 00 GMT, and the heights of the topography of 500 mbar for each of the 120 grid points in figure 1. The static stability of the reference atmosphere as a function of the height of the 500 mbar level is given by the straight line.

Mean value of σ at 120 grid points	: $38 \times 10^{-7} \text{ m}^4 \text{ kg}^{-2} \text{ s}^{-2}$
Mean value of $\sigma_{r.a.}$ at 120 grid points	: $38 \times 10^{-7} \text{ m}^4 \text{ kg}^{-2} \text{ s}^{-2}$
Value of σ for the ICAO standard atmosphere:	$37 \times 10^{-7} \text{ m}^4 \text{ kg}^{-2} \text{ s}^{-2}$
Mean value of $\sigma_{r.a.}$ for the polar jetstream	: $37 \times 10^{-7} \text{ m}^4 \text{ kg}^{-2} \text{ s}^{-2}$

It must be mentioned here that all computations carried out with (3.27) possess a relatively large truncation error due to the use of differences. An estimation of the truncation error is possible, because the static stability of the ICAO standard atmosphere is exactly known at each pressure level. The static stability σ in (3.25) can also be expressed as

$$\sigma = \frac{R^2 \cdot T}{g \cdot p^2} \left(\frac{g}{c_p} + \frac{dT}{dz} \right) \quad (3.28)$$

According to the definition of the standard atmosphere, $\frac{dT}{dz} = -0.0065^\circ\text{C}$ per standard geopotential meter in the troposphere. Further, T is specified for a chosen pressure at sea level, so that according to the hydrostatic law T is known at every pressure p , and consequently also σ . At 500 mbar $\sigma = 28 \times 10^{-7} \text{ m}^4 \text{ kg}^{-2} \text{ s}^{-2}$. So the truncation error caused by the use of difference approximations is about 30%. However, mutual comparison is possible, because in all computations the same difference approximation has been used.

The above computations suggest that the mean values of the static stabilities at 500 mbar of the real atmosphere and the reference atmosphere agree with each other and can also be used as a mean value for the polar jetstream of the reference atmosphere.

3.3 *Some considerations with respect to the formulation of the thermodynamic equation and the choice of the static stability*

In section 1 the thermodynamic equation was not taken into consideration, for the reference atmosphere could be completely defined with the relations (3.1), (3.2), (3.3) and (3.4). It will be shown now that for the reference atmosphere defined in this way the thermodynamic equation (2.14), without the heat term Q , is valid at 500 mbar for some specified wavelengths only. These wavelengths depend on the choice of the static stability and the geostrophic wind of the basic flow.

Substituting (3.5) and (3.9) into (2.14) the following expression is found for the thermodynamic equation at 500 mbar:

$$\frac{dA}{dp} \dot{\psi}_5 + \frac{\sigma_5}{f_0^2} \int_0^{p_5} (A \cdot K - A^2) dp \cdot RVA = 0 \quad (3.29)$$

The quasi-geostrophic vorticity equation (3.2) at 500 mbar becomes

$$\nabla^2 \dot{\psi}_5 + J(\psi_5, \nabla^2 \psi_5 + f) = (A_5 \cdot K - A_5^2) RVA = (1 - K) J(\psi_5, \nabla^2 \psi_5) \approx 0 \quad (3.30)$$

because $A_5 = 1$ and $K = 0.99 \approx 1$, which value was computed in 2.1. From section 2.2 it follows that the mean latitude of the positive RVA-areas 1–9 of the polar jetstream is 48°N , while the latitudes of the individual areas vary between 38°N and 59°N . With reasonable accuracy one can assume, therefore, that the polar jetstream is situated along 48°N , and the use of the β -plane approximation of the equations for 45°N is reasonably justified in this case. Further, it is assumed that the streamfunction ψ of the jetstream not only locally satisfies (3.15), but as well for the whole jetstream region with the x -axis directed along the 45°N latitude circle and the y -axis perpendicular to it. So for the considerations given here the jetstream is represented by a simple sine-wave. Then using (3.15) and substituting the result of (3.16) into (3.29) and (3.30), taking the Laplacian operator ∇^2 of (3.29) and eliminating the tendency $\dot{\psi}_5$ from (3.29) and (3.30), one can derive a relation between the static stability σ_5 at 500 mbar and the wavelength of the wave, resulting in

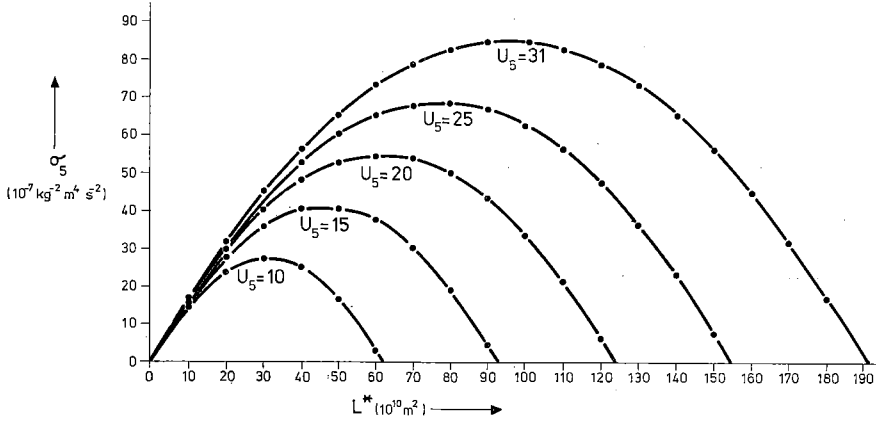


Fig. 10 Relation, valid for the reference atmosphere at 500 mbar for 25 March 1971, 00 GMT, between the static stability σ_5 , the geostrophic windspeed U_5 (ms^{-1}) of the basic zonal flow and the 'quadratic wavelength' L^* .

$$\frac{\sigma_5}{f_0^2} = \frac{\left(\frac{dA}{dp}\right)_{p_5} \cdot \left(1 - \frac{\beta \cdot L^*}{U_5}\right) \cdot L^*}{\int_0^{p_5} (A - A^2) dp} \quad (3.31)$$

with $K = 1$ and a 'quadratic wavelength' $L^* \equiv 1/(\mu_x^2 + \mu_y^2) = \frac{L_x^2}{4\pi^2[1 + (L_x/L_y)^2]}$

Taking the values of f_0 and β for 45°N and those of A from table 2 a relation results between σ_5 , U_5 and L^* , which is given in figure 10 for different values of these parameters. This figure clearly shows that for given values of σ_5 and U_5 one can find two, one or no values of L^* . From 3.2 it follows that $\sigma_{r.a.}$ of the reference atmosphere approximately equals that of the ICAO standard atmosphere. According to table 6 the value of the ICAO standard atmosphere is $28 \times 10^{-7} \text{ m}^4 \text{ kg}^{-2} \text{ s}^2$. Assuming the same value of the truncation error of $\sigma_{r.a.}$, it also becomes $\sigma_{r.a.} \approx 28 \times 10^{-7} \text{ m}^4 \text{ kg}^{-2} \text{ s}^2$. Taking for σ_5 the value of $\sigma_{r.a.}$, one can read the values of L^* , namely L_1^* and L_2^* , from figure 10. In table 5 the possible values of L_x given by $(L_x)_1$ and $(L_x)_2$ are given as functions of U_5 and L_x/L_y . For the computations of table 5 three values of L_x/L_y have been chosen, namely 0, 0.5 and 1, for these values are most common in the real atmosphere. If n denotes the number of waves around the latitude circle 45°N , then it follows from table 5 that two kinds of waves are possible, namely waves with n

U_5 ms ⁻¹	10	15	20	25	31	10	15	20	25	31
L_x/L_y	$(L_x)_1$ km					$(L_x)_2$ km				
0	3400	2800	2700	2700	2600	3400	5400	6400	7400	8300
0.5	3800	3100	3100	3000	2900	3800	6000	7200	8200	9200
1	4900	4000	3900	3800	3700	4900	7600	9100	10400	11700

Table 5 The computed wavelengths $(L_x)_1$ and $(L_x)_2$ according to (3.31) for several values of U_5 and ratios L_x/L_y .

varying from 6 to 11, and waves with n from 2 to 8. These kinds of waves roughly agree with the long and ultra-long waves of the atmosphere. Table 5 also shows that the wavelengths $(L_x)_1$ for a fixed value of L_x/L_y are fairly independent of U_5 unlike those of $(L_x)_2$, which vary more than a factor two.

The computations show that two groups of waves with wavelengths from ~ 2500 km to ~ 4000 km and with wavelengths from ~ 3500 km to ~ 12000 km are possible.

In 2.2 a value of $U_5 = 31 \text{ ms}^{-1}$ was computed for the polar jetstream at 25-3-71, 00 GMT. It follows from table 5 that for this value of U_5 the wavelengths of the long waves of the reference atmosphere must be about 2500–4000 km. Figure 7 shows that the long waves in the polar jetstream have those wavelengths. This result for that date supports the conclusion drawn in section 3.1, that for the long waves the behaviour of the real atmosphere shows resemblance with that of the reference atmosphere. So it indicates that the long waves from 2500 to 4000 km can be reasonably well described by a numerical model using the thermodynamic equation at 500 mbar with a value of the static stability in accordance with the one valid for the ICAO standard atmosphere. Such a model will show an equivalent barotropic behaviour for these waves.

However, in the real atmosphere also short frontal waves occur. These waves are of great importance for day-to-day weather forecasting, because clouds and precipitation are associated with them. Therefore it would be very favourable if these waves could also be described by a numerical model. Because in general the air in these waves is saturated, the values of the static stability to be used should be in accordance with saturated adiabatic lapse rates. In table 6 several values of static stabilities are given, which have been computed for various pressure levels and various temperatures at 1000 mbar and are based on saturated adiabatic lapse rates. Besides, the values according to the ICAO standard atmosphere have been computed. For that purpose the static stability (3.25) has been rewritten with the help of the hydrostatic law as

$$\sigma = \frac{R}{p} \left(\frac{1}{c_p \cdot \rho} - \frac{\partial T}{\partial p} \right) \quad (3.32)$$

Using this formula and the 'Tables of precipitable water and other factors for a saturated pseudo-adiabatic atmosphere of U.S. Weather Bureau (1951)', the values of the static stabilities have been computed. $\frac{\partial T}{\partial p}$ of (3.32) has been approximated by

$(T_{p+\Delta p} - T_{p-\Delta p})/(2\Delta p)$, where Δp denotes a pressure difference of 50 mbar. In the case of the ICAO standard atmosphere formula (3.28) has been used.

Table 6 shows that for temperatures of 10°–14°C at 1000 mbar, which are not unusual in warm sectors of frontal waves, the values of the static stabilities at 500 mbar of saturated adiabatic lapse rates are much lower than that of the ICAO standard atmosphere at the same level. So these values do not agree with the value of the reference atmosphere. Nevertheless it is important to know what wavelengths result from (3.31), if one takes values of σ_5 in accordance with those of the saturated adiabatic lapse rates with temperatures of 10°C and 14°C at 1000 mbar. These values are respectively 10×10^{-7} and $15 \times 10^{-7} \text{ m}^4\text{kg}^{-2}\text{s}^2$. Figure 10 shows that for these values the solutions for the wavelengths of the short waves are nearly independent of U_5 . The solutions for the wavelengths of the ultra-long waves are not taken into consideration, because ultra-long waves, which are fully saturated with water vapour, have no real physical meaning. The computed short wavelengths are given in table 7 for a value of $U_5 = 31 \text{ ms}^{-1}$.

Table 7 shows that the wavelengths are smaller than those of table 5. The wavelength

p mbar	σ of ICAO standard atmosphere	σ of an atmosphere with a saturated adiabatic lapse rate			
	($10^{-7} \text{ m}^4 \text{ kg}^{-2}\text{s}^2$)	($10^{-7} \text{ m}^4 \text{ kg}^{-2}\text{s}^2$)			
300	69	< 1	2	4	16
350	52	< 1	3	7	23
400	41	< 1	5	12	30
450	33	1	8	14	29
500	28	2	10	15	28
550	24	3	11	17	27
600	20	4	12	17	25
650	17	5	13	17	24
700	15	5	13	16	22
750	13	6	12	16	21
800	12	7	12	15	19
850	11	7	11	14	17

temp. at 1000 mbar	14°C	0°C	10°C	14°C	20°C
-----------------------	------	-----	------	------	------

Table 6 Values of the static stability of an atmosphere with a saturated adiabatic lapse rate and of the ICAO standard atmosphere for various temperatures at 1000 mbar.

σ_5	$10 \times 10^{-7} \text{m}^4 \text{kg}^{-2} \text{s}^2$			$15 \times 10^{-7} \text{m}^4 \text{kg}^{-2} \text{s}^2$		
L_x/L_y	0	0.5	1	0	0.5	1
L_x (km)	1400	1600	2000	1900	2100	2700

Table 7 The wavelengths computed from (3.31) with $U_5 = 31 \text{ ms}^{-1}$ and with the values of the static stability at 500 mbar for saturated adiabatic lapse rates related to temperatures of 10°C and 14°C at 1000 mbar.

of 1600 km, which belongs to $\sigma_5 = 10 \times 10^{-7} \text{ m}^4 \text{kg}^{-2} \text{s}^2$ and $L_x/L_y = 0.5$, agrees with that of the mean wavelength of the RVA-pattern at 25-3-71, 00 GMT, as can be seen from table 4 in 2.2. As is shown in the next section, the wavelengths of table 7 also agree with those of the frontal waves at sea level in the Atlantic region.

It can now be concluded that the relation (3.31) between the static stability at 500 mbar and L^ holds for both short baroclinic frontal waves and long equivalent barotropic waves.*

Concerning the design of a baroclinic model aiming to describe developing short frontal waves and which makes use of the thermodynamic equation at 500 mbar with a constant value of the static stability in accordance with a saturated adiabatic lapse rate and temperatures from $\sim 10^\circ \text{C}$ to $\sim 14^\circ \text{C}$ at 1000 mbar, it can be remarked that the long waves, which are equivalent barotropic at the initial time $t = t_0$, will not remain so during the integration of the equations. *So the use of 'saturated adiabatic' values for the static stability in the thermodynamic equation at 500 mbar will violate the equivalent barotropic behaviour of the long waves in the real atmosphere.*

Up to now only the use of the thermodynamic equation (2.14) at 500 mbar has been discussed. However, in the baroclinic model described in Chapter IV, the thermodynamic equation is integrated from 300 to 500 mbar from 500 to 850 mbar. Therefore, further discussions are necessary on the integrals given below.

$$\int_{p_3}^{p_5} \left[\frac{\partial \psi}{\partial p} + J \left(\psi, \frac{\partial \psi}{\partial p} \right) + \frac{\sigma}{f_o} \omega \right] dp = - \int_{p_3}^{p_5} \frac{R \cdot Q}{c_p \cdot f_o \cdot p} dp \quad (3.33)$$

and

$$\int_{p_5}^{p_{8.5}} \left[\frac{\partial \psi}{\partial p} + J \left(\psi, \frac{\partial \psi}{\partial p} \right) + \frac{\sigma}{f_o} \omega \right] dp = - \int_{p_5}^{p_{8.5}} \frac{R \cdot Q}{c_p \cdot f_o \cdot p} dp \quad (3.34)$$

Equations (3.33) and (3.34) are meant to describe the thickness patterns of the short waves, which are related to the frontal waves at sea level. As the air in those waves is generally saturated, one has to choose the values of the static stability σ belonging to saturated adiabatic lapse rates. Table 6 shows that for a given temperature at 1000 mbar the static stability is not strongly dependent on pressure p . Therefore, it is permitted to take constant values of σ in (3.33) and (3.34). These are denoted by σ_{3-5} for the layer from 300 to 500 mbar, and by $\sigma_{5-8.5}$ for the layer from 500 to 850 mbar. Taking for σ_{3-5} and for $\sigma_{5-8.5}$ the average values belonging to saturated adiabatic lapse rates with temperatures of 10°C and 14°C at 1000 mbar, for the layers 300–500 and 500–850 mbar respectively, it can be shown that the long waves of the reference atmosphere do not satisfy the integrated thermodynamic equations (3.33) and (3.34). For that purpose (3.5) and (3.9) of the reference atmosphere are substituted into (3.33) and (3.34). It is assumed therefore that $Q = 0$ for the reference atmosphere. So one gets

$$(A_3 - 1) \psi_5 - \frac{\sigma_{3-5}}{f_0^2} \int_{p_3}^{p_5} \int_0^p (A \cdot K - A^2) dp \Big] dp \cdot \text{RVA} = 0 \quad (3.35)$$

and

$$(1 - A_{8.5}) \psi_5 - \frac{\sigma_{5-8.5}}{f_0^2} \int_{p_5}^{p_{8.5}} \int_0^p (A \cdot K - A^2) dp \Big] dp \cdot \text{RVA} = 0 \quad (3.36)$$

It will be shown that for the long waves of the reference atmosphere, which satisfy the sine-wave formula (3.15), (3.35) and (3.36) are not valid. Using (3.15), (3.16) and the quasi-geostrophic vorticity equation (3.30) with $K = 1$, equations (3.35) and (3.36) can be reduced, in a similar way as was done for (3.29), to the following relations between the quadratic wavelength L^* and the static stabilities σ_{3-5} and $\sigma_{5-8.5}$.

$$\frac{\sigma_{3-5}}{f_0^2} = \frac{(1 - A_3)(1 - \beta \cdot L^*/U_5)L^*}{\int_{p_3}^{p_5} \int_0^p (A - A^2) dp \Big] dp} \quad (3.37)$$

and

$$\frac{\sigma_{5-8.5}}{f_0^2} = \frac{(A_{8.5} - 1)(1 - \beta \cdot L^*/U_5)L^*}{\int_{p_5}^{p_{8.5}} \int_0^p (A - A^2) dp \Big] dp} \quad (3.38)$$

Taking again the values of f_0 and β at 45°N , $U_5 = 31 \text{ ms}^{-1}$ and the values of A from the reference atmosphere at 25-3-'71, 00 GMT the values of L_x , which correspond to the chosen values of σ_{3-5} and $\sigma_{5-8.5}$, can be computed for several ratios of L_x/L_y . For that purpose the mean values of the static stabilities σ_{3-5} and $\sigma_{5-8.5}$ have been computed with the aid of table 6, and these are given in table 8. As was the case for (3.31), for every value of σ in table 8, two values of L_x can be computed for a given ratio L_x/L_y , namely an ultra-long (planetary wave) and a short wave. The ultra-long wavelengths are not taken into consideration here. The computed short wavelengths are given in table 9.

temperature at 1000 mbar	σ_{3-5} ($10^{-7}\text{m}^4\text{kg}^{-2}\text{s}^2$)	$\sigma_{5-8.5}$ ($10^{-7}\text{m}^4\text{kg}^{-2}\text{s}^2$)
10 °C	5.6	11.8
14 °C	10.4	15.9

Table 8 Mean values of the static stability for the layers 300—500 and 500—850 mbar of an atmosphere with a saturated adiabatic lapse rate.

σ	σ_{3-5}		$\sigma_{5-8.5}$	
	10 °C	14 °C	10 °C	14 °C
temperature at 1000 mbar	10 °C	14 °C	10 °C	14 °C
L_x/L_y	L_x (km)	L_x (km)	L_x (km)	L_x (km)
0	1100	1400	1400	1700
0.5	1200	1600	1600	1900
1	1500	2000	2000	2400

Table 9 The computed short wavelengths from (3.37) and (3.38) with $U_5 = 31 \text{ ms}^{-1}$ and the mean values of the static stability for saturated adiabatic lapse rates according to table 8.

This table clearly shows that for the values of the static stability in table 8 no solutions exist corresponding to the wavelengths from 2500 to 4000 km (long waves). The computed wavelengths agree with those of table 7, which have been obtained by applying the thermodynamic equation at 500 mbar. It has to be remarked that the computed wavelengths depend on the values of $A(p)$ and U_5 for one date, namely 25-3-'71, 00 GMT. However, the solution for the short wavelengths is very insensitive to variations of U_5 , because $\beta \cdot L^*/U_5 \ll 1$ holds. Since the values of $A(p)$ for 25-3-'71, 00 GMT, are fairly representative for polar jetstream conditions over the North Atlantic and Western Europe, the computed short wavelengths are representative.

Moreover, computations with A -values for other dates did not lead to essentially different solutions for the wavelengths.

It is of interest to know what kind of values of the static stability one gets if a wavelength of about 3000 km is introduced into (3.37) and (3.38). The relevant computed values of the static stability are given in table 10 for the three chosen values of L_x/L_y . Following this procedure much higher values result. These agree more with those of the ICAO standard atmosphere around 500 mbar.

The results obtained for the integrated forms (3.33) and (3.34) of the thermodynamic equation agree with those following from the application of that equation at 500 mbar. *So the long waves of the reference atmosphere do not satisfy (3.33) and (3.34) if one uses 'saturated adiabatic' values of the static stability.*

L_x/L_y	$\sigma_{3-5}(10^{-7}\text{m}^4\text{kg}^{-2}\text{s}^2)$	$\sigma_{5-8.5}(10^{-7}\text{m}^4\text{kg}^{-2}\text{s}^2)$
0	38	41
0.5	32	34
1	21	23

Table 10 The computed values of the static stability from (3.37) and (3.38) with $U_5 = 31 \text{ ms}^{-1}$ and $L_x = 3000 \text{ km}$.

The results obtained in this way indicate that the use of a constant value of the static stability in the integrated forms (3.33) and (3.34) of the thermodynamic equation is not permitted, because every atmospheric flow pattern consists of baroclinic short waves and equivalent barotropic long waves, which are both important for short range numerical weather prediction.

A possible way to overcome this difficulty will be proposed now. It is based on modified forms of the equations (3.33) and (3.34), which are given below.

$$\int_{p_3}^{p_5} \left[\frac{\partial \psi}{\partial p} + J\left(\psi, \frac{\partial \psi}{\partial p}\right) + \frac{\sigma_{3-5}}{f_0} \omega \right] dp + \varepsilon_3 = - \int_{p_3}^{p_5} \frac{R \cdot Q}{c_p \cdot f_0 \cdot p} dp \quad (3.39)$$

and

$$\int_{p_5}^{p_{8.5}} \left[\frac{\partial \psi}{\partial p} + J\left(\psi, \frac{\partial \psi}{\partial p}\right) + \frac{\sigma_{5-8.5}}{f_0} \omega \right] dp + \varepsilon_{8.5} = - \int_{p_5}^{p_{8.5}} \frac{R \cdot Q}{c_p \cdot f_0 \cdot p} dp \quad (3.40)$$

ε_3 and $\varepsilon_{8.5}$ being corrections added to the equations, and defined as

$$\varepsilon_3 \equiv (A_3 - 1)\dot{\psi}_5 - \frac{\sigma_{3-5}}{f_0^2} \left[\int_{p_3}^{p_5} \int_0^p (A \cdot K - A^2) dp \right] dp \cdot \text{RVA} \quad (3.41)$$

and

$$\varepsilon_{8.5} \equiv (1 - A_{8.5})\dot{\psi}_5 - \frac{\sigma_{5-8.5}}{f_0^2} \left[\int_{p_5}^{p_{8.5}} \int_0^p (A \cdot K - A^2) dp \right] dp \cdot \text{RVA} \quad (3.42)$$

The tendency $\dot{\psi}_5$ at 500 mbar equals the one contained in the vorticity equation (3.30).

It can be shown that for $Q = 0$, all waves, which satisfy the definition of the reference atmosphere in 1, also satisfy equations (3.39) and (3.40). This follows from the substitution of (3.5) and (3.9) valid for the reference atmosphere, and of (3.41) and (3.42) into (3.39) and (3.40). So the long waves of the real atmosphere, which are equivalent barotropic, will meet the requirements of the integrated forms of the thermodynamic equation when the correction terms ε_3 and $\varepsilon_{8.5}$ are added.

ε_3 and $\varepsilon_{8.5}$ generally not being equal to zero, equations (3.39) and (3.40) are not identical with respectively (3.33) and (3.34). However, for the short baroclinic frontal waves, of which the behaviour of the thickness fields is defined by (3.33) and (3.34), ε_3 and $\varepsilon_{8.5}$ should have to equal zero. It can be shown that this is true if σ_{3-5} and $\sigma_{5-8.5}$ equal the mean values of the static stability belonging to saturated adiabatic lapse rates with temperatures from 10°C to 14°C at 1000 mbar. For that purpose it is assumed that the streamfunction ψ_5 at 500 mbar locally satisfies (3.15). As has been shown in 2.2, this is a reasonable approximation because of the elliptic shape of the RVA-areas. Using (3.30) with $K = 1$, ε_3 and $\varepsilon_{8.5}$ can be expressed, after some computational work, as

$$\begin{aligned} \varepsilon_3 = & -U_5 \psi_5^* \mu_x \left\{ (A_3 - 1) \left(1 - \frac{\beta \cdot L^*}{U_5} \right) \right. \\ & \left. + \frac{\sigma_{3-5}}{f_0^2 \cdot L^*} \left[\int_{p_3}^{p_5} \int_0^p (A - A^2) dp \right] dp \right\} \cos(\mu_y \cdot y) \cos(\mu_x \cdot x) \end{aligned} \quad (3.43)$$

and

$$\begin{aligned} \varepsilon_{8.5} = & -U_5 \psi_5^* \mu_x \left\{ (1 - A_{8.5}) \left(1 - \frac{\beta \cdot L^*}{U_5} \right) \right. \\ & \left. + \frac{\sigma_{5-8.5}}{f_0^2 \cdot L^*} \left[\int_{p_5}^{p_{8.5}} \int_0^p (A - A^2) dp \right] dp \right\} \cos(\mu_y \cdot y) \cos(\mu_x \cdot x) \end{aligned} \quad (3.44)$$

ε_3 and $\varepsilon_{8.5}$ are zero for all values of x and y if the terms between the braces of (3.43) and (3.44) are zero. So (3.37) and (3.38) must hold. The wavelengths following from these relations have already been computed and given in table 9. These do have the required low values.

It can be concluded that equations (3.39) and (3.40) are consistent with the equivalent barotropic long waves and the baroclinic short waves, having saturated adiabatic lapse rates with temperatures from 10°C to 14°C at 1000 mbar. These equations are used for the baroclinic model in Chapter IV. Since it has been shown that (3.37) and (3.38) are fairly realistic relations between wavelengths and static stabilities, it is possible to use these relations for the specification of the static stabilities in (3.39) and (3.40). For those computations one has to make a choice of L^* . This procedure offers the possibility by varying the quantity L^* or L_x (after a choice of L_x/L_y) to change the values of the static stability in the equations of the baroclinic model.

For the baroclinic model, the values for the polar jetstream in table 4 are taken to compute the static stability. It follows from table 9 that for $L_x \approx 1600$ km and for $L_x/L_y \approx 0.5$, σ_{3-5} and $\sigma_{5-8.5}$ agree with respectively saturated potential temperatures of 10°C for the layer 500–850 mbar and of 14°C for the layer 300–500 mbar. This choice of L_x and L_x/L_y implies a stable thermal stratification of the troposphere between 300 and 850 mbar. It is interesting to mention that the mean saturated potential temperature of the layer 300–500 mbar of the ICAO standard atmosphere is 14°C and that of the layer 500–850 mbar 12°C.

In the next section the relation between the RVA at 500 mbar and the frontal waves at sea level is outlined. It will then be shown that the computed wavelengths of table 9, belonging to the saturated adiabatic lapse rates and which agree with the mean wavelength of the RVA on 25-3-71, 00 GMT also agree with the mean wavelength of the most frequently occurring frontal waves at sea level.

For the baroclinic model the integrals in (3.39) and (3.40) must be evaluated. Therefore knowledge of ω as a function of pressure p is necessary. Because ω is evaluated with the aid of the continuity equation (3.3) knowledge of the horizontal divergence D is also necessary. For the equivalent barotropic long waves the profile in the vertical of D is known and is given by (3.6). However, for the baroclinic short frontal waves the profile of D has to be further investigated. This investigation is carried out in 3.5 with the aid of a simple two-parameter model.

3.4 *Relation between the advection of relative vorticity at 500 mbar and the frontal waves at sea level*

Frontal waves at sea level are connected with cyclonic development near the fronts. Development at sea level was investigated by SUTCLIFFE (1939, 1947) and SUTCLIFFE and FORSDYKE (1950). They found a relationship between the isobaric divergence at 1000

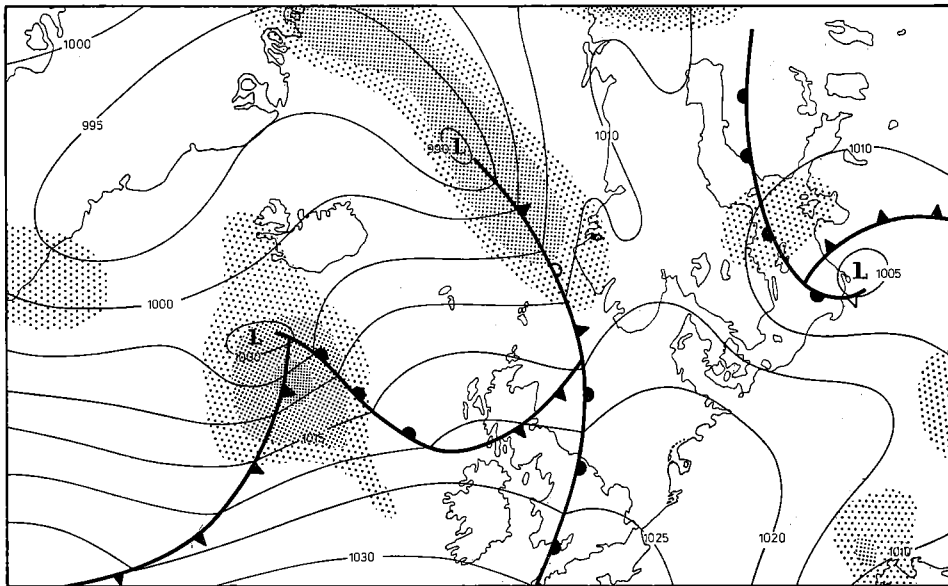
mbar and the advection of thermal vorticity connected with the thermal wind between 1000 and 500 mbar. PETERSSSEN (1955) reviewed and extended SUTCLIFFE's theory of development with particular reference to cyclonic development. It was suggested that cyclogenesis resulted from the release of some kind of instability by finite perturbations, which could be identified with the wave-shaped motion patterns in the middle and upper troposphere. PETERSSSEN, DUNN and MEANS (1955) tested the following working hypothesis: 'Cyclonic development at sea level occurs when and where an area of positive vorticity advection in the upper troposphere becomes superimposed upon a frontal zone at sea level'. They found this hypothesis to be useful for prediction purposes.

Recently, DUSHAN (1973) investigated the SUTCLIFFE-PETERSSSEN development theory for two cases over the Eastern United States. He found that advection of vorticity at the level of non-divergence exerts the dominant influence for initial cyclonic development and that the thermal terms (advection of thickness, stability and diabatic influence) become only important after the development has begun.

The studies mentioned show the importance of the advection of positive vorticity in the higher levels of the troposphere for the development (production of positive vorticity) at sea level. Investigations of charts of advection of relative vorticity at 500 mbar and of pressure charts at sea level with analyzed fronts clearly show that the following relationships exist: *centres of young frontal waves (wave tops) tend to coincide with the centres of positive RVA-areas during the early stages of development. During the development the RVA-value increases. After the start of the occlusion process the RVA-centre tends to coincide with the occlusion point at sea level and the RVA-value reaches a maximum. At the decaying stage of the cyclone the value decreases.* A picture of the characteristic relationship between the positive RVA at 500 mbar and the developing frontal wave at sea level is given in figure 11.

A practical method to define the fronts at sea level with the aid of the RVA-charts computed from the numerical forecasts of the 500 mbar heights was developed by BIJVOET at the Royal Netherlands Meteorological Institute. Since 1968, these charts, based on the numerical 500 mbar prognoses of NMC-Washington D.C., have been used by the medium-range forecast section for the forecasts up to three days ahead.

An example of the above-mentioned relations is given in the figures 12a-12e, which show a series of surface pressure analyses with fronts and isolines of computed RVA. The subsequent analyses are given with intervals of one day. Especially interesting is the wave centred at 45°N and 43°W at 16-3-71, 00 GMT (fig. 12a). The following positions of this system are 47°N and 23°W (fig. 12b), 49°N and 9°W (fig. 12c), 52°N and 5°W (fig. 12d) and 50°N and 2°W (fig. 12e). First one sees the developing RVA in relation with the developing wave (fig. 12a, b, c) and then the fast decrease in relation with the decay at sea level of the wave (fig. 12d, e). The relation described above does not seem to be fully satisfied in this case. The fact that the surface analyses

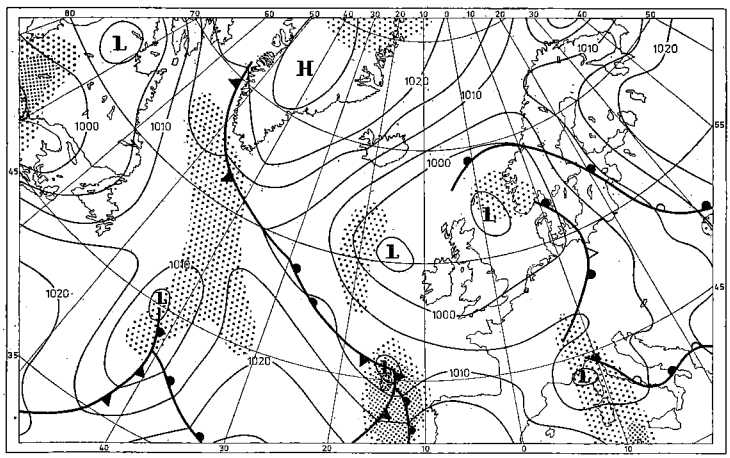


Units of the RVA: \dots $0.6-1.2 \times 10^{-9} \text{ s}^{-2}$ \times $1.2-2.4 \times 10^{-9} \text{ s}^{-2}$ \blacksquare $> 2.4 \times 10^{-9} \text{ s}^{-2}$

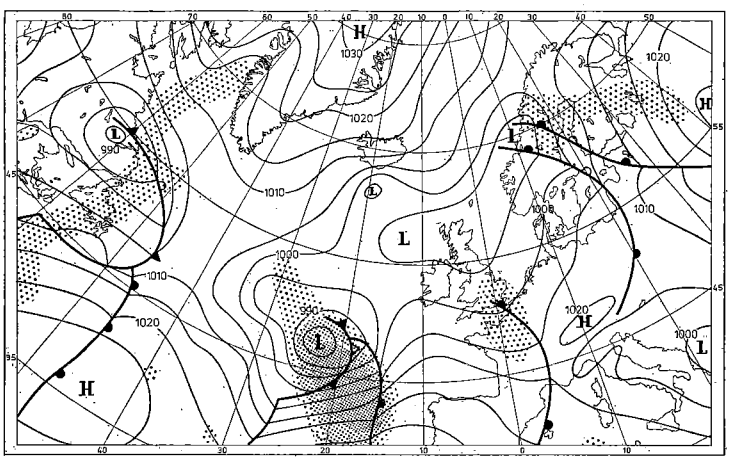
Fig. 11 Sea level pressure analysis and the advection of positive relative vorticity (RVA > 0) at 500 mbar, valid for 19 July 1974, 12 GMT. Isobars are labelled in mbar.

were handmade and the RVA-values were computed from objective 500 mbar analyses with the aid of sparsely available upper-air observations over the Atlantic can be the cause of a certain inconsistency between the RVA-pattern and the development at sea level.

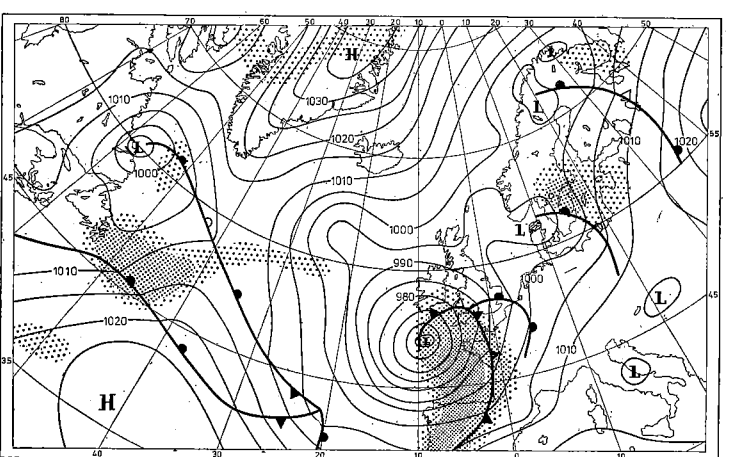
The relatively close relation between the RVA-pattern at 500 mbar and the frontal waves clearly shows that the mean wavelength of the RVA-areas and the wavelengths of the developing disturbances at sea level must be of the same order. DODDS (1971) investigated the behaviour of depressions at sea level and in doing so, he selected those for the years 1965, 1966 and 1967. These depressions had reached their minimum central pressure in an area bounded by the latitudes 40°N and 65°N and the longitudes 40°W and 40°E . The total number of depressions was 288 for these three years. Table 11 shows the frequency of depressions as a function of the diameter at the time of minimum central pressure. The diameter of each depression was defined by DODDS in measuring the length of the linesegment (through the centre in west-east direction) between the two intersection points with the outermost closed isobar. The wavelength of each system can be regarded as roughly twice its diameter.



a



b



c

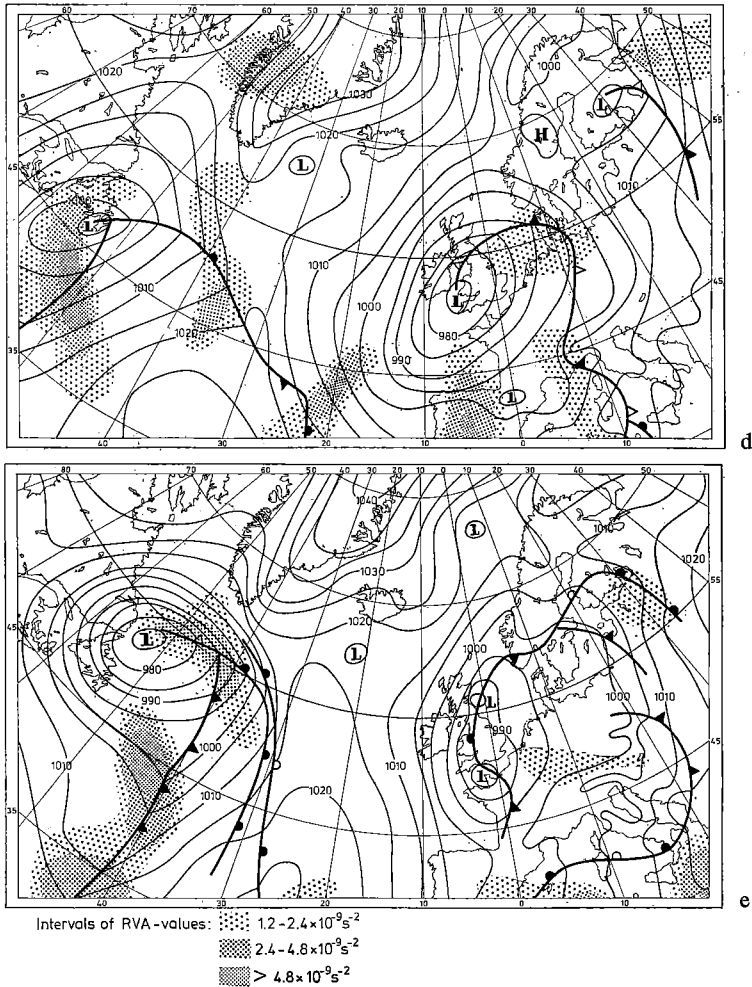


Fig. 12 Analysis of sea level pressure and advection of positive relative vorticity ($\text{RVA} > 0$) at 500 mbar for a period of 5 days.

- a. Valid for 16 March 1971, 00 GMT
- b. Valid for 17 March 1971, 00 GMT
- c. Valid for 18 March 1971, 00 GMT
- d. Valid for 19 March 1971, 00 GMT
- e. Valid for 20 March 1971, 00 GMT.

diameter km	frequency %	diameter km	frequency %	diameter km	frequency %
300	< 1	1500	9	2700	3
500	5	1700	9	2900	2
700	10	1900	6	3100	< 1
900	18	2100	4	3300	1
1100	13	2300	3	3500	1
1300	12	2500	3	3700	1

Table 11 Frequency of depressions at sea level as a function of the mean diameter measured at the time of minimum central pressure after DODDS (1971).

As the depressions DODDS investigated were short waves as well as long waves, the mean wavelength being ~ 2800 km was not a good measure to compare with the dimensions of the RVA-areas. Table 11 shows that the frequency of the long waves is small compared with that of the short waves. Therefore the wavelengths of the depressions with the greatest frequency are a better estimate. These wavelengths vary from 1600 to 2000 km. The mean wavelength of RVA-areas, which appeared to be about 1600 km at 25-3-'71, 00 GMT (see table 4 in 2.2), and the wavelengths of table 9 agree fairly well with those of the greatest frequency at sea level. However, to avoid difficulties in defining shallow depressions and in specifying depressions within systems having more than one centre, DODDS ignored depressions with fewer than three closed isobars drawn at 4 mbar intervals at the times the systems had reached their minimum central pressures. Therefore, an underestimate of the frequency of the short waves seems to be possible.

3.5 *Divergence D and ω of young developing frontal waves and a comparison with those of the reference atmosphere*

In this section the divergence D and the vertical velocity ω of young developing frontal waves are examined, with the aid of a simple two-parameter model. The two chosen parameters are the heights of the 500 mbar and the 1000 mbar levels, with the additional assumption that the heights of all pressure levels in the troposphere satisfy

$$z = z_{10} + C_1(p) \cdot (z_5 - z_{10}) + C_2(p) \quad (3.45)$$

with $C_1(p_5) = 1$ and $C_1(p_{10}) = C_2(p_5) = C_2(p_{10}) = 0$

z_5 and z_{10} are the heights of the 500 mbar and the 1000 mbar levels respectively. These are in principle mutually independent, so that the above assumption is an extension of (3.1) valid for the reference atmosphere. The functions C_1 and C_2 are

defined by the assumption that the reference atmosphere has to be a special case of (3.45). So, after the substitution of (3.1) into the left and right hand sides of (3.45) the following two relations result.

$$C_1 = (A - A_{10})/(1 - A_{10}) \quad \text{and} \quad C_2 = B + (C_1 - 1)B_{10} \quad (3.46)$$

with $A_{10} \equiv A$ at 1000 mbar and $B_{10} \equiv B$ at 1000 mbar.

z_{10} is split up into one part based on the reference atmosphere and another on the departure z^* from it.

$$z_{10} = A \cdot z_5 + B_{10} + z^* \quad (3.47)$$

Substituting this formula into (3.45) and making use of the results of (3.46) then gives

$$z = A \cdot z_5 + C^* \cdot z^* + B \quad \text{with} \quad C^* \equiv (1 - A)/(1 - A_{10}) \quad (3.48)$$

or, using the definition of the quasi-geostrophic streamfunction

$$\psi = A \cdot \psi_5 + C^* \cdot \psi^* + \frac{g \cdot B}{f_0} \quad \text{with} \quad \psi^* \equiv \frac{g \cdot z^*}{f_0} \quad (3.49)$$

For the considerations given in this section it is again assumed that the values of A for 25-3-71, 00 GMT are sufficiently representative to be used for the calculations.

It can be seen from figure 6 that $\omega = 0$ at $p = p_2$ and $p = p_{10}$ for the reference atmosphere. Therefore, the boundary condition $\omega = 0$ is applied at the levels p_2 and p_{10} .

Below 300 mbar the A -profile is to a high degree linear as follows from figure 4. In order to simplify the following computations it is assumed that A is exactly linear between p_2 and p_{10} . This assumption introduces an error between p_2 and p_3 , but this has no great influence on the computed values of the horizontal divergence D and the vertical velocity ω , as will be shown later on. Using the value of $A_{10} = 0.2$ from table 2, A can be expressed as

$$A = -1.6 p/p_{10} + 1.8 \quad (3.50)$$

After some computational work it follows that

$$\int_{p_2}^{p_{10}} A dp \approx \int_{p_2}^{p_{10}} A^2 dp \quad (3.51)$$

This result is not surprising, because it can easily be shown for each atmosphere satisfying (3.1), (3.2) and (3.3) with the conditions $\omega = 0$ at 200 mbar and 1000 mbar and $D = 0$ at 500 mbar, that (3.51) is exactly valid.

To get the equations of the two-parameter model, the vorticity equation, the continuity equation and the thermodynamic equation are used. The first equation is obtained by integrating the vorticity equation (3.2) over the whole troposphere from p_2 to p_{10} and using the continuity equation (3.3) together with the boundary conditions $\omega = 0$ at p_2 and p_{10} . This results in

$$\int_{p_2}^{p_{10}} [\nabla^2 \psi + J(\psi, \nabla^2 \psi + f)] dp = 0 \quad (3.52)$$

The second equation is given by the integrated continuity equation (3.3). Using the condition that $\omega = 0$ at p_{10} , it becomes

$$\omega = \int_p^{p_{10}} D dp \quad (3.53)$$

The third equation is the vorticity equation (3.2) itself. A fourth equation is needed, because there are four unknown quantities, namely ψ_s , ψ^* , D and ω . Because the short waves are of interest here and as for these waves the thermodynamic equation has to be used for the description of the dynamics of the thermal fields, one of the integrated forms of this equation can be used.

Developing young frontal waves at sea level are in many cases accompanied by precipitation at intensities of 1mm/hour or more, so the release of latent heat has to be taken into account, as was shown by the scale analysis of PHILLIPS (1963). The very important role of the release of latent heat for development at sea level was also confirmed by the investigations of DANARD (1964, 1966).

Much of the release of latent heat takes place in the lower troposphere, i.e. below 500 mbar, but above the boundary layer, so that the integrated form (3.34) can be applied. The heat term Q serves to include the release of latent heat.

Now 4 constants are defined as follows:

$$K_1 \equiv 1 - A_{10}, \quad K_2 \equiv \int_{p_2}^{p_{10}} C^* dp / \int_{p_2}^{p_{10}} A dp, \quad K_3 \equiv \int_{p_2}^{p_{10}} (C^*)^2 dp / \int_{p_2}^{p_{10}} A dp$$

and $K_4 \equiv 1 - A_{8,5}$ (3.54)

With the aid of (3.49), (3.51) and (3.54), equation (3.52) become

$$\nabla^2 \psi_5 + J(\psi_5, \nabla^2 \psi_5 + f) = -K_2[\nabla^2 \psi^* + J(\psi^*, f)] - K_3 \cdot J(\psi^*, \nabla^2 \psi^*) \quad (3.55)$$

Substituting (3.49) into the vorticity equation (3.2) and using (3.55), (3.2) can be written as

$$\begin{aligned} f_0 D = & (A - A^2) J(\psi_5, \nabla^2 \psi_5) + (A \cdot K_2 - C^*)[\nabla^2 \psi^* + J(\psi^*, f)] + \\ & + [A \cdot K_3 - (C^*)^2] J(\psi^*, \nabla^2 \psi^*) - A \cdot C^* [J(\psi_5, \nabla^2 \psi^*) + \\ & + J(\psi^*, \nabla^2 \psi_5)] \end{aligned} \quad (3.56)$$

With the aid of (3.49), (3.54) and after applying the Laplacian operator, the equation (3.34) becomes

$$-K_4 \nabla^2 \psi_5 + \frac{K_4}{K_1} \nabla^2 [\psi^* + J(\psi_5, \psi^*)] + \nabla^2 \int_{ps}^{ps.5} \left(\frac{\sigma \cdot \omega}{f_0} + \frac{R \cdot Q}{c_p \cdot f_0 \cdot p} \right) dp = 0 \quad (3.57)$$

Of special interest are the divergence D and ω in the centre of the perturbation ψ^* where $\frac{\partial \psi^*}{\partial x} = 0$ and $\frac{\partial \psi^*}{\partial y} = 0$. For that point it is assumed that the relative vorticity of ψ^* is maximum, so that $\frac{\partial}{\partial x} (\nabla^2 \psi^*) = \frac{\partial}{\partial y} (\nabla^2 \psi^*) = 0$. So for the centre of the perturbation the equations (3.55) and (3.56) become fairly simple, namely

$$\nabla^2 \psi_5 + J(\psi_5, \nabla^2 \psi_5 + f) = -K_2 \nabla^2 \psi^* \quad (3.58)$$

and

$$f_0 D = (A - A^2) J(\psi_5, \nabla^2 \psi_5) + (A \cdot K_2 - C^*) \nabla^2 \psi^* \quad (3.59)$$

For a further simplification of (3.57) it is assumed that $\nabla^2 [J(\psi_5, \psi^*)] \approx 0$ in the centre of the perturbation. In general this is a reasonable assumption. It is exactly true, if ψ_5 satisfies (3.15) in the vicinity of the disturbance and ψ^* is assumed to equal

$$\psi^* = \psi_{10}^* \cos(\mu_y \cdot y) \sin(\mu_x \cdot x + \varphi) \quad (3.60)$$

Equation (3.57) reduces to

$$-K_4 \nabla^2 \psi_5 + \frac{K_4}{K_1} \nabla^2 \psi^* + \nabla^2 \int_{ps}^{ps.5} \left(\frac{\sigma \cdot \omega}{f_0} + \frac{R \cdot Q}{c_p \cdot f_0 \cdot p} \right) dp = 0 \quad (3.61)$$

In young developing frontal disturbances, which are not yet occluded, release of

latent heat generally takes place. For such disturbances it may be assumed that this release of latent heat occurs in the whole column of air between 500 and 850 mbar in the vicinity of the disturbance at sea level, and that the lapse rate equals the saturated adiabatic one. It can be shown that for such conditions the following relation holds (see for instance HALTINER (1971))

$$\sigma \cdot \omega = - \frac{R \cdot Q}{c_p \cdot p} \quad (3.62)$$

With this relation, (3.61) becomes

$$-\nabla^2 \psi_5 + \frac{1}{K_1} \nabla^2 \psi^* = 0 \quad (3.63)$$

(3.58), (3.59) and (3.63) are the set of equations for the centre of the young developing wave. (3.63) combined with (3.58) results in

$$\nabla^2 \psi^* = - \frac{K_1}{1 + K_1 \cdot K_2} J(\psi_5, \nabla^2 \psi_5 + f) \quad (3.64)$$

so that *the development of the perturbation at sea level is proportional to the advection of absolute vorticity at 500 mbar.*

The combination of (3.64) and (3.59) gives for the horizontal divergence D

$$f_0 D = (A - A^2) J(\psi_5, \nabla^2 \psi_5) + (C^* - A \cdot K_2) \frac{K_1}{1 + K_1 \cdot K_2} J(\psi_5, \nabla^2 \psi_5 + f) \quad (3.65)$$

so that the divergence is composed of two parts. *The first term on the right hand side of (3.65) refers to the reference atmosphere, as one can see by comparing it with (3.6).* The second part is the departure from the divergence of the reference atmosphere. It is shown below that this departure is caused by the release of latent heat. For that purpose it is investigated what the expression for D would become if $Q = 0$. It is supposed that $\sigma = \sigma_{5-8.5}$ and that relation (3.38) holds. After the substitution of (3.59) into (3.53) and of (3.53) into (3.61), equations (3.58) and (3.61) contain two unknown quantities, namely $\nabla^2 \psi_5$ and $\nabla^2 \psi^*$. Assuming that ψ_5 satisfies (3.15) and using relation (3.38), it follows that $\nabla^2 \psi^* = 0$ for the waves having the wavelengths of table 9. As one can see from (3.59) only the part of D which is related to the reference atmosphere is maintained. *This proves that the second term on the right hand side of (3.65) is connected with the release of latent heat.*

For waves having wavelengths of about 1000–3000 km it can easily be shown with

the aid of (3.15) that $J(\psi_5, f) \ll J(\psi_5, \nabla^2 \psi_5)$, so that the influence of the coriolis parameter f can be neglected in (3.65). Using now the definition of RVA as given by (3.8), equation (3.65) becomes

$$f_o D = - \left[(A - A^2) + (C^* - A \cdot K_2) \frac{K_1}{1 + K_1 \cdot K_2} \right] \cdot \text{RVA} \quad (3.66)$$

It follows from the integrated continuity equation (3.53) that ω is given by

$$f_o \omega = - \left[\int_p^{p_{10}} (A - A^2) dp + \frac{K_1}{1 + K_1 \cdot K_2} \int_p^{p_{10}} (C^* - A \cdot K_2) dp \right] \cdot \text{RVA} \quad (3.67)$$

Because $A(p)$ is taken to be a linear function of p , it follows from (3.48) that C is a linear function of p as well. Using the value $A_{10} = 0.2$, the constants K_1 and K_2 can easily be computed from (3.54) and are found to be $K_1 = 0.8$ and $K_2 = 0.2/0.84$. With these values (3.66) and (3.67) can be calculated further, resulting in

$$f_o D = - [(A - A^2) + (0.672C^* - 0.160A)] \cdot \text{RVA} \quad (3.68)$$

and

$$f_o \omega = - \left[\int_p^{p_{10}} (A - A^2) dp + \int_p^{p_{10}} (0.672C^* - 0.160A) dp \right] \cdot \text{RVA} \quad (3.69)$$

D and ω both consist of 'dry' parts and 'moist' parts. The dry parts of D and ω , which are those according to the reference atmosphere, are given by

$$f_o \cdot D_d = D'_d \cdot \text{RVA} \quad \text{and} \quad f_o \cdot \omega_d = \omega'_d \cdot \text{RVA} \quad \text{with}$$

$$D'_d \equiv -(A - A^2) \quad \text{and} \quad \omega'_d \equiv \int_p^{p_{10}} D'_d dp \quad (3.70)$$

The moist parts, which are caused by the release of latent heat, are defined as

$$f_o \cdot D_m = D'_m \cdot \text{RVA} \quad \text{and} \quad f_o \cdot \omega_m = \omega'_m \cdot \text{RVA} \quad \text{with}$$

$$D'_m \equiv -(0.672C^* - 0.160A) \quad \text{and} \quad \omega'_m \equiv \int_p^{p_{10}} D'_m dp \quad (3.71)$$

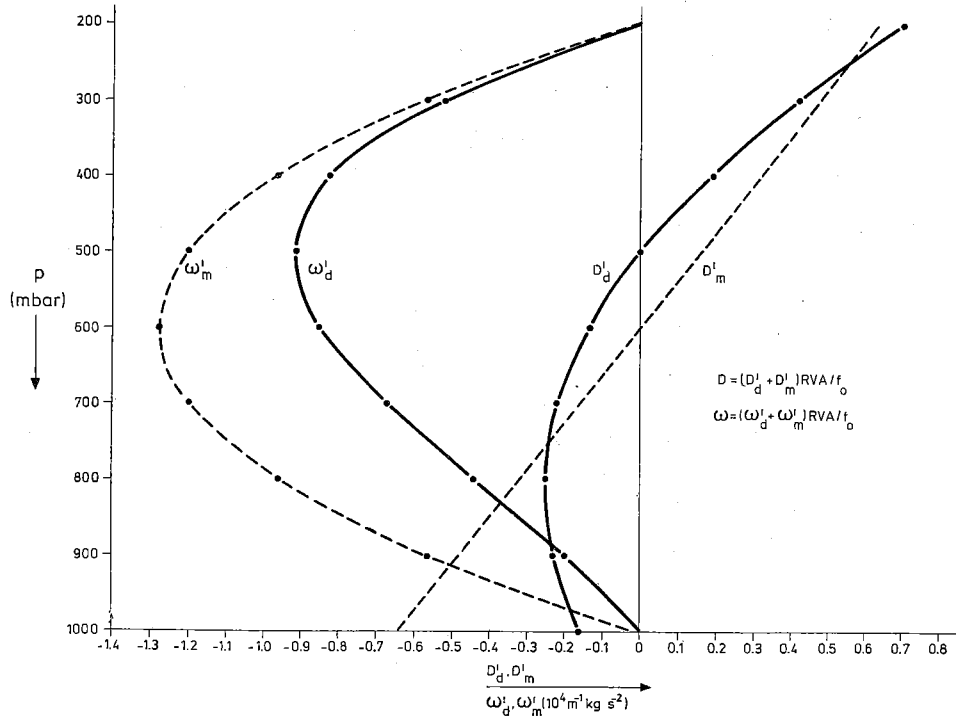


Fig. 13 The profiles of the horizontal divergences D'_d and D'_m and the vertical velocities ω'_d and ω'_m for the centre at sea level of a young developing short frontal wave according to the two-parameter model developed in III 3.5. The subscripts d and m refer to the 'dry' and to the 'moist' parts, respectively.

Numerical values for several pressure levels are given in table 12 and the profiles as a function of the pressure are given in figure 13. This figure clearly shows that the profile of D'_m is linear. This is a result of the fact that in the troposphere the function A was supposed to be linear, so that according to (3.71) and (3.48) D'_m is also linear. It can be seen in table 12 and figure 13 that the level of non-divergence where $D'_d + D'_m = 0$ is found at about 550 mbar. This is somewhat lower than the level of non-divergence in the reference atmosphere, which was found at about 500 mbar.

In view of the various assumptions made in the theory described above, a verification is necessary by which the theoretical results are compared with real observations. For that purpose D and ω computed from (3.70) and (3.71) are compared with some observed values. The way in which D is determined must be independent of the theory, so that only D determined from real wind observations, and ω determined

p	A	C^*	D'_d	D'_m	ω_d	ω'_m	$D' = D'_d + D'_m$	$\omega' = \omega'_d + \omega'_m$
mbar					$10^4 \text{m}^{-1} \text{kg s}^{-2}$	$10^4 \text{m}^{-1} \text{kg s}^{-2}$		
200	1.48	-0.60	+0.71	+0.64	0	0	+1.35	0
300	1.32	-0.40	+0.42	+0.48	-0.52	-0.56	+0.90	-1.08
400	1.16	-0.20	+0.19	+0.32	-0.82	-0.96	+0.51	-1.78
500	1	0	0	+0.16	-0.91	-1.20	+0.16	-2.11
600	0.84	+0.20	-0.13	0	-0.85	-1.28	-0.13	-2.13
700	0.68	+0.40	-0.22	-0.16	-0.67	-1.20	-0.38	-1.87
800	0.52	+0.60	-0.25	-0.32	-0.44	-0.96	-0.57	-1.40
900	0.36	+0.80	-0.23	-0.48	-0.20	-0.56	-0.71	-0.76
1000	0.20	+1.00	-0.16	-0.64	0	0	-0.80	0

Table 12 Numerical values of the 'dry' and 'moist' parts of the divergence and ω as a function of the pressure for the perturbation ψ^* at sea level.

from the integrated continuity equation are suitable. Case studies that can be used for this purpose are rare however, due to the fact that the horizontal wind is nearly non-divergent, so that relatively large errors in the computations of D can be expected. Only cases with strong development show horizontal divergences large enough to be computed with a certain accuracy from real wind observations. Three such case studies could be selected, namely the one by PALMÉN (1958), by PALMÉN and HOLOPAINEN (1962) and by DANARD (1964). All three studies satisfied the necessary criteria, namely that a non-occluded disturbance was present and that the development at sea level was large enough to be certain that the centre of the perturbation z^* of (3.47) almost coincided with the centre of z_{10} . With the aid of the 500 mbar analyses, RVA was computed by finite difference approximations in the point above the centre at sea level. Then, from (3.70) and (3.71), D and ω could be computed for specified pressure levels and compared with the real values. The computed RVA values from the studies by PALMÉN, PALMÉN and HOLOPAINEN and DANARD were $5.8 \times 10^{-9} \text{s}^{-2}$, $1.4 \times 10^{-9} \text{s}^{-2}$ and $3.2 \times 10^{-9} \text{s}^{-2}$ respectively. The comparisons between the results from the case studies and the present computations are given in the tables 13, 14 and 15. Table 15 also contains a comparison of the moist parts of ω at 600 mbar, as DANARD computed it for the layer between 500 and 700 mbar.

Tables 13, 14 and 15 clearly show that a good agreement exists between the values of D and ω , which were defined with the aid of real wind observations, and the computed ones. The neglect of surface friction can possibly account for the fact that the absolute value of the computed divergence at 1000 mbar is smaller than the observed divergence.

Table 12 shows that in the troposphere the dry and moist parts of ω are of the same order of magnitude and that the largest value of ω_m is found at 600 mbar. These results are in excellent agreement with the conclusions of DANARD (1964).

p mbar	D computed with (3.68) 10^{-5}s^{-1}	D according to PALMÉN 10^{-5}s^{-1}	ω computed with (3.69) $10^{-1}\text{m}^{-1}\text{kg s}^{-3}$	ω according to PALMÉN $10^{-1}\text{m}^{-1}\text{kg s}^{-3}$
300	+5.2	+4	-6.3	-1.1
400	+3.0	+4	-10.3	-5.3
500	+0.9	+3	-12.2	-9.3
600	-0.8	+1	-12.4	-11.5
700	-2.2	-1	-10.8	-11.7
800	-3.3	-3	-8.1	-9.2
900	-4.1	-5	-4.4	-6.5
1000	-4.6	-7	0	0

Table 13 Comparison of the computed D 's and ω 's with those according to PALMÉN (1958).

p mbar	D computed with (3.68) 10^{-5}s^{-1}	D according to PALMÉN and HOLOPAINEN 10^{-5}s^{-1}	ω computed with (3.69) $10^{-1}\text{m}^{-1}\text{kg s}^{-3}$	ω according to PALMÉN and HOLOPAINEN $10^{-1}\text{m}^{-1}\text{kg s}^{-3}$
200	+1.9	+1.8	0	-2.7
300	+1.3	+1.3	-1.5	-4.2
400	+0.7	+0.2	-2.5	-5.1
500	+0.2	-0.8	-3.0	-4.8
600	-0.2	-1.1	-3.0	-3.8
700	-0.5	-0.2	-2.6	-3.2
800	-0.8	-1.0	-2.0	-2.7
900	-1.0	-1.1	-1.1	-1.7
1000	-1.1	-2.1	0	0

Table 14 Comparison of the computed D 's and ω 's with those according to PALMÉN and HOLOPAINEN (1962).

p mbar	ω computed with (3.69) $10^{-1}\text{m}^{-1}\text{kg s}^{-3}$	ω according to DANARD $10^{-1}\text{m}^{-1}\text{kg s}^{-3}$	moist part of ω computed $10^{-1}\text{m}^{-1}\text{kg s}^{-3}$	moist part of ω according to DANARD $10^{-1}\text{m}^{-1}\text{kg s}^{-3}$
200	0	-3	0	—
400	-5.7	-6	-3.1	—
600	-6.8	-7	-4.1	-5
800	-4.5	-4	-3.1	—

Table 15 Comparison of the computed ω 's with those according to DANARD (1964).

The results of table 12 further indicate that the upward velocities in areas with precipitation where $\omega = \omega_d + \omega_m$ are in general more than twice as large as those in areas without precipitation, where $\omega = \omega_d$. PALMÉN (1958) and PALMÉN and HOLOPAINEN (1962) obtained the same results.

Finally, one can conclude that in the centre at sea level of a young developing frontal wave the vertical profiles of D and ω consist of two parts, namely one part which equals that of the reference atmosphere, and a second part caused by the release of latent heat. These results are used to evaluate the integrals of ω in (3.39) and (3.40) and these evaluations are carried out in Chapter IV.

4 Stability analysis of the quasi-geostrophic equations

4.1 General theory

The basic equations used in the stability analysis are the quasi-geostrophic vorticity equation (2.10), the continuity equation (2.13) and the thermodynamic equation (2.14). The boundary conditions are $\omega = 0$ at $p = p_u$ and p_l . p_u is the pressure at the upper boundary level and p_l that at the lower boundary level. As will be shown in 4.2, the release of latent heat is taken into account by replacing the static stability σ by a new value, which is much lower than the original one. Therefore, in carrying out the following computations, it can be assumed for simplicity's sake that $Q = 0$. The static stability σ is taken constant for the layer between p_u and p_l . Table 6 in 3.3 shows that this is a sufficient approximation for an atmosphere with a saturated adiabatic lapse rate.

To carry out the stability analysis a rectangular frame is chosen with the x -axis along the west-to-east direction and the y -axis pointing from south to north. The origin is taken at 45°N . The quasi-geostrophic streamfunction ψ is split up in the following way:

$$\psi = \bar{\psi} + \psi' \quad (3.72)$$

where $\bar{\psi}$ is the zonal mean of ψ . It is assumed that the local time-dependency of $\bar{\psi}$ is small compared with that of ψ' , so that $\bar{\psi} \ll \psi'$.

For the sake of simplicity it is also assumed that $\bar{\psi}$ depends linearly on y and p , so that the geostrophic wind $U \equiv -\frac{\partial\bar{\psi}}{\partial y}$ of the basic zonal flow is independent of y

and $\frac{dU}{dp}$ is independent of p .

With the aid of (3.72) and (2.13) the equations (2.10) and (2.14) with $Q = 0$ can be written as

$$\nabla^2\psi' + J(\bar{\psi}, \nabla^2\psi') + J(\psi', f) + J^*(\psi', \nabla^2\psi') = f_0 \frac{\partial\omega}{\partial p} \quad (3.73)$$

and

$$\frac{\partial \psi'}{\partial p} + J\left(\bar{\psi}, \frac{\partial \psi'}{\partial p}\right) + J\left(\psi', \frac{\partial \bar{\psi}}{\partial p}\right) + J^*\left(\psi', \frac{\partial \psi'}{\partial p}\right) = -\frac{\sigma}{f_0} \omega \quad (3.74)$$

The non-linear advection terms marked with the symbol * can be neglected if the amplitude of the perturbation ψ' is small enough. This is generally true in the early stage of development. The influence of the Rossby parameter $\beta \equiv \frac{df}{dy}$ can be neglected for waves with wavelengths smaller than roughly 3000 km. So for waves with small amplitudes and wavelengths $\leq \sim 3000$ km, equations (3.73) and (3.74) become

$$\nabla^2 \psi' + U \frac{\partial}{\partial x} (\nabla^2 \psi') = f_0 \frac{\partial \omega}{\partial p} \quad (3.75)$$

and

$$\frac{\partial \dot{\psi}'}{\partial p} + U \frac{\partial}{\partial x} \left(\frac{\partial \psi'}{\partial p} \right) - \frac{dU}{dp} \frac{\partial \psi'}{\partial x} = -\frac{\sigma}{f_0} \omega \quad (3.76)$$

These linear equations are used to carry out the stability analysis. This is done in the way EADY (1949) suggested. However, EADY used the primitive equations formulated in the x, y, z coordinate system. To obtain solutions showing real features of synoptic systems, he had to make assumptions which were in agreement with the geostrophic approximations.

In 3.1 it was concluded that the height fields and the thermal fields of the long and short waves move with nearly the same speeds, show the same developments and have a phase shift between the two patterns, which is nearly constant with respect to time. Therefore, possible wave solutions of (3.75) and (3.76) of the following form are sought:

$$\psi' = \psi^* \cos(\mu_y \cdot y) e^{i\mu_x(x-ct)} \quad (3.77)$$

and

$$\omega = \omega^* \cos(\mu_y \cdot y) e^{i\mu_x(x-ct)} \quad (3.78)$$

ψ^* and ω^* depend only on p and may be real or complex. The wave velocity c is independent of x, y, p and t and may also be real or complex. Such wave solutions satisfy the above-mentioned requirements with respect to the height and thermal fields. As is shown later on, in the case of complex values, the waves are subject to a phase shift in the vertical.

Substitutions of (3.77) and (3.78) into (3.75) and (3.76) lead to

$$i\mu_x(\mu_x^2 + \mu_y^2)(c - U)\psi^* = f_0 \frac{d\omega^*}{dp} \quad (3.79)$$

and

$$i\mu_x \left[(c - U) \frac{d\psi^*}{dp} + \frac{dU}{dp} \psi^* \right] = \frac{\sigma}{f_0} \omega^* \quad (3.80)$$

Now (3.79) is multiplied with $\frac{\sigma}{f_0^2}$ and (3.80) is differentiated with respect to p .

Keeping in mind that $\frac{d^2U}{dp^2} = 0$, one gets the following ordinary second-order differential equation

$$\frac{d^2\psi^*}{dp^2} - \lambda^2\psi^* = 0 \quad \text{with} \quad \lambda^2 \equiv \frac{\sigma}{f_0^2} (\mu_x^2 + \mu_y^2) \quad (3.81)$$

The general solution of this equation reads

$$\psi^* = \psi_1^* e^{\lambda \cdot p} + \psi_2^* e^{-\lambda \cdot p} \quad (3.82)$$

The coefficients ψ_1^* and ψ_2^* are specified by the use of the boundary condition $\omega^* = 0$ at $p = p_u$ and $p = p_1$, which by substitution into (3.80) leads to

$$\left(c - U_1 + \frac{1}{\lambda} \frac{dU}{dp} \right) e^{+\lambda \cdot p_1} \psi_1^* - \left(c - U_1 - \frac{1}{\lambda} \frac{dU}{dp} \right) e^{-\lambda \cdot p_1} \psi_2^* = 0 \quad (3.83)$$

and

$$\left(c - U_u + \frac{1}{\lambda} \frac{dU}{dp} \right) e^{+\lambda \cdot p_u} \psi_1^* - \left(c - U_u - \frac{1}{\lambda} \frac{dU}{dp} \right) e^{-\lambda \cdot p_u} \psi_2^* = 0 \quad (3.84)$$

with

$$U = U_1 \text{ at } p_1 \text{ and } U = U_u \text{ at } p_u.$$

This set of equations only has a non-trivial solution if the determinant is equal to zero. Thus

$$\begin{aligned} & \left(c - U_1 + \frac{1}{\lambda} \frac{dU}{dp} \right) \left(c - U_u - \frac{1}{\lambda} \frac{dU}{dp} \right) e^{2\alpha} - \\ & - \left(c - U_1 - \frac{1}{\lambda} \frac{dU}{dp} \right) \left(c - U_u + \frac{1}{\lambda} \frac{dU}{dp} \right) = 0 \end{aligned} \quad (3.85)$$

with $\alpha \equiv \lambda(p_1 - p_u)$.

This is a quadratic equation in the velocity c , which can be rewritten as

$$c^2 - (U_u + U_l)c + U_u U_l - \left(\frac{1}{\lambda} \frac{dU}{dp} \right)^2 - \frac{1}{\lambda} \frac{dU}{dp} (U_u - U_l) \coth(\alpha) = 0 \quad (3.86)$$

As U depends linearly on p , $\frac{1}{\lambda} \frac{dU}{dp}$ can be written as

$$\frac{1}{\lambda} \frac{dU}{dp} = \frac{1}{\lambda} \frac{U_l - U_u}{p_l - p_u} = - \frac{U_u - U_l}{\alpha} \quad (3.87)$$

The quadratic equation (3.86) then becomes

$$c^2 - (U_u + U_l)c + U_u U_l + (U_u - U_l)^2 [-\alpha^{-2} + \alpha^{-1} \coth(\alpha)] = 0 \quad (3.88)$$

The solution of this equation is

$$c = \frac{U_u + U_l}{2} \pm \frac{U_u - U_l}{2} f(\alpha)^{\frac{1}{2}} \quad \text{with} \quad f(\alpha) \equiv 1 + 4\alpha^{-2} - 4\alpha^{-1} \coth(\alpha) \quad (3.89)$$

The wave will be stable for those values of α for which $f(\alpha) > 0$ and unstable waves occur for $f(\alpha) < 0$. (3.89) shows that unstable waves move with the velocity $(U_u + U_l)/2$. This means that for these unstable waves the 'steering' level is found at the middle pressure level between the upper and the lower boundaries, because U is a linear function of p .

(3.77) shows that in the case of $f(\alpha) < 0$ the maximum instability is found for the value of α for which the absolute value of the complex part of $\mu_x c$ is maximum. The definitions of α and of λ show that μ_x satisfies

$$\mu_x = \frac{f_0 \alpha}{p_l - p_u} [\sigma \{1 + (L_x/L_y)^2\}]^{-\frac{1}{2}} \quad (3.90)$$

Thus

$$\mu_x c = \mu_x \frac{U_u + U_l}{2} \pm \frac{(U_u - U_l) f_0}{2(p_l - p_u)} [\sigma \{1 + (L_x/L_y)^2\}]^{-\frac{1}{2}} g(\alpha)^{\frac{1}{2}} \quad (3.91)$$

with

$$g(\alpha) \equiv \alpha^2 f(\alpha) = \alpha^2 + 4 - 4\alpha \coth(\alpha) \quad (3.92)$$

The maximum instability is found at the minimum value of $g(\alpha)$. In table 16, $f(\alpha)$

and $g(\alpha)$ are given for different values of α . The maximum instability is found at $\alpha \approx 1.6$, while neutral waves are found at $\alpha \approx 2.4$.

α	$g(\alpha)$	$f(\alpha)$	α	$g(\alpha)$	$f(\alpha)$	α	$g(\alpha)$	$f(\alpha)$
0	0	-0.33	1.1	-0.29	-0.24	2.2	-0.18	-0.04
0.1	-0.00	-0.33	1.2	-0.32	-0.22	2.3	-0.10	-0.01
0.2	-0.01	-0.33	1.3	-0.34	-0.20	2.4	+0.00	+0.00
0.3	-0.03	-0.33	1.4	-0.37	-0.19	2.5	+0.11	+0.02
0.4	-0.05	-0.32	1.5	-0.38	-0.17	3.0	+0.94	+0.10
0.5	-0.08	-0.31	1.6	-0.38	-0.15	4.0	+3.99	+0.25
0.6	-0.11	-0.30	1.7	-0.38	-0.13	5.0	+9.00	+0.26
0.7	-0.14	-0.29	1.8	-0.36	-0.11	10	+64	+0.64
0.8	-0.18	-0.28	1.9	-0.34	-0.09	100	+9604	+0.96
0.9	-0.22	-0.27	2.0	-0.30	-0.07	∞	∞	1
1.0	-0.25	-0.25	2.1	-0.25	-0.06			

Table 16 The values of f defined in (3.89) and g defined in (3.92) for several values of α defined in (3.85).

In the following section the case of a young developing frontal wave is investigated with the aid of the theory given above.

4.2 The case of a young developing frontal wave

For developing waves the real atmosphere must have a preference for the system that shows maximum instability. As shown in table 16 the corresponding value of α is about 1.6. The relation between the static stability σ and the wavelength is given by (3.90) for a given value of α . (3.90) can be rewritten as

$$L_x = \frac{2\pi(p_1 - p_u)}{f_0\alpha} [\sigma\{1 + (L_x/L_y)^2\}]^{\frac{1}{2}} \quad (3.93)$$

The following values are chosen: $p_u = p_2$ (200 mbar) and $p_l = p_{10}$ (1000 mbar); $L_x = 1600$ km and $L_x/L_y = 0.5$ (approximately the mean values for the RVA-pattern at 500 mbar as defined in section 2.2); $\alpha \approx 1.6$ (the value of maximum instability). With these values the static stability σ can be computed from (3.93), resulting in $2.1 \times 10^{-7} \text{ m}^4\text{kg}^{-2}\text{s}^2$. As has been remarked in 3.3, for a developing frontal wave with precipitation one expects a value of the static stability according to a saturated adiabatic lapse rate leading to about $10 \times 10^{-7} \text{ m}^4\text{kg}^{-2}\text{s}^2$ (see table 6). This value is about five times as much than the one computed here. The difference can be explained by taking into account the release of latent heat, which was ignored in the stability

analysis in 4.1. This can be done in the following way. The thermodynamic equation with release of latent heat is given by (2.14). In case $Q > 0$ (release of latent heat), $\frac{\sigma}{f_0} \omega + \frac{R \cdot Q}{c_p \cdot f_0 \cdot p} = 0$. This relationship between Q and ω was also used in section 3.5. It is possible to introduce an 'effective' static stability parameter $\tilde{\sigma}$ into the thermodynamic equation,

$$\frac{\partial \psi}{\partial p} + J\left(\psi, \frac{\partial \psi}{\partial p}\right) + \frac{\tilde{\sigma}}{f_0} \omega = 0 \quad (3.94)$$

with $\tilde{\sigma} = \sigma$ for $Q = 0$ and $\tilde{\sigma} = 0$ for $Q > 0$.

In the stability analysis a mean value of σ for the whole layer of air between p_u and p_1 was used. Now a new mean value $\tilde{\sigma}_m$ of $\tilde{\sigma}$ can be defined as follows. Suppose there is release of latent heat between the two pressure levels \tilde{p}_u and \tilde{p}_1 , with $p_u \leq \tilde{p}_u < \tilde{p}_1 \leq p_1$, then $\tilde{\sigma} = \sigma$ for $p_u \leq p < \tilde{p}_u$, $\tilde{\sigma} = 0$ for $\tilde{p}_u \leq p \leq \tilde{p}_1$ and $\tilde{\sigma} = \sigma$ for $\tilde{p}_1 < p \leq p_1$. The mean value $\tilde{\sigma}_m$ of $\tilde{\sigma}$ then becomes

$$\tilde{\sigma}_m = \frac{[(\tilde{p}_u - p_u) + (p_1 - \tilde{p}_1)]\sigma}{p_1 - p_u} \quad (3.95)$$

In the extreme case there is release of latent heat in the whole column between 200 and 1000 mbar. Then $p_u = \tilde{p}_u$ and $p_1 = \tilde{p}_1$ and $\tilde{\sigma}_m = 0$. In general, however, there is no release of latent heat above 300 mbar nor below 950 mbar, so that $\tilde{p}_u = 300$ mbar and $\tilde{p}_1 = 950$ mbar are more realistic. So for these values with $\sigma \approx 10 \times 10^{-7} \text{ m}^4 \text{ kg}^{-2} \text{ s}^2$, $\tilde{\sigma}_m \approx 2 \times 10^{-7} \text{ m}^4 \text{ kg}^{-2} \text{ s}^2$, which is in accordance with the required value.

Without release of latent heat $\tilde{\sigma}_m = \sigma \approx 10 \times 10^{-7} \text{ m}^4 \text{ kg}^{-2} \text{ s}^2$ and using the values $L_x = 1600$ km, $L_x/L_y = 0.5$, $p_u = p_2$ and $p_1 = p_{10}$, then according to the definition of α in (3.85), $\alpha \approx 3.5$. For this value of α it follows from table 16 that $f(\alpha) > 0$ and the wave must be stable.

The important conclusion that can be drawn is that there is a strong evidence that the short frontal waves with wavelengths of about 1000-2500 km, which are related with the areas of advection of relative vorticity at 500 mbar, can only be unstable if latent heat is released. This conclusion has been confirmed by the experiments with the BK3-model with inclusion of the release of latent heat by HEIJBOER and EXTER BLOKLAND, DEN (1974).

The above conclusion also agrees with that of the simple two-parameter model in section 3.5, namely that without release of latent heat no production of vorticity occurs in the centre of a perturbation at sea level.

In the following two sections the spatial structure of certain stable and unstable waves are investigated and compared with the results in 3.

4.3 *Spatial structure of stable waves*

First the coefficients ψ_1^* and ψ_2^* are specified. Using (3.87) and (3.89), the equation (3.83) can be written after some computational work as

$$(\alpha - 2 + G) e^{+\lambda \cdot p_1} \psi_1^* - (\alpha + 2 + G) e^{-\lambda \cdot p_1} \psi_2^* = 0 \quad (3.96)$$

with $G \equiv \pm \alpha f(\alpha)^{\frac{1}{2}} = \pm g(\alpha)^{\frac{1}{2}}$

The mean pressure p_m at the middle level is given by $p_m = (p_u + p_l)/2$, so that p_m is found to be 600 mbar. It follows from (3.82) that at this level

$$e^{+\lambda \cdot p_m} \psi_1^* + e^{-\lambda \cdot p_m} \psi_2^* = \psi_m^* \quad (3.97)$$

ψ_m^* is the amplitude of the perturbation ψ' at the middle level and can be chosen arbitrarily. Here it is supposed to be real. With the aid of the definition of α , p_l and p_u can be expressed as

$$p_l = p_m + \frac{\alpha}{2\lambda} \quad \text{and} \quad p_u = p_m - \frac{\alpha}{2\lambda} \quad (3.98)$$

Using the result of (3.98), ψ_1^* and ψ_2^* can be solved from (3.96) and (3.97). Substitutions of these results into (3.82) lead to

$$\psi^* = F_p \cdot \psi_m^* \quad \text{with} \quad F_p \equiv \frac{(\alpha + 2 + G) e^{\lambda \cdot (p - p_m)} + (\alpha - 2 + G) e^\alpha e^{-\lambda \cdot (p - p_m)}}{(\alpha + 2 + G) + (\alpha - 2 + G) e^\alpha} \quad (3.99)$$

The computations presented above are valid for stable as well as for unstable waves. In the case of stable waves both $f(\alpha)$ and $g(\alpha)$ are > 0 , so that F_p is real. With the aid of (3.77) the real part of ψ' is found to be

$$\psi' = F_p \cdot \psi_m' = F_p \cdot \psi_m^* \cos(\mu_y \cdot y) \cos[\mu_x(x - c \cdot t)] \quad (3.100)$$

The velocity c of (3.89) is written as

$$c = U_m \pm \frac{U_u - U_l}{2} f(\alpha)^{\frac{1}{2}} \quad \text{with} \quad U_m \equiv \frac{1}{2}(U_u + U_l) \quad (3.101)$$

The horizontal divergence D can be computed by substitution of (3.99) into (3.79) and differentiation of (3.78) with respect to p . Then, after elimination of $\frac{d\omega^*}{dp}$ and taking the real part, $f_0 D$ becomes

$$f_0 D = \mu_x(\mu_x^2 + \mu_y^2) (c - U) F_p \psi_m^* \cos(\mu_y \cdot y) \sin[\mu_x(x - c \cdot t)] \quad (3.102)$$

The advection of the relative vorticity RVA at 500 mbar is given by $-U_5 \frac{\partial}{\partial x} (\nabla^2 \psi')$ and can be expressed with the aid of (3.100) as

$$\text{RVA} = -U_5 \mu_x (\mu_x^2 + \mu_y^2) F_5 \psi_m^* \cos(\mu_y \cdot y) \sin[\mu_x(x - c \cdot t)] \quad (3.103)$$

where U_5 and F_5 represent the values of U and F_p at 500 mbar respectively.

Using (3.103), (3.102) can be written as

$$f_0 D = - \frac{(c - U) F_p}{U_5 F_5} \text{RVA} \quad (3.104)$$

The level of non-divergence is found at that level where $c = U$, so that according to (3.89), $U = U_m \pm \frac{1}{2}(U_u - U_l)f(\alpha)^\pm$. Due to the fact that U_m is the velocity at 600 mbar and $U_u - U_l > 0$ and $f(\alpha) > 0$, the level of non-divergence is found above 600 mbar in the case of the positive sign and below that for the negative sign. Thus probably only the positive sign has a real meaning, because in the troposphere, if there exists a level of non-divergence, it is nearly always found close to 500 mbar.

The formula for ω is obtained by differentiation of (3.99) with respect to p , substitution of the result into (3.80). After the elimination of ψ_m^* from (3.80) and (3.103) and taking the real part of (3.78), the expression for ω reads

$$f_0 \lambda^2 \omega = \frac{(c - U) \frac{dF_p}{dp} + \frac{dU}{dp} F_p}{U_5 F_5} \text{RVA} \quad (3.105)$$

By differentiating this formula with respect to p it can be easily shown that the extreme value of ω is found at the level where $c = U$.

The stable wave shows resemblance with the reference atmosphere, which was defined in 1, because at all pressure levels the wave moves with the same velocity and there is no phase shift in the vertical. The divergence D and the vertical velocity ω become functions of the RVA, which was also true for the reference atmosphere.

As the level of non-divergence was also found at 500 mbar for the reference atmosphere, it may be of interest to compute the parameters describing the behaviour of

the wave with the level of non-divergence at 500 mbar and compare them with those for the reference atmosphere. For that purpose it is assumed that the basic zonal wind U satisfies the relation $U = A \cdot U_5$ with A is a linear function of p as is the case for the reference atmosphere in 3.5 in table 12. Using $U_m = A_6 \cdot U_5$, $U_u = A_2 \cdot U_5$ and $U_l = A_{10} \cdot U_5$, it follows from (3.101) with the positive sign, that for the level of non-divergence at 500 mbar where $c = U_5$,

$$f(\alpha) = \left[\frac{2(1 - A_6)}{A_2 - A_{10}} \right]^2 \quad (3.106)$$

The upper and lower boundaries are again p_u at 200 mbar and p_l at 1000 mbar. Taking $A_2 = 1.48$, $A_6 = 0.84$ and $A_{10} = 0.20$ according to table 12, $f(\alpha) = 0.0625$ and thus $\alpha \approx 2.75$ and $G = \alpha \cdot f(\alpha)^{\frac{1}{2}} \approx 0.69$. With the aid of (3.99), F_p can be computed and is given in table 17.

A new quantity F' is defined as

$$F' \equiv F_p / F_5 \quad (3.107)$$

Due to $c = U_5$ and $U = A \cdot U_5$, (3.104) can be written as

$$f_o D = D' \cdot RVA \quad \text{with} \quad D' \equiv -(1 - A)F' \quad (3.108)$$

The computed values of F' and D' are also given in table 17.

With the aid of (3.87), (3.107), $c = U_5$ and $U = A \cdot U_5$, (3.105) can be expressed as

$$f_o \omega = \omega' \cdot RVA \quad \text{with} \quad \omega' \equiv \frac{(p_l - p_u)^2}{\alpha^2} \left[(1 - A) \frac{dF'}{dp} - \frac{A_u - A_l}{p_l - p_u} F' \right] \quad (3.109)$$

ω' is given in table 17.

Comparisons of F' , D' and ω' of table 17 with A , D'_a and ω'_a of table 12 for the reference atmosphere respectively, show that to a certain extent there is a quantitative agreement especially in the middle troposphere around the 500 mbar level. Due to the different approach in this section compared with the considerations that led to the values given in table 12, an exact agreement could not be expected.

It follows from (3.103) that the maximum value of the RVA at the steering level (denoted by $|RVA_s|_{\max}$) is given by

$$|RVA_s|_{\max} = U_5 \mu_x (\mu_x^2 + \mu_y^2) F_5 \psi_m^* \quad (3.110)$$

p mbar	F	F'	D'	ω' $10^4 \text{m}^{-1} \text{kg s}^{-2}$
200	3.23	2.54	+1.22	0
300	2.33	1.83	+0.59	-0.97
400	1.70	1.34	+0.21	-1.40
500	1.27	1	0	-1.51
600	1	0.79	-0.13	-1.44
700	0.85	0.67	-0.21	-1.25
800	0.79	0.62	-0.30	-0.96
900	0.85	0.67	-0.43	-0.56
1000	0.97	0.76	-0.61	0

Table 17 Computed quantities for the stable wave with a level of non-divergence at 500 mbar.

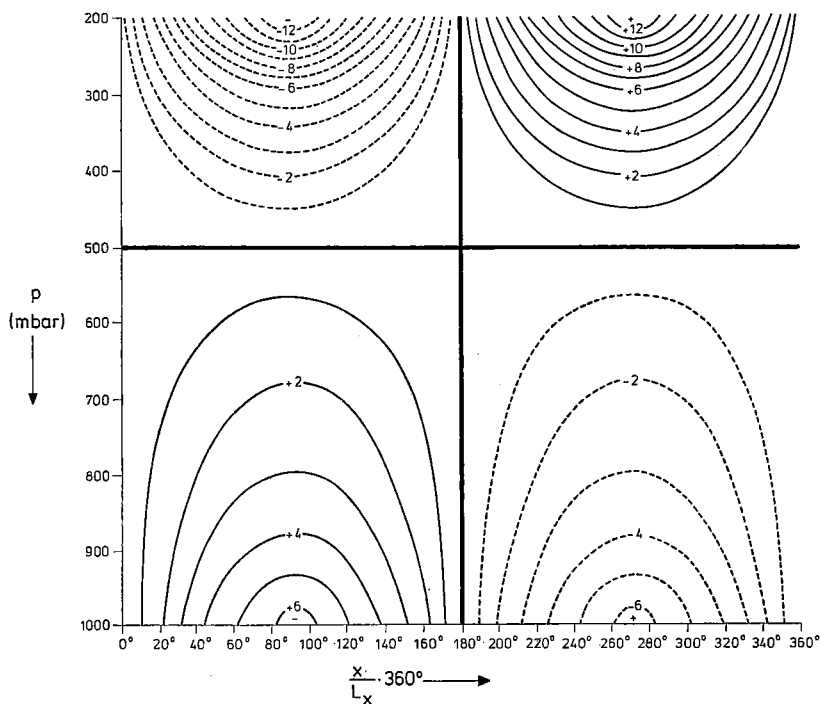


Fig. 14 Vertical cross-section of the divergence-field of a stable wave

($a = \frac{p_l - p_u}{f_0} [\sigma(\mu_x^2 + \mu_y^2)]^{\frac{1}{2}} \approx 2.75$) with the level of non-divergence at 500 mbar.

Isolines of negative divergence are dashed.

Isolines of positive divergence are drawn.

Unit of divergence is $10^3 \cdot |RVA_s|_{\max} \text{s}^{-1}$.

$|RVA_s|_{\max}$ is the maximum absolute value of the advection of relative vorticity at the steering level (500 mbar).

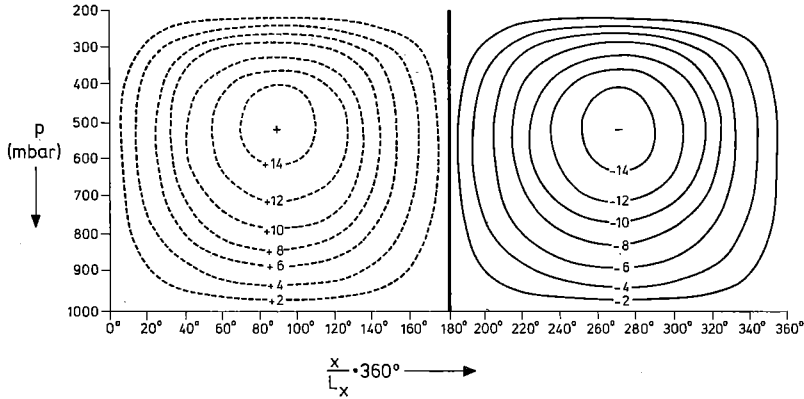


Fig. 15 Vertical cross-section of the ω -field of a stable wave

($a = \frac{P_1 - P_n}{f_0} [\sigma(\mu_x^2 + \mu_y^2)]^{\frac{1}{2}} \approx 2.75$) with the level of non-divergence at 500 mbar.

Isolines of positive ω are dashed.

Isolines of negative ω are drawn.

Unit of ω is $10^7 \cdot |\text{RVA}_s|_{\max} \text{m}^{-1} \text{kg s}^{-3}$.

$|\text{RVA}_s|_{\max}$ is the maximum absolute value of the advection of relative vorticity at the steering level (500 mbar).

Using this formula and (3.103), the expressions (3.108) and (3.109) can be written as

$$f_o D = - |\text{RVA}_s|_{\max} \cdot D' \cdot \cos(\mu_y \cdot y) \sin[\mu_x(x - c \cdot t)] \quad (3.111)$$

and

$$f_o \omega = - |\text{RVA}_s|_{\max} \cdot \omega' \cdot \cos(\mu_y \cdot y) \sin[\mu_x(x - c \cdot t)] \quad (3.112)$$

Vertical cross-sections for D and ω have been computed for the middle of the wave where $\cos(\mu_y \cdot y) = 1$ along the x -axis at $t = 0$. These cross-sections are given in the figures 14 and 15.

In the next section the spatial structure of the unstable wave is investigated in a similar way.

4.4 Spatial structure of unstable waves

In the case of an unstable wave $f(\alpha) < 0$, so that F_p in (3.99) and c in (3.101) are complex. Therefore the velocity c can also be written as

$$c = c_r + c_i \cdot i \quad \text{with} \quad c_r \equiv \frac{1}{2}(U_u + U_l) \quad \text{and} \quad c_i \equiv \pm \frac{1}{2}(U_u - U_l) \cdot [-f(\alpha)]^{\frac{1}{2}} \quad (3.113)$$

After considerable computational work, F_p in (3.99) can be expressed as

$$F_p = F_r + F_i \cdot i$$

with

$$F_r \equiv \frac{1}{2}[e^{+\lambda(p-p_m)} + e^{-\lambda(p-p_m)}], \quad F_i \equiv \frac{-4 e^\alpha G' [e^{+\lambda(p-p_m)} - e^{-\lambda(p-p_m)}]}{[\alpha + 2 + (\alpha - 2)e^\alpha]^2 - (1 + e^\alpha)^2 g(\alpha)} \quad (3.114)$$

and

$$G' \equiv \pm [-g(\alpha)]^{\frac{1}{2}}$$

For $c_i > 0$ the wave will amplify, whereas for negative values of c_i it damps. This means that only the solution with the positive sign is of interest. With the aid of (3.77), (3.99), (3.113) and (3.114) the real part of ψ' can be written as

$$\psi' = e^{\mu_x c_i t} [F_r \cos \mu_x(x - c_r t) - F_i \sin \mu_x(x - c_r t)] \cos(\mu_y \cdot y) \cdot \psi_m^* \quad (3.115)$$

with

$$\mu_x c_i = \frac{f_o(U_u - U_l) \cdot [-g(\alpha)]^{\frac{1}{2}}}{2(p_l - p_u) [\sigma\{1 + (L_x/L_y)^2\}]^{\frac{1}{2}}}$$

The steering level is found where $c_r = U$. According to (3.113) and the linearity of U this must be the 600 mbar level. For this level where $p = p_m$, $F_r = 1$ and $F_i = 0$ yield.

After differentiation of (3.78) with respect to p and using (3.79), (3.99) and (3.114), the real part of $f_o D$ becomes

$$f_o D = \mu_x(\mu_x^2 + \mu_y^2) e^{\mu_x c_i t} [\{(c_r - U)F_i + c_i F_r\} \cos \mu_x(x - c_r t) + \{(c_r - U)F_r - c_i F_i\} \sin \mu_x(x - c_r t)] \cos(\mu_y \cdot y) \cdot \psi_m^* \quad (3.116)$$

With the aid of (3.78), (3.80), (3.99) and (3.114) the real part of $\frac{\sigma}{f_o} \omega$ can be computed and reads

$$\begin{aligned} \frac{\sigma}{f_o} \omega = & -\mu_x e^{\mu_x c_i t} \left[\left\{ (c_r - U) \frac{dF_i}{dp} + c_i \cdot \frac{dF_r}{dp} + \frac{dU}{dp} \cdot F_i \right\} \cos \mu_x(x - c_r t) \right. \\ & \left. + \left\{ (c_r - U) \frac{dF_r}{dp} - c_i \cdot \frac{dF_i}{dp} + \frac{dU}{dp} \cdot F_r \right\} \sin \mu_x(x - c_r t) \right] \cos(\mu_y \cdot y) \cdot \psi_m^* \end{aligned} \quad (3.117)$$

The sine and cosine components of (3.115) can be composed to a single cosine-wave, which reads

$$\psi' = \frac{F_r}{\cos \gamma} e^{\mu_x c t} \psi_m^* \cos(\mu_y \cdot y) \cdot \cos[\mu_x(x - c_r t) + \gamma] \quad (3.118)$$

with $\text{tg}(\gamma) = F_i/F_r$

The formula for the thermal field $T' \equiv -\frac{f_o p}{R} \frac{d\psi'}{dp}$ of the perturbation can be derived by differentiation of (3.115) to p and by composing the sine and cosine waves. It reads

$$T' = -\frac{f_o p}{R \cdot \cos \delta} \frac{dF_r}{dp} e^{\mu_x c t} \psi_m^* \cos(\mu_y \cdot y) \cos[\mu_x(x - c_r t) + \delta] \quad (3.119)$$

$$\text{with } \text{tg}(\delta) = \frac{dF_i}{dp} \Bigg| \frac{dF_r}{dp}$$

Unlike the stable wave in 4.3, the unstable wave shows a phase shift γ in the vertical for the streamfunction ψ' and a phase shift δ for the thermal field T' . These phase shifts do not depend on x , y and t .

With the aid of (3.118) the advection of relative vorticity at each pressure level, which is given by $-U \frac{\partial}{\partial x} (\nabla^2 \psi')$, can be computed and shows an exponential growth like the fields of the streamfunction ψ' and temperature T' .

$$\begin{aligned} \text{RVA}(x, y, p, t) = \\ -U \frac{\partial}{\partial x} (\nabla^2 \psi') = -\frac{F_r}{\cos \gamma} e^{\mu_x c t} \mu_x (\mu_x^2 + \mu_y^2) U \psi_m^* \cdot \cos(\mu_y \cdot y) \sin[\mu_x(x - c_r t) + \gamma] \end{aligned} \quad (3.120)$$

This exponential development is in qualitative agreement with the behaviour of the RVA at 500 mbar of developing frontal waves. See, for instance, the wave which is described in 3.4 and is shown in figure 12.

For the purpose of a more quantitative comparison with the results of 3.5, the spatial structure will be further investigated for the most unstable wave. For such a wave $\alpha \approx 1.6$ as was shown in table 16. So $f(\alpha) \approx -0.15$, $g(\alpha) \approx -0.38$ and $G' = [-g(\alpha)]^{\frac{1}{2}} \approx 0.62$. With the aid of (3.114), F_r and F_i have been computed. The phase shifts γ and δ have been computed with the aid of (3.118) and (3.119) and are given in table 18, which table also contains the amplitude $F_r/\cos \gamma$ of the perturbation

ψ' . As in the previous section it is supposed that the zonal wind U satisfies the relation

$$U = A \cdot U_5 = A' \cdot U_6, \quad A' \text{ being } A' \equiv A/A_6 \quad (3.121)$$

It follows from (3.120) that the maximum value of the RVA at the steering level of 600 mbar is given by

$$|RVA_s|_{\max} = e^{\mu_x c_r t} \mu_x (\mu_x^2 + \mu_y^2) U_6 \psi_m^* \quad (3.122)$$

Using (3.113) and (3.122), (3.116) can be rewritten as

$$\begin{aligned} f_o D = & -|RVA_s|_{\max} \cdot [D_1' \cos(\mu_y \cdot y) \sin \mu_x(x - c_r t) \\ & + D_2' \cos(\mu_y \cdot y) \cos \mu_x(x - c_r t)] \end{aligned} \quad (3.123)$$

with $D_1' \equiv -[(1 - A')F_r - \frac{1}{2}(A_u' - A_i')] \{-f(\alpha)\}^{\frac{1}{2}} F_i]$

and $D_2' \equiv -[(1 - A')F_i + \frac{1}{2}(A_u' - A_i')] \{-f(\alpha)\}^{\frac{1}{2}} F_r]$.

In a similar way and using the definitions of λ in (3.81) and of α in (3.85), (3.117) becomes

$$\begin{aligned} f_o \omega = & -|RVA_s|_{\max} \cdot [\omega_1' \cos(\mu_y \cdot y) \sin \mu_x(x - c_r t) \\ & + \omega_2' \cos(\mu_y \cdot y) \cos \mu_x(x - c_r t)] \end{aligned} \quad (3.124)$$

with

$$\omega_1' \equiv \frac{(p_1 - p_u)^2}{\alpha^2} \left[(1 - A') \frac{dF_r}{dp} - \frac{1}{2}(A_u' - A_i') \{-f(\alpha)\}^{\frac{1}{2}} \frac{dF_i}{dp} - \frac{A_u' - A_i'}{p_1 - p_u} F_r \right]$$

and

$$\omega_2' \equiv \frac{(p_1 - p_u)^2}{\alpha^2} \left[(1 - A') \frac{dF_i}{dp} + \frac{1}{2}(A_u' - A_i') \{-f(\alpha)\}^{\frac{1}{2}} \frac{dF_r}{dp} - \frac{A_u' - A_i'}{p_1 - p_u} F_i \right]$$

D_1' , D_2' , ω_1' and ω_2' are given in table 18.

The results of this section can be compared with the results of 3.5 in which the divergence D' and the vertical velocity ω' in a young developing frontal wave were investigated with the aid of a simple two-parameter model. The divergence D' and the vertical velocity ω' were computed in the centre of the perturbation part ψ^* of the wave.

According to (3.118) this centre can be identified with the point at 1000 mbar of the perturbation ψ' for which $\cos(\mu_y \cdot y) = 1$ and $\cos(\mu_x \cdot x + \gamma) = -1$. According

p mbar	$F_r/\cos \gamma$	γ	δ	D'_1	D'_2	ω'_1 $10^4\text{m}^{-1}\text{kg s}^{-2}$	ω'_2 $10^4\text{m}^{-1}\text{kg s}^{-2}$
200	+1.90	+45°	+68°	+1.42	+0.63	0	0
300	+1.53	+39°	+71°	+0.96	+0.20	-1.20	-0.41
400	+1.24	+30°	+76°	+0.59	-0.08	-1.97	-0.45
500	+1.07	+17°	+83°	+0.28	-0.24	-2.40	-0.28
600	+1	0°	+90°	0	-0.30	-2.54	0
700	+1.07	-17°	+98°	-0.28	-0.24	-2.40	+0.28
800	+1.24	-30°	+104°	-0.59	-0.08	-1.97	+0.45
900	+1.53	-39°	+110°	-0.96	+0.20	-1.20	+0.41
1000	+1.90	-45°	+114°	-1.42	+0.63	0	0

Table 18 Computed quantities for the most unstable wave with $\alpha = 1.6$.

to table 18, $\gamma = -45^\circ$ at 1000 mbar, so that $\mu_x \cdot x = 225^\circ$. It follows from (3.120) and (3.122) that the advection of relative vorticity at 500 mbar (RVA) is related to the maximum value at the steering level 600 mbar for that point as

$$\text{RVA} = -\frac{F_r(p_5)}{\cos 17^\circ} \sin(\mu_x \cdot x + 17^\circ) \cdot |\text{RVA}_s|_{\max} = 0.942 |\text{RVA}_s|_{\max} \quad (3.125)$$

Due to $\cos(\mu_x \cdot x) = \sin(\mu_x \cdot x) = -\sin 45^\circ$, (3.123) and (3.124) then become

$$f_0 D = D' \cdot \text{RVA} \quad \text{with} \quad D' \equiv 0.751(D'_1 + D'_2)$$

and

$$f_0 \omega = \omega' \cdot \text{RVA} \quad \text{with} \quad \omega' \equiv 0.751(\omega'_1 + \omega'_2) \quad (3.126)$$

p mbar	D' of the unstable wave —	D' according to table 12 —	ω' of the unstable wave $10^4\text{m}^{-1}\text{kg s}^{-2}$	ω' according to table 12 $10^4\text{m}^{-1}\text{kg s}^{-2}$
200	+1.52	+1.35	0	0
300	+0.87	+0.90	-1.21	-1.08
400	+0.45	+0.51	-1.82	-1.78
500	+0.03	+0.16	-2.01	-2.11
600	-0.23	-0.13	-1.91	-2.13
700	-0.39	-0.38	-1.59	-1.87
800	-0.44	-0.57	-1.14	-1.40
900	-0.57	-0.71	-0.59	-0.76
1000	-0.59	-0.80	0	0

Table 19 Comparison of the computed D' and ω' of the most unstable wave and those from the two-parameter model of 3.5 for the centre of the perturbation at 1000 mbar.

Now, with the aid of table 18, D' and ω' can be calculated and compared with $D' = D'_d + D'_m$ and $\omega' = \omega'_d + \omega'_m$ of table 12 in section 3.5. The results are given in table 19, which show a good agreement between both sets of values.

From these results it can be concluded that *concerning the divergence- and ω -values the most unstable wave of the stability analysis agrees with the young developing frontal waves of the real atmosphere.*

Finally, a further insight in the structure of the unstable wave is given in figures 16 and 17, which give a vertical cross-section of D and ω along the x -axis in the middle of the wave for which $\cos(\mu_y \cdot y) = 1$. Unlike in the case of a stable wave, figure 16

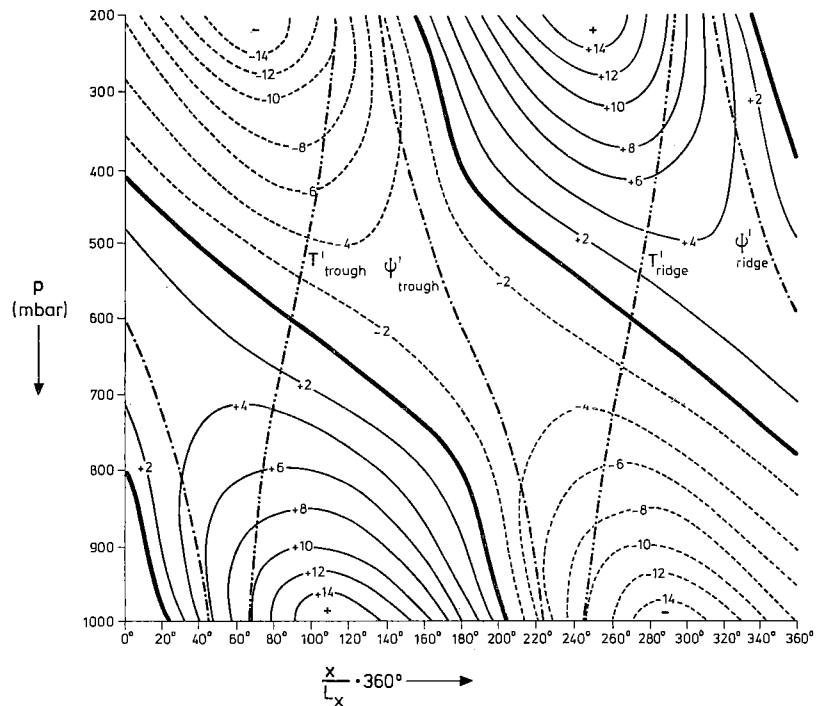


Fig. 16 Vertical cross-section of the divergence-field of the most unstable wave ($\alpha \approx 1.6$).

Isolines of negative divergence are dashed.

Isolines of positive divergence are drawn.

----- Through or ridge line of the streamfunction ψ' .

----- Through or ridge line of the thermal field T' .

Unit of divergence is $10^3 |RVA_s|_{\max} s^{-1}$.

$|RVA_s|_{\max}$ is the maximum absolute value of the advection of relative vorticity at the steering level (600 mbar).

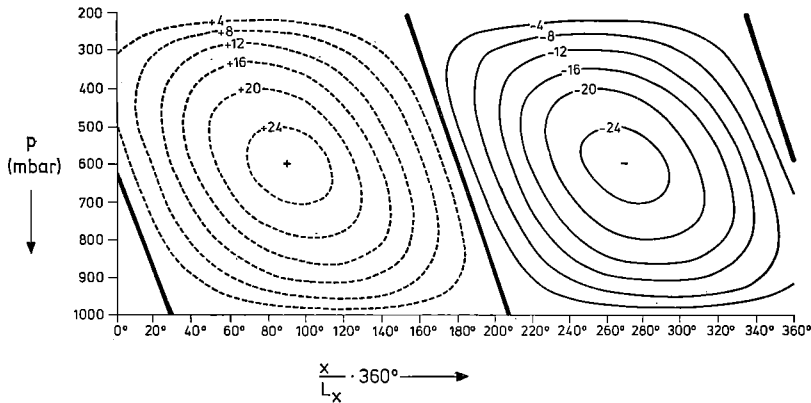


Fig. 17 Vertical cross-section of the ω -field of the most unstable wave ($a \approx 1.6$).
 Isolines of positive ω are dashed.
 Isolines of negative ω are drawn.
 Unit of ω is $10^7 |RVA_s|_{\max} m^{-1} kg s^{-3}$.
 $|RVA_s|_{\max}$ is the maximum absolute value of the advection of relative vorticity at the steering level (600 mbar).

clearly shows that *there exists no constant pressure level of non-divergence for the unstable wave investigated here*. This result was also found by CRESSMAN (1961) in a diagnostic study of mid-tropospheric development.

5 Conclusions with regard to the construction of a baroclinic model

The following four conclusions can be drawn from the foregoing considerations:

1. The importance of the release of latent heat

The stability analysis in section 4 indicates that the short frontal waves with wavelengths of about 1000–2500 km can only be unstable if latent heat is released. The release of latent heat can give a plausible explanation for the low values of the static stability, which are necessary to make the short waves unstable.

From the scale analysis given by PHILLIPS (1963) it also follows that the release of latent heat has to be taken into account if one wants to describe the behaviour of synoptic systems with the aid of the quasi-geostrophic equations.

In section 3.5 it has been shown that in the centre of the perturbation at sea level of a young developing frontal wave, the ω -values increase with about a factor two through the influence of the release of latent heat. *Therefore the release of latent heat*

has to be taken into account in a baroclinic model which one desires to be capable of predicting the deepening of short frontal waves.

2. Profile of the horizontal divergence in the vertical

For the construction of the baroclinic BK3-model in Chapter IV the integrated thermodynamic equations over the layers 300–500 and 500–850 mbar are used. To carry out the integrations of ω , knowledge of the profile of the horizontal divergence D in the vertical is necessary. The results in section 3.5 indicate that D and ω can be split up into a ‘dry’ and a ‘moist’ part, each possessing a different profile and a different level on non-divergence. See also table 12 and figure 13. The dry part of D has the same profile as the reference atmosphere and a level of non-divergence at ~ 500 mbar. The moist part of D has a linear profile and a level of non-divergence at ~ 600 mbar.

Because the basic equations of the baroclinic model are linear with regard to D and ω , it is possible to split up these quantities into ‘dry’ and ‘moist’ parts. This approach is followed in Chapter IV, where the dry part of D is profiled in accordance with the reference atmosphere for the layers 300–500 and 500–1000 mbar, and the moist part is taken linear for the layers 200–300, 300–500, 500–850 and 850–1000 mbar.

3. The choice of the static stability parameters

For a baroclinic model, which is able to describe the development of the short frontal waves with precipitation, values of the static stability parameter in accordance with those of saturated adiabatic lapse rates seem to be a logical choice. However, for the upper troposphere these values are much lower than those of the ICAO standard atmosphere. See also table 6 in section 3.3. In the dry parts of the atmosphere at sufficient distance from the frontal areas one will find values of the static stability more in accordance with those of the ICAO standard atmosphere. This problem of a variable static stability in the real atmosphere can be solved to a certain extent by the introduction of a so-called correction term into the integrated thermodynamic equation, which is approximately zero if the static stability is that of a saturated adiabatic lapse rate.

As has been argued in section 3.3, the use of such a correction term leads to a correct description of the long waves, if they are equivalent barotropic and probably also for the short waves, because in that case the equations are equal to the original ones without correction.

For short range prognoses up to 36 hours ahead the results of barotropic prognoses at 500 mbar show that an equivalent barotropic description is a good first-order approximation of the behaviour of long waves, although in some cases, notably in the winter season, the baroclinicity of those waves may also be of importance for the short range predictions.

4. The number of levels

The stability analysis in section 4 gives some insight into the choice of the number of levels for the baroclinic model. This analysis gives a fairly simple but not unrealistic description of a developing baroclinic wave. The streamfunction ψ of this wave consists of three parameters, namely one describing the basic streamfunction, which is independent of time, and two more describing the perturbation ψ' , which are dependent on time. According to (3.72) and (3.115), ψ can be written as

$$\psi = A(p) \cdot P_0(y) + F_r(p) \cdot P_1(x, y, t) - F_i(p) \cdot P_2(x, y, t) \quad (3.127)$$

with

$$P_0(y) = -U_5 \cdot y,$$

$$P_1(x, y, t) = e^{\mu_x c_i t} \cos(\mu_y \cdot y) \cos[\mu_x(x - c_r t)] \psi_m^*$$

and

$$P_2(x, y, t) = e^{\mu_x c_i t} \cos(\mu_y \cdot y) \sin[\mu_x(x - c_r t)] \psi_m^*$$

After the choice of two levels at pressures p_1 and p_2 , the parameters P_1 and P_2 can be expressed as linear combinations of the streamfunctions $\psi(x, y, p_1, t)$, $\psi(x, y, p_2, t)$ and $P_0(y)$. Thus two parameters are equivalent with two levels if $P_0(y)$ is a known function. The above results were based on the linearized quasi-geostrophic equations with a prescribed basic zonal streamfunction. For these equations one needs at least two parameters or two levels to describe the development of a baroclinic disturbance. However, in these equations the basic streamfunction cannot change with time. In reality, however, it will change by a non-linear interaction with the perturbation. So in a model using only two parameters the basic streamfunction and the perturbation will be completely time-dependent on each other.

Supposing now that the perturbation is a short baroclinic frontal wave superimposed on a nearly equivalent barotropic long wave, which acts as the basic streamfunction for the baroclinic perturbation, a third parameter is needed to describe at least the equivalent barotropic behaviour of this long wave.

So the number of parameters or levels must be three at least.

CHAPTER IV

DESIGN OF THE BAROCLINIC MODEL

1 Outline of the design

Starting from the quasi-geostrophic basic equations in Chapter II, several ways present themselves for constructing a baroclinic model. However, one can distinguish two main possibilities which in principle depend on the vertical resolution used in the model.

First, with a high resolution in the vertical, the use of difference forms of the vorticity equation and the thermodynamic equation is suitable. After eliminating ω in the difference equations, one gets a set of Helmholtz-equations for the geopotential heights of each chosen pressure level. These equations are coupled and have to be solved simultaneously.

It is also possible to derive the omega-equation by differentiating the vorticity equation with respect to pressure p and applying the Laplacian operator to the thermodynamic equation. After subtraction of the two resulting equations one gets the omega-equation, which can be solved by a three-dimensional iterative technique with the boundary conditions $\omega = 0$ at the upper and lower boundaries of the atmosphere, as well as at the lateral boundaries of the chosen computational grid. After that, one can compute the horizontal divergence from the difference form of the continuity equation and then compute the time derivatives of the geopotential heights from the vorticity equation and the thermodynamic equation at the chosen pressure levels. The above-described method has the advantage that it is easy to formulate the prognostic equations and it is suitable if one wants to reckon with a high vertical resolution.

If, in order to restrict computing time, a low vertical resolution is necessary, the second main possibility with the integrated form of the basic equations can be used. This method has the advantage that quasi-discontinuities such as temperature inversions are smoothed out. The integrated form of the basic equations can be applied in several ways. In the case of a model based on three pressure levels, one needs three prognostic equations, which may be the integrated vorticity equation for the whole atmosphere between the lower and the upper level and the integrated thermodynamic equations for the two layers bounded by the three levels of the model. This method was applied in the operational threeparameter model of the Swedish Meteorological Service described by BENGTTSSON and MOEN (1969).

Another way leading to relatively simple equations for a three-parameter model is the use of the vorticity equation at the three chosen pressure levels, the integrated thermodynamic equation for the two layers bounded by the three chosen levels, and

the integrated continuity equation for the whole column of the atmosphere. This set of six equations contains six unknowns, namely three horizontal divergences and three time derivatives of the geopotential heights. After eliminating the three divergences one gets the three required prognostic equations. That method will be used for the baroclinic model called BK3 in this treatise. This BK3-model was developed in continuation of experiments with an earlier version of a three-parameter model developed by GALEN, VAN (1969).

However, the application of the integrated equations involves a new difficulty. To carry out the integrations one needs to know the vertical structure of the horizontal divergence. This, in addition, implies a more detailed knowledge of those waves in the atmosphere which are important for short-range weather prediction. For that purpose the results obtained in Chapter III are suitable, because it was indicated that the reference atmosphere gives a reasonable description of the behaviour of long waves with wavelengths of ~ 2500 to ~ 4000 km. It was also shown that in the centres of young developing frontal waves where release of latent heat takes place the divergence can be split up into a dry part being the divergence of the reference atmosphere and a linear moist part. *If the integrated thermodynamic equations (3.39) and (3.40) with the corrections ε_3 and $\varepsilon_{8.5}$ are used, it will be possible to design a model, which is fully consistent with the reference atmosphere, because each wave satisfying (3.1) of the reference atmosphere at $t = t_0$ will continue to satisfy (3.1) during the time-integration of these equations.* This will be further elaborated in the next sections.

2 Prognostic equations

For the description of the prognostic system the equations in the β -plane approximation described in Chapter II are used. In section 5 they are replaced by the equations valid for stereographic projection.

For the choice of the pressure levels in the troposphere the reference atmosphere described in Chapter III can give a good guidance. The graph of the divergence for that model atmosphere is shown in figure 6, and it was shown in section III.2.1 that the three characteristic levels, where D is maximum, $D = 0$ and D is minimum, were 230, 510 and 810 mbar respectively. Due to the fact that the aerological observations of radiosondes are given at standard pressure levels, the most suitable choice is to take those levels in the troposphere which are close to these characteristic levels, i.e. 300, 500 and 850 mbar. These pressures are denoted by p_3 , p_5 and $p_{8.5}$ respectively. It should be noted here that the standard pressure level at 250 mbar is closer to 230 mbar, but in order to ensure that the highest level of the model is mostly in the troposphere the choice of 300 mbar is more suitable.

To get the prognostic set of equations of the BK3-model, the quasi-geostrophic vorticity equation (2.10) is applied to the levels 300, 500 and 850 mbar.

$$\nabla^2 \dot{\psi}_3 + J(\psi_3, \nabla^2 \psi_3 + f) + f_o D_3 = 0, \quad (4.1)$$

$$\nabla^2 \dot{\psi}_5 + J(\psi_5, \nabla^2 \psi_5 + f) + f_o D_5 = 0, \quad (4.2)$$

and

$$\nabla^2 \dot{\psi}_{8.5} + J(\psi_{8.5}, \nabla^2 \psi_{8.5} + f) + f_o D_{8.5} = 0, \quad (4.3)$$

where the dot denotes $\frac{\partial}{\partial t}$

The continuity equation (2.13) is integrated in the vertical over the whole atmosphere from 0 to 1000 mbar, denoted by p_{10} . Using the boundary conditions (2.8), namely $\omega = 0$ at 0 and 1000 mbar, this integral becomes

$$\int_0^{p_{10}} D \, dp = 0 \quad (4.4)$$

The thermodynamic equation is integrated from 300 to 500 mbar and from 500 to 850 mbar. These equations are given by (3.39) and (3.40), and are given again below, for the sake of convenience.

$$\int_{p_3}^{p_5} \left[\frac{\partial \dot{\psi}}{\partial p} + J\left(\psi, \frac{\partial \psi}{\partial p}\right) + \frac{\sigma_{3-5}}{f_o} \omega \right] dp + \varepsilon_3 = - \int_{p_3}^{p_5} \frac{R \cdot Q}{c_p \cdot f_o \cdot p} dp \quad (4.5)$$

and

$$\int_{p_5}^{p_{8.5}} \left[\frac{\partial \dot{\psi}}{\partial p} + J\left(\psi, \frac{\partial \psi}{\partial p}\right) + \frac{\sigma_{5-8.5}}{f_o} \omega \right] dp + \varepsilon_{8.5} = - \int_{p_5}^{p_{8.5}} \frac{R \cdot Q}{c_p \cdot f_o \cdot p} dp \quad (4.6)$$

ω is defined by the continuity equation as

$$\omega = - \int_0^p D \, dp = \int_p^{p_{10}} D \, dp \quad (4.7)$$

Equations (4.1)-(4.7) are the prognostic equations of the BK3-model. They contain the unknown quantities $\dot{\psi}$, D and ω , which can be computed at times when the streamfunction is known at 300, 500 and 850 mbar. In the moist version of the model the release of latent heat is taken into account, so that in that case $Q > 0$. Because $\dot{\psi}$, D and ω appear linear in the equations, it is possible to split up the equations into a moist and a dry part. This is done in the following way as

$$\dot{\psi} = \dot{\psi}_d + \dot{\psi}_m, \quad D = D_d + D_m \quad \text{and} \quad \omega = \omega_d + \omega_m \quad (4.8)$$

The subscripts d and m refer to the dry and moist part respectively.

The set of 'dry' equations can be defined as

$$\nabla^2 \dot{\psi}_{d3} + J(\psi_3, \nabla^2 \psi_3 + f) + f_o \cdot D_{d3} = 0, \quad (4.9)$$

$$\nabla^2 \dot{\psi}_{d5} + J(\psi_5, \nabla^2 \psi_5 + f) + f_o \cdot D_{d5} = 0, \quad (4.10)$$

$$\nabla^2 \dot{\psi}_{d8.5} + J(\psi_{8.5}, \nabla^2 \psi_{8.5} + f) + f_o \cdot D_{d8.5} = 0, \quad (4.11)$$

$$\int_0^{p_{10}} D_d dp = 0, \quad (4.12)$$

$$\int_{p_3}^{p_5} \left[\frac{\partial \dot{\psi}_d}{\partial p} + J\left(\psi, \frac{\partial \psi}{\partial p}\right) + \frac{\sigma_{3-5}}{f_o} \omega_d \right] dp + \varepsilon_3 = 0, \quad (4.13)$$

$$\int_{p_5}^{p_{8.5}} \left[\frac{\partial \dot{\psi}_d}{\partial p} + J\left(\psi, \frac{\partial \psi}{\partial p}\right) + \frac{\sigma_{5-8.5}}{f_o} \omega_d \right] dp + \varepsilon_{8.5} = 0, \quad (4.14)$$

and

$$\omega_d = - \int_0^p D_d dp = \int_p^{p_{10}} D_d dp \quad (4.15)$$

The set of 'moist' equations results after the subtraction of (4.9)-(4.15) from (4.1)-(4.7) respectively.

$$\nabla^2 \dot{\psi}_{m3} + f_o \cdot D_{m3} = 0, \quad (4.16)$$

$$\nabla^2 \dot{\psi}_{m5} + f_o \cdot D_{m5} = 0, \quad (4.17)$$

$$\nabla^2 \dot{\psi}_{m8.5} + f_o \cdot D_{m8.5} = 0, \quad (4.18)$$

$$\int_0^{p_{10}} D_m dp = 0, \quad (4.19)$$

$$\int_{p_3}^{p_5} \left[\frac{\partial \dot{\psi}_m}{\partial p} + \frac{\sigma_{3-5}}{f_o} \omega_m \right] dp = - \int_{p_3}^{p_5} \frac{R \cdot Q}{c_p \cdot f_o \cdot p} dp, \quad (4.20)$$

$$\int_{p_5}^{p_{8.5}} \left[\frac{\partial \psi_m}{\partial p} + \frac{\sigma_{5-8.5}}{f_o} \omega_m \right] dp = - \int_{p_5}^{p_{8.5}} \frac{R \cdot Q}{c_p \cdot f_o \cdot p} dp, \quad (4.21)$$

and

$$\omega_m = - \int_0^p D_m dp = \int_p^{p_{10}} D_m dp \quad (4.22)$$

Addition of the moist set of equations to the dry set immediately leads to the original set of equations (4.1)-(4.7).

Experiments with the inclusion of the release of latent heat in the model using (4.16)-(4.22) have been described by HEIJBOER and EXTER BLOKLAND, DEN (1974). The way in which latent heat is included is shown in section 4.

In the further description of the dry part of the model the subscripts d are omitted. The correction terms ε_3 and $\varepsilon_{8.5}$ and the static stability parameters σ_{3-5} and $\sigma_{5-8.5}$ of the equations (4.13) and (4.14) were discussed in section III 3.3 and are given below for convenience.

$$\varepsilon_3 \equiv (A_3 - 1) \psi_5^* + \frac{\sigma_{3-5}}{f_o^2} \left[\int_{p_3}^{p_5} \int_0^p (A \cdot K - A^2) dp \right] dp \cdot J(\psi_5, \nabla^2 \psi_5) \quad (4.23)$$

and

$$\varepsilon_{8.5} \equiv (1 - A_{8.5}) \psi_5^* + \frac{\sigma_{5-8.5}}{f_o^2} \int_{p_5}^{p_{8.5}} \left[\int_0^p (A \cdot K - A^2) dp \right] dp \cdot J(\psi_5, \nabla^2 \psi_5) \quad (4.24)$$

with

$$\nabla^2 \psi_5^* = -J(\psi_5, \nabla^2 \psi_5 + f) \quad \text{and} \quad K = 1 \quad (4.25)$$

In these formulas RVA is replaced by $-J(\psi_5, \nabla^2 \psi_5)$. The symbol * is used for the barotropic tendency ψ_5^* in (4.25) to mark the difference with the baroclinic tendency ψ_5 in (4.10). The static stability parameters are given by (3.37) and (3.38) and read

$$\frac{\sigma_{3-5}}{f_o^2} = \frac{(1 - A_3) (1 - \beta \cdot L^* / U_5) L^*}{\int_{p_3}^{p_5} \left[\int_0^p (A - A^2) dp \right] dp} \quad (4.26)$$

and

$$\frac{\sigma_{5-8.5}}{f_0^2} = \frac{(A_{8.5} - 1)(1 - \beta \cdot L^*/U_5)L^*}{\int_{p_5}^{p_{8.5}} \left[\int_0^p (A - A^2) dp \right] dp} \quad (4.27)$$

with

$$L^* \equiv \frac{L_x^2}{4\pi^2[1 + (L_x/L_y)^2]}$$

For the computation of the integrals in (4.12), (4.13), (4.14) and (4.15) knowledge of the divergence D as a function of pressure p is necessary. The way in which D is defined in the vertical is discussed in the next session.

3 The dry model

3.1 Vertical profile of the horizontal divergence D

After substitution of (4.15) into (4.13) and (4.14) six equations remain in which the integrals of the divergence D have to be evaluated. After the choice of three characteristic pressure levels for D one has to specify D as a function of p between those levels, so that it is possible to carry out these integrations. Then the six equations contain six unknown quantities, namely the three height tendencies at the levels of 300, 500 and 850 mbar and the three divergences at the three characteristic levels. It is not necessary that the three characteristic pressure levels for the divergence D coincide with those levels chosen for the geopotential heights. The three pressures are denoted by p_h , p_i and p_j with $p_h < p_i < p_j \leq p_{10}$, and the three divergences by D_h , D_i and D_j respectively. It is now assumed that D can be profiled in the following way.

$$0 \leq p \leq p_h : \quad D = F_h'(p) \cdot D_h = F_h'(p) \cdot (D_i + D_{hi}) \quad (4.28)$$

where $D_{hi} \equiv D_h - D_i$, $F_h'(0) = 0$ and $F_h'(p_h) = 1$.

$$p_h \leq p \leq p_i : \quad D = D_i + F_i'(p) \cdot D_{hi} \quad (4.29)$$

where $F_i'(p_h) = 1$ and $F_i'(p_i) = 0$.

$$p_i \leq p \leq p_{10} : \quad D = D_i + F_j'(p) \cdot D_{ij} \quad (4.30)$$

where $D_{ij} \equiv D_i - D_j$, $F_j'(p_i) = 0$ and $F_j'(p_j) = -1$.

Assuming that the D -profile of the reference atmosphere, given by (3.6), has to be a special case of (4.28), (4.29) and (4.30), F'_h , F'_i and F'_j can be defined. For that purpose (3.6) is substituted into (4.28), (4.29) and (4.30), giving the following results.

$$F'_h = F(p)/F(p_h) \quad \text{for } 0 \leq p \leq p_h \quad (4.31)$$

$$F'_i = [F(p) - F(p_i)]/[F(p_h) - F(p_i)] \quad \text{for } p_h \leq p \leq p_i \quad (4.32)$$

$$F'_j = -[F(p) - F(p_i)]/[F(p_j) - F(p_i)] \quad \text{for } p_i \leq p \leq p_{10} \quad (4.33)$$

The function F is given by $F(p) \equiv A \cdot K - A^2$ with A the function defined in (3.1) and K the constant defined in (3.7).

In section III 2.1 two characteristic pressure levels with respect to divergence were found in the troposphere for the reference atmosphere, namely the level for which $A = K/2$ (maximum value of D), and the level where $A = K$ (D is equal to zero). These levels were 810 and 510 mbar, respectively. Now D_j is chosen at the level p_j for which $A(p_j) = K/2$ and D_i at the level p_i with $A(p_i) = K$. From this choice it follows that $F(p_i) = 0$ and $F(p_j) = K^2/4$. There remains the choice of D_h at the level p_h in the troposphere. D_h is chosen at the level for which $F(p_h) = -F(p_j)$, so that $A^2(p_h) - A(p_h) \cdot K = K^2/4$. This quadratic equation in A has two roots of which only the positive one has a real meaning, so that $A(p_h) = (1 + \sqrt{2})K/2$. This choice of the level p_h will lead to the relatively simple relation (4.34) as is shown.

Using $F(p_i) = 0$ and $F(p_h) = -F(p_j) = -K^2/4$, it follows after the substitution of these results into (4.31), (4.32) and (4.33) that

$$F'_h = F'_i = F'_j = -4F/(K^2) \quad (4.34)$$

Thus the characteristic levels p_h , p_i and p_j for D can be computed, as A is a known function of p . The equations which have to be solved for that purpose are summarized below.

$$A(p_h) = (1 + \sqrt{2})K/2, \quad (4.35)$$

$$A(p_i) = K, \quad (4.36)$$

and

$$A(p_j) = K/2 \quad (4.37)$$

Taking the value of $K = 0.99$ for 25-3-'71, 00 GMT, it follows that $A(p_h) = 1.20$, so that according to table 2 in section III 2.1, p_h is found at 375 mbar. This level in the troposphere is relatively far remote from the level at 230 mbar, where the maximum value of the divergence was found for the reference atmosphere. However, it follows from table 18 in III 4.4 that according to the stability analysis for the most unstable wave

the divergence D consists of two parts D_1' and D_2' of which each part possesses its own characteristic levels. These levels for D_1' are 600 mbar ($D_1' = 0$), 200 and 1000 mbar (maximum absolute value). Those levels for D_2' are 600 mbar (minimum value), 200 and 1000 mbar (maximum value), and two levels where $D_2' = 0$, namely one between 300 and 400 mbar and one between 800 and 900 mbar.

So the choice of 375, 510 and 810 mbar in the troposphere for p_h , p_i and p_j , respectively, seems a reasonable compromise between the characteristic levels of the reference atmosphere for 25-3-'71, 00 GMT, the levels of the stable wave according to table 17 and those of the most unstable wave in table 18 in III 4.4.

After the specification of p_h , p_i and p_j it is possible to compute the integrals of D_d and ω_d in (4.12), (4.13) and (4.14) with the aid of (4.28), (4.29), (4.30) and (4.34). This is carried out in the next section.

3.2 Integrations of the prognostic equations

To simplify the following computations it is assumed that $K = 1$. This implies that the level of non-divergence of the reference atmosphere is exactly 500 mbar, as follows from (3.6).

The integral (4.12) can be split up into

$$\int_0^{p_h} D dp + \int_{p_h}^{p_i} D dp + \int_{p_i}^{p_{10}} D dp = 0$$

Using (4.28)-(4.30) and (4.34) with $K = 1$ one obtains after some computations that

$$D_i = \alpha^*(D_{ij} - D_{hi}) \quad (4.38)$$

$$\text{with } \alpha^* \equiv \left[4 \int_{p_i}^{p_{10}} F dp \right] / \left[4 \int_{p_h}^{p_{10}} F dp + \int_{p_h}^{p_{10}} dp \right]$$

Further (4.15) can be expressed as

$$\omega(p) = \int_p^{p_{10}} dp \cdot D_i - 4 \int_p^{p_{10}} F dp \cdot D_{ij} \quad \text{for } p_i \leq p \leq p_{10}, \quad (4.39)$$

$$\omega(p) = \omega(p_i) + \int_p^{p_i} dp \cdot D_i - 4 \int_p^{p_i} F dp \cdot D_{hi} \quad \text{for } p_h \leq p \leq p_i, \quad (4.40)$$

and

$$\omega(p) = \omega(p_h) - 4 \int_p^{p_h} F dp \cdot (D_i + D_{hi}) \quad \text{for } 0 \leq p \leq p_h \quad (4.41)$$

Because $p_i = p_5$, due to $K = 1$, and $p_{8.5} < p_{10}$, the integral of ω in (4.14) can be computed with the aid of (4.38) and (4.39) as follows.

$$\int_{p_5}^{p_{8.5}} \omega dp = -a'_0 D_{ij} - a'_1 D_{hi} \quad (4.42)$$

with

$$a'_1 \equiv \alpha^* \int_{p_5}^{p_{8.5}} \left(\int_p^{p_{10}} dp \right) dp$$

and

$$a'_0 \equiv 4 \int_{p_5}^{p_{8.5}} \left(\int_p^{p_{10}} F dp \right) dp - a'_1$$

With the aid of (4.40) and (4.41) the similar integral in (4.13) can be computed as

$$\int_{p_3}^{p_5} \omega dp = \int_{p_3}^{p_h} \omega dp + \int_{p_h}^{p_5} \omega dp = -b'_0 D_{ij} - b'_1 D_{hi} \quad (4.43)$$

with

$$b'_0 \equiv 4 \int_{p_3}^{p_5} \left(\int_{p_5}^{p_{10}} F dp \right) dp - \beta^*, \quad b'_1 \equiv 4 \int_{p_3}^{p_5} \left(\int_p^{p_5} F dp \right) dp + \beta^*$$

and

$$\beta^* \equiv \left[\int_{p_h}^{p_5} \left(\int_p^{p_{10}} dp \right) dp + \int_{p_3}^{p_h} \left(\int_{p_h}^{p_{10}} dp \right) dp - 4 \int_{p_3}^{p_h} \left(\int_p^{p_h} F dp \right) dp \right] \alpha^*$$

For the further computation of the integrals of (4.13) and (4.14) it is assumed that the quasi-geostrophic streamfunction ψ satisfies for

$$p_3 \leq p \leq p_5 : \quad \psi = \psi_5 + C_3(p) \cdot \psi'_3 + E_3(p) \quad (4.44)$$

with

$$\psi'_3 \equiv \psi_3 - \psi_5, \quad C_3(p_3) = 1, \quad C_3(p_5) = 0, \quad E_3(p_3) = E_3(p_5) = 0,$$

and for

$$p_5 \leq p \leq p_{8.5} : \quad \psi = \psi_5 + C_{8.5}(p) \cdot \psi'_{8.5} + E_{8.5}(p) \quad (4.45)$$

with

$$\psi'_{8.5} \equiv \psi_5 - \psi_{8.5}, \quad C_{8.5}(p_5) = 0, \quad C_{8.5}(p_{8.5}) = -1, \quad E_{8.5}(p_5) = E_{8.5}(p_{8.5}) = 0$$

ψ_3 , ψ_5 and $\psi_{8.5}$ are the streamfunctions at respectively 300, 500 and 850 mbar. The functions C_3 , $C_{8.5}$, E_3 and $E_{8.5}$ need not further be specified for the computations of the integrals of (4.13) and (4.14). Using (4.42), (4.43), (4.44) and (4.45) the integrals in (4.13) and (4.14) are determined completely and the equations become

$$\psi'_3 + J(\psi_5, \psi'_3) + \frac{\sigma_{3-5}}{f_0} (b'_0 D_{ij} + b'_1 D_{hi}) - \varepsilon_3 = 0 \quad (4.46)$$

and

$$\psi'_{8.5} + J(\psi_5, \psi'_{8.5}) + \frac{\sigma_{5-8.5}}{f_0} (a'_0 D_{ij} + a'_1 D_{hi}) - \varepsilon_{8.5} = 0 \quad (4.47)$$

with a'_0 and a'_1 given in (4.42) and b'_0 and b'_1 in (4.43). It follows from (4.28), (4.34) and (4.38) that

$$D_3 - D_5 = d'_0 D_{ij} + d'_1 D_{hi} \quad (4.48)$$

with

$$d'_0 \equiv -\alpha^* [1 + 4F(p_3)] \quad \text{and} \quad d'_1 \equiv -4F(p_3) - d'_0$$

In a similar way it can be deduced with the aid of (4.30) and (4.34) that

$$D_5 - D_{8.5} = c'_0 D_{ij} \quad (4.49)$$

with $c'_0 \equiv 4F(p_{8.5})$

Subtracting the vorticity equation (4.10) from (4.9), using (4.48) yields

$$\nabla^2 \psi'_3 + J(\psi_5, \nabla^2 \psi'_3) + J(\psi'_3, \nabla^2 \psi_5 + \nabla^2 \psi'_3 + f) = -f_0 d'_0 D_{ij} - f_0 d'_1 D_{hi} \quad (4.50)$$

In a similar way it can be shown that with the aid of (4.10), (4.11) and (4.49)

$$\nabla^2 \dot{\psi}'_{8.5} + J(\psi_5, \nabla^2 \psi'_{8.5}) + J(\psi'_{8.5}, \nabla^2 \psi_5 - \nabla^2 \psi'_{8.5} + f) = -f_0 c'_0 D_{ij} \quad (4.51)$$

Taking $D_i = D_5$, equation (4.10) can be written as

$$\nabla^2 \dot{\psi}'_5 + J(\psi_5, \nabla^2 \psi_5 + f) = -f_0 D_i \quad (4.52)$$

The basic set of prognostic equations of the dry BK3-model is now formed by (4.38), (4.46), (4.47), (4.50), (4.51) and (4.52). These six equations contain the six unknown quantities D_i , D_{hi} , D_{ij} , $\dot{\psi}'_5$, $\dot{\psi}'_3$ and $\dot{\psi}'_{8.5}$. The correction terms ε_3 and $\varepsilon_{8.5}$ are given by (4.23) and (4.24). The barotropic tendency $\dot{\psi}'_5$ is given by (4.25). The formulas for the static stability parameters σ_{3-5} and $\sigma_{5-8.5}$ are (4.26) and (4.27).

3.3 Equations of the dry BK3-model in β -plane approximation

To get the equations of the dry BK3-model, the three divergences D_{hi} , D_{ij} and D_i are eliminated. For that purpose D_{ij} and D_{hi} are solved from the set of equations (4.46) and (4.47) with the following results.

$$\begin{aligned} D_{ij} = & -\frac{f_0 \cdot b'_1}{\sigma_{5-8.5} \cdot \Delta} [\dot{\psi}'_{8.5} + J(\psi_5, \psi'_{8.5}) - \varepsilon_{8.5}] \\ & + \frac{f_0 \cdot a'_1}{\sigma_{3-5} \cdot \Delta} [\dot{\psi}'_3 + J(\psi_5, \psi'_3) - \varepsilon_3] \end{aligned} \quad (4.53)$$

and

$$\begin{aligned} D_{hi} = & +\frac{f_0 \cdot b'_0}{\sigma_{5-8.5} \cdot \Delta} [\dot{\psi}'_{8.5} + J(\psi_5, \psi'_{8.5}) - \varepsilon_{8.5}] \\ & -\frac{f_0 \cdot a'_0}{\sigma_{3-5} \cdot \Delta} [\dot{\psi}'_3 + J(\psi_5, \psi'_3) - \varepsilon_3] \end{aligned} \quad (4.54)$$

with $\Delta \equiv a'_0 \cdot b'_1 - a'_1 \cdot b'_0$

With the aid of (4.23), (4.24), (4.26), (4.27) and the definitions of a'_0 , a'_1 , b'_0 and b'_1 given by (4.42) and (4.43) it can be shown after some computational work that

$$\frac{b'_0 + b'_1}{\sigma_{5-8.5}} \varepsilon_{8.5} - \frac{a'_0 + a'_1}{\sigma_{3-5}} \varepsilon_3 = 0 \quad (4.55)$$

Substitution of the results of (4.53), (4.54) and (4.55) into (4.38) then yields

$$D_i = -\frac{f_0 \alpha^*(b'_0 + b'_1)}{\sigma_{5-8.5} \cdot \Delta} [\dot{\psi}'_{8.5} + J(\psi_5, \psi'_{8.5})] + \frac{f_0 \alpha^*(a'_0 + a'_1)}{\sigma_{3-5} \cdot \Delta} [\dot{\psi}'_3 + J(\psi_5, \psi'_3)] \quad (4.56)$$

To obtain the equations of the BK3-model (4.53) and (4.54) are substituted into (4.50) and (4.51), using (4.23) and (4.24). Further (4.56) is substituted into (4.52). The resulting equations finally become

$$\nabla^2 \dot{\psi}'_5^* = -J(\psi_5, \nabla^2 \psi_5 + f), \quad (4.57)$$

$$(\nabla^2 - a_{00}) \dot{\psi}'_{8.5} + a_{01} \dot{\psi}'_3 = -J(\psi_5, \nabla^2 \psi'_{8.5} - a_{00} \psi'_{8.5} + a_{01} \psi'_3 - a_{04} \nabla^2 \psi_5) - J(\psi'_{8.5}, \nabla^2 \psi_5 - \nabla^2 \psi'_{8.5} + f) - a_{05} \dot{\psi}'_5^*, \quad (4.58)$$

$$(\nabla^2 - a_{10}) \dot{\psi}'_3 + a_{11} \dot{\psi}'_{8.5} = -J(\psi_5, \nabla^2 \psi'_3 - a_{10} \psi'_3 + a_{11} \psi'_{8.5} - a_{14} \nabla^2 \psi_5) - J(\psi'_3, \nabla^2 \psi_5 + \nabla^2 \psi'_3 + f) - a_{15} \dot{\psi}'_5^*, \quad (4.59)$$

and

$$\nabla^2 \dot{\psi}'_5 = -J(\psi_5, \nabla^2 \psi_5 + f - a_{00} \psi'_{8.5} + a_{01} \psi'_3) + a_{05} \dot{\psi}'_{8.5} - a_{15} \dot{\psi}'_3 \quad (4.60)$$

with

$$a_0 \equiv \frac{f_0^2}{\sigma_{5-8.5}} \frac{\alpha^*(b'_0 + b'_1)}{\Delta}, \quad a_1 \equiv \frac{f_0^2}{\sigma_{3-5}} \frac{\alpha^*(a'_0 + a'_1)}{\Delta}, \quad (4.61)$$

$$a_{00} \equiv \frac{f_0^2}{\sigma_{5-8.5}} \frac{c'_0 \cdot b'_1}{\Delta}, \quad a_{01} \equiv \frac{f_0^2}{\sigma_{3-5}} \frac{c'_0 \cdot a'_1}{\Delta}, \quad (4.62)$$

$$a_{10} \equiv \frac{f_0^2}{\sigma_{3-5}} \frac{d'_1 \cdot a'_0 - d'_0 \cdot a'_1}{\Delta} \quad \text{and} \quad a_{11} \equiv \frac{f_0^2}{\sigma_{5-8.5}} \frac{d'_1 \cdot b'_0 - d'_0 \cdot b'_1}{\Delta} \quad (4.63)$$

The coefficients resulting from the correction terms ε_3 and $\varepsilon_{8.5}$ are

$$a_{04} \equiv c'_0/4 = F(p_{8.5}), \quad a_{05} \equiv a_{00}(1 - A_{8.5}) - a_{01}(A_3 - 1) \quad (4.64)$$

$$a_{14} \equiv (d'_0 + d'_1)/4 = -F(p_3) \quad \text{and} \quad a_{15} \equiv a_{10}(A_3 - 1) - a_{11}(1 - A_{8.5}) \quad (4.65)$$

Due to $-\int_0^p (A - A^2) dp = \int_p^{p_{10}} (A - A^2) dp$ for $K = 1$, the two static stability parameters σ_{3-5} and $\sigma_{5-8.5}$, which are given by (4.26) and (4.27), can also be expressed as

$$\frac{\sigma_{3-5}}{f_0^2} = \frac{(A_3 - 1)(1 - \beta \cdot L^*/U_5)L^*}{\int_{p_3}^{p_5} \left[\int_p^{p_{10}} (A - A^2) dp \right] dp} \quad (4.66)$$

and

$$\frac{\sigma_{5-8.5}}{f_0^2} = \frac{(1 - A_{8.5})(1 - \beta \cdot L^*/U_5)L^*}{\int_{p_5}^{p_{8.5}} \left[\int_p^{p_{10}} (A - A^2) dp \right] dp} \quad (4.67)$$

3.4 Computation of the coefficients

The coefficients of the equations are given by the formulas (4.61)–(4.65) of the previous section. They depend on the A -values of the reference atmosphere, which have been evaluated in Chapter III for the date 25-3-'71, 00 GMT, and also on the two static stability parameters σ_{3-5} and $\sigma_{5-8.5}$. The relations for the coefficients contain double integrals. When the function A is approximated by an analytical expression, these double integrals can fairly easily be computed. Inspection of table 2 and of figure 4 shows that from 300 to 1000 mbar A is approximately a linear function of p . To define this function it is assumed that the values of A at 500 and 850 mbar given in that table are exactly fulfilled. Then the linear function becomes $A = -1.6286 p/p_{10} + 1.8143$. Using this formula, A has been computed for several values of p and compared with the values in table 2. See table 20.

pressure mbar	linear approximation of A	A according to table 2
300	1.3257	1.33
400	1.1629	1.16
500	1.0000	1.00
600	0.8371	0.84
700	0.6743	0.67
800	0.5114	0.51
850	0.4300	0.43
900	0.3486	0.35
1000	0.1857	0.20

Table 20 Comparison of a linear approximation of A with the values in table 2.

With the help of (4.35), (4.36) and (4.37) in 3.1 and the assumption that $K = 1$ the three characteristic levels of D can be computed, which results in $A(p_h) = 1.2071$ and

$p_h = 372.8$ mbar, $A(p_i) = 1$ and $p_i = p_5 = 500$ mbar, $A(p_j) = 0.5$ and $p_j = 807.0$ mbar. These values of p_h , p_i and p_j are nearly the same as those computed in 3.1.

Now it is possible to compute α^* , a'_0 , a'_1 , b'_0 and b'_1 from (4.38), (4.42) and (4.43). c'_0 , d'_0 and d'_1 can be computed from (4.49) and (4.48). The values are given below.

$$\begin{aligned}\alpha^* &= 0.3962, \\ a'_0 &= 5.193 \times 10^8 \text{ m}^{-2}\text{kg}^2\text{s}^{-4}, \quad a'_1 = 4.507 \times 10^8 \text{ m}^{-2}\text{kg}^2\text{s}^{-4}, \\ b'_0 &= 2.667 \times 10^8 \text{ m}^{-2}\text{kg}^2\text{s}^{-4}, \quad b'_1 = 3.769 \times 10^8 \text{ m}^{-2}\text{kg}^2\text{s}^{-4}, \\ \Delta &\equiv a'_0 b'_1 - a'_1 b'_0 = 7.560 \times 10^{16} \text{ m}^{-4}\text{kg}^4\text{s}^{-8}, \\ c'_0 &= 0.9804, \quad d'_0 = 0.2881, \quad d'_1 = 1.4390\end{aligned}\tag{4.68}$$

(4.61)–(4.63) show that the parts of the coefficients not depending on the static stability parameters are

$$\begin{aligned}a_{00}^* &\equiv \frac{\alpha^*(b'_0 + b'_1)}{\Delta} = 0.3373 \times 10^{-8} \text{ m}^2\text{kg}^{-2}\text{s}^4, \\ a_{11}^* &\equiv \frac{\alpha^*(a'_0 + a'_1)}{\Delta} = 0.5084 \times 10^{-8} \text{ m}^2\text{kg}^{-2}\text{s}^4, \\ a_{00}^* &\equiv \frac{c'_0 b'_1}{\Delta} = 0.4888 \times 10^{-8} \text{ m}^2\text{kg}^{-2}\text{s}^4, \\ a_{01}^* &\equiv \frac{c'_0 a'_1}{\Delta} = 0.5845 \times 10^{-8} \text{ m}^2\text{kg}^{-2}\text{s}^4, \\ a_{10}^* &\equiv \frac{d'_1 a'_0 - d'_0 a'_1}{\Delta} = 0.8168 \times 10^{-8} \text{ m}^2\text{kg}^{-2}\text{s}^4, \\ a_{11}^* &\equiv \frac{d'_1 b'_0 - d'_0 b'_1}{\Delta} = 0.3638 \times 10^{-8} \text{ m}^2\text{kg}^{-2}\text{s}^4\end{aligned}\tag{4.69}$$

The static stability parameters σ_{3-5} and $\sigma_{5-8.5}$ can be computed with the aid of (4.66) and (4.67) respectively. Each of them depends on two parts, namely one part defined by the A -values of the reference atmosphere and the other part depending on the wavelength L_x , the ratio L_x/L_y and the zonal wind U_5 of the basic flow. The numerical values of L_x/L_y and U_5 , which were valid for the polar jetstream at 25-3-'71, 00 GMT, have been taken from table 4. The values of A have been taken from table 20. For L_x the mean value of the lengths of the line segments between the points of maximum RVA-values of the polar jetstream was chosen. This length was 1550 km. The results of all computations together with the numerical values of U_5 , L_x , L_x/L_y and β are given below.

$$U_5 = 31 \text{ ms}^{-1}, \quad L_x = 1550 \times 10^3 \text{ m}, \quad L_x/L_y = 0.48,$$

$$\beta = 1.619 \times 10^{-11} \text{ m}^{-1} \text{ s}^{-1} \text{ at } 45^\circ \text{N},$$

$$\frac{A_3 - 1}{\int_{p_3}^{p_5} \left[\int_p^{p_{10}} (A - A^2) dp \right] dp} = 0.2025 \times 10^{-8} \text{ m}^2 \text{ kg}^{-2} \text{ s}^4,$$

$$\frac{1 - A_{8.5}}{\int_{p_5}^{p_{8.5}} \left[\int_p^{p_{10}} (A - A^2) dp \right] dp} = 0.2350 \times 10^{-8} \text{ m}^2 \text{ kg}^{-2} \text{ s}^4,$$

$$\beta L^*/U_5 = 0.0258, \quad (1 - \beta L^*/U_5)L^* = 4.818 \times 10^{10} \text{ m}^2,$$

$$\frac{\sigma_{3-5}}{f_0^2} = 97.57 \text{ m}^4 \text{ kg}^{-2} \text{ s}^4, \quad \frac{\sigma_{5-8.5}}{f_0^2} = 113.2 \text{ m}^4 \text{ kg}^{-2} \text{ s}^4,$$

$$a_0 = 2.980 \times 10^{-11} \text{ m}^{-2}, \quad a_1 = 5.211 \times 10^{-11} \text{ m}^{-2},$$

$$a_{00} = 4.318 \times 10^{-11} \text{ m}^{-2}, \quad a_{01} = 5.991 \times 10^{-11} \text{ m}^{-2},$$

$$a_{10} = 8.371 \times 10^{-11} \text{ m}^{-2}, \quad a_{11} = 3.214 \times 10^{-11} \text{ m}^{-2},$$

$$a_{04} = 0.2451, \quad a_{05} = 0.5100 \times 10^{-11} \text{ m}^{-2},$$

$$a_{14} = 0.4312, \quad a_{15} = 0.8945 \times 10^{-11} \text{ m}^{-2} \quad (4.70)$$

The numerical values of the coefficients are specifically related to the data of 25-3-'71, 00 GMT. However, in principle it is possible to define the coefficients for every moment according to the method described in this article. As has already been outlined in III 2.1, the A -values of table 2 are fairly realistic for polar jetstream conditions over the Atlantic and Western Europe. Therefore these A -values have been used for all experiments described in Chapter V.

Concerning the static stability parameters which have been computed with the aid of (4.66) and (4.67), using a value of 1550 km for L_x , the use of a value between 1600 and 2000 km is perhaps more realistic as can be seen from table 11, where the frequency of the diameters of depressions at sea level is given. These values are based on 288 cases for the years 1965, 1966 and 1967, whereas the wavelength of 1550 km is based only on the situation of 25-3-'71, 00 GMT. A value of 1800 km for L_x results in somewhat higher values of the static stabilities of the model, making the model more stable. However, a dry version of the model, which is perhaps too unstable, is not so serious for the experiments described in Chapter V, since it has been shown in these

experiments that explosive development at sea level (deepening of 20 mbar or more in 24 hours) is not possible with the dry version of the model, but only with the moist one.

4 The inclusion of the release of latent heat

4.1 Description of the method

The 'moist' set of equations is given by (4.16)–(4.22) with the boundary conditions $\omega_m = 0$ for $p = 0$ and $p = 1000$ mbar. The lateral boundary condition is $\psi'_{m3} = \psi'_{m5} = \psi'_{m8.5} = 0$ at the boundary of the computational area.

Subtraction of (4.17) from (4.16) and (4.18) from (4.17) gives

$$\nabla^2 \psi'_{m3} = -f_o \cdot D'_{m3} \quad (4.71)$$

and

$$\nabla^2 \psi'_{m8.5} = -f_o \cdot D'_{m8.5} \quad (4.72)$$

with

$$\psi'_{m3} \equiv \psi_{m3} - \psi_{m5}, \quad \psi'_{m8.5} \equiv \psi_{m5} - \psi_{m8.5}, \quad D'_{m3} \equiv D_{m3} - D_{m5} \quad \text{and}$$

$$D'_{m8.5} \equiv D_{m5} - D_{m8.5}$$

Equations (4.20) and (4.21) can also be written as

$$\psi'_{m3} = \int_{p_3}^{p_5} \frac{R \cdot Q}{c_p f_o p} dp + \frac{\sigma_{3-5}}{f_o} \int_{p_3}^{p_5} \omega_m dp \quad (4.73)$$

and

$$\psi'_{m8.5} = \int_{p_5}^{p_{8.5}} \frac{R \cdot Q}{c_p f_o p} dp + \frac{\sigma_{5-8.5}}{f_o} \int_{p_5}^{p_{8.5}} \omega_m dp \quad (4.74)$$

For the computations of the integral of D_m in (4.19) and those of ω_m in (4.73) and (4.74) the profile of D_m as a function of p has to be known. It is assumed that in the stratosphere with $p \leq 200$ mbar $D_m = 0$, so that according to the continuity equation

$\frac{\partial \omega_m}{\partial p} = 0$ or $\omega_m = 0$. According to the conclusion 2 in section III 5 for the troposphere

below 200 mbar, a linear profile is chosen between the levels 200, 300, 500, 850 and 1000 mbar. The formulas are given below.

$$0 \leq p \leq 200 \text{ mbar: } D_m = 0 \quad (4.75)$$

$$200 \leq p \leq 300 \text{ mbar: } D_m = \frac{p - p_2}{p_3 - p_2} D_{m3} = \frac{p - p_2}{p_3 - p_2} (D_{m5} + D'_{m3}) \quad (4.76)$$

$$300 \leq p \leq 500 \text{ mbar: } D_m = D_{m5} + \frac{p_5 - p}{p_5 - p_3} D'_{m3} \quad (4.77)$$

$$500 \leq p \leq 850 \text{ mbar: } D_m = D_{m5} - \frac{p - p_5}{p_{8.5} - p_5} D'_{m8.5} \quad (4.78)$$

$$850 \leq p \leq 1000 \text{ mbar: } D_m = D_{m8.5} = D_{m5} - D'_{m8.5} \quad (4.79)$$

Thus below 850 mbar D_m is constant and equals $D_{m8.5}$. It appeared that the results of the calculations with other linear profiles of D_m below 850 mbar were not significantly different from those with a constant D_m .

Now using (4.22) and (4.75)–(4.79), ω_m and the integrals of ω_m in (4.73) and (4.74) can be computed for the chosen layers. The results are given below.

$0 \leq p \leq 200 \text{ mbar:}$

$$\omega_m = 0 \quad (4.80)$$

$200 \leq p \leq 300 \text{ mbar:}$

$$\omega_m = -\frac{1}{2} \frac{(p - p_2)^2}{(p_3 - p_2)} (D_{m5} + D'_{m3}) \quad (4.81)$$

and

$$\omega_{m3} = -\frac{1}{2}(p_3 - p_2) (D_{m5} + D'_{m3}) \quad (4.82)$$

$300 \leq p \leq 500 \text{ mbar:}$

$$\omega_m = -[p - p_3 + \frac{1}{2}(p_3 - p_2)]D_{m5} - \left[\frac{1}{2}(p_5 - p_2) - \frac{1}{2} \frac{(p_5 - p)^2}{(p_5 - p_3)} \right] D'_{m3} \quad (4.83)$$

and

$$\omega_{m5} = -\frac{1}{2}(2p_5 - p_2 - p_3) D_{m5} - \frac{1}{2}(p_5 - p_2) D'_{m3} \quad (4.84)$$

Applying (4.83) one gets

$$\int_{p_3}^{p_5} \omega_m dp = -\frac{p_5 - p_3}{6} [3(p_5 - p_2)D_{m5} + (2p_5 + p_3 - 3p_2)D'_{m3}] \quad (4.85)$$

$500 \leq p \leq 850$ mbar:

$$\omega_m = -[p - \frac{1}{2}(p_2 + p_3)]D_{m5} - \frac{1}{2}(p_5 - p_2)D'_{m3} + \frac{1}{2} \frac{(p - p_5)^2}{(p_{8.5} - p_5)} D'_{m8.5} \quad (4.86)$$

and

$$\omega_{m8.5} = -\frac{1}{2}(2p_{8.5} - p_3 - p_2)D_{m5} - \frac{1}{2}(p_5 - p_2)D'_{m3} + \frac{1}{2}(p_{8.5} - p_5)D'_{m8.5} \quad (4.87)$$

Applying (4.86) one gets

$$\int_{p_5}^{p_{8.5}} \omega_m dp = -\frac{p_{8.5} - p_5}{6} [3(p_{8.5} + p_5 - p_2 - p_3)D_{m5} + 3(p_5 - p_2)D'_{m3} - (p_{8.5} - p_5)D'_{m8.5}] \quad (4.88)$$

$850 \leq p \leq 1000$ mbar:

$$\omega_m = -[p - \frac{1}{2}(p_2 + p_3)]D_{m5} - \frac{1}{2}(p_5 - p_2)D'_{m3} + [p - \frac{1}{2}(p_{8.5} + p_5)]D'_{m8.5} \quad (4.89)$$

and

$$\omega_{m10} = -\frac{1}{2}(2p_{10} - p_2 - p_3)D_{m5} - \frac{1}{2}(p_5 - p_2)D'_{m3} + \frac{1}{2}(2p_{10} - p_{8.5} - p_5)D'_{m8.5} \quad (4.90)$$

Using the boundary condition $\omega_{m10} = 0$, (4.90) can be expressed as

$$(2p_{10} - p_2 - p_3)D_{m5} = (2p_{10} - p_{8.5} - p_5)D'_{m8.5} - (p_5 - p_2)D'_{m3} \quad (4.91)$$

If the integrals of the heating terms in (4.73) and (4.74) are known, then after substitution of the results of (4.85) into (4.73) and of (4.88) into (4.74), equations (4.17), (4.71), (4.72), (4.73), (4.74), and (4.91) contain six unknowns, namely ψ_{m5} , ψ'_{m3} , $\psi'_{m8.5}$, D_{m5} , $D'_{m8.5}$ and D'_{m3} . After elimination of the three moist divergences, one Poisson-equation and two Helmholtz-equations result, which could be solved with the use of the lateral boundary condition $\psi'_{m3} = \psi'_{m8.5} = \psi_{m5} = 0$. However, a difficulty presents itself, because the heating function Q is not completely known. It consists of the sum of a so-called dry and a moist part (see (4.93)) of which only the dry part is known. There is a possibility to overcome this difficulty, and as can be seen this will also result in a simplification of the equations.

Substitution of (4.17), (4.71) and (4.72) into (4.91) results in the following Poisson-equation.

$$\nabla^2 [(2p_{10} - p_2 - p_3)\psi_{m5} - (2p_{10} - p_{8.5} - p_5)\psi'_{m8.5} + (p_5 - p_2)\psi'_{m3}] = 0$$

In accordance with the condition that $\psi'_{m3} = \psi'_{m5} = \psi'_{m8.5} = 0$ at the boundary of the computational area, the solution of this equation reads

$$(2p_{10} - p_2 - p_3)\psi'_{m5} - (2p_{10} - p_{8.5} - p_5)\psi'_{m8.5} + (p_5 - p_2)\psi'_{m3} = 0 \quad (4.92)$$

If q denotes the specific humidity and q_s its saturated value, then in the case of release of latent heat $q = q_s$ and $\frac{dq_s}{dt} = \frac{dq}{dt} < 0$. Then the heating term Q equals $Q = -L \frac{dq_s}{dt}$ with L the latent heat of condensation. It can be shown that after some computational work (see for instance HALTNER (1971)) that

$$\frac{R \cdot Q}{c_p f_o p} = - \frac{R \cdot L}{c_p f_o p} \frac{dq_s}{dt} = - \frac{\sigma_{s.ad.} \omega}{f_o}$$

with $\sigma_{s.ad.}$ the static stability with respect to a saturated adiabatic lapse rate. Since ω can be split up into a dry and a moist part as $\omega = \omega_d + \omega_m$, the heating term Q can also be divided as follows

$$\frac{R \cdot Q}{c_p f_o p} = - \frac{\sigma_{s.ad.}}{f_o} \omega_d - \frac{\sigma_{s.ad.}}{f_o} \omega_m \quad (4.93)$$

Now the following assumptions are made:

1. If there is no release of latent heat in the layer between 500 and 850 mbar, also no release is permitted in the layer between 300 and 500 mbar.
2. Only release of latent heat is taken into account if there is condensation in the whole column of air between 500 and 850 mbar, so that with the use of (4.93), (4.74) can be expressed as

$$\psi'_{m8.5} = - \int_{p_5}^{p_{8.5}} \frac{\sigma_{s.ad.}}{f_o} (\omega_m + \omega_d) dp + \frac{\sigma_{5-8.5}}{f_o} \int_{p_5}^{p_{8.5}} \omega_m dp \approx - \frac{\sigma_{5-8.5}}{f_o} \int_{p_5}^{p_{8.5}} \omega_d dp$$

because of $\sigma_{5-8.5} \approx \sigma_{s.ad.}$ due to the value of the static stability parameter $\sigma_{5-8.5}$, which is approximately equal to $\sigma_{s.ad.}$ for a saturated potential temperature of 10°C. See (4.70) in 3.4 and table 8 in III 3.3.

3. If there is release of latent heat in the layer between 500 and 850 mbar, it is assumed for the layer between 300 and 500 mbar that latent heat is partly released,

namely between p_x and p_5 with $p_3 < p_x < p_5$. Then using (4.93), (4.73) can be expressed as

$$\psi'_{m3} = - \int_{p_x}^{p_5} \frac{\sigma_{s.ad.}}{f_0} (\omega_d + \omega_m) dp + \frac{\sigma_{3-5}}{f_0} \int_{p_3}^{p_5} \omega_m dp \approx \frac{\sigma_{3-5}}{f_0} \left(\int_{p_3}^{p_x} \omega_m dp - \int_{p_x}^{p_5} \omega_d dp \right)$$

due to $\sigma_{3-5} \approx \sigma_{s.ad.}$. In section III 3.5 it has been shown that in the centre of a young developing frontal wave in which release of latent heat is taking place, ω_d and ω_m have the same negative sign and are of the same order of magnitude between 300 and 500 mbar (see table 12), so that near 400 mbar a level \tilde{p}_x exists where

$$\int_{p_x}^{\tilde{p}_x} \omega_m dp = \int_{\tilde{p}_x}^{p_5} \omega_d dp.$$

Here it is assumed that $p_x = \tilde{p}_x$. Of course this assumption is in general not exactly valid for developing frontal waves, although the assumption that latent heat is partly released in the layer from 300 to 500 mbar is not unrealistic for such waves, so that in many cases p_x will be close to \tilde{p}_x . To investigate the consequences if $p_x \neq \tilde{p}_x$, other possibilities, namely $p_x = p_5$ and $p_x = p_3$ are considered in 4.3.

Due to the three assumptions, (4.73) and (4.74) reduce to

$$\psi'_{m3} = 0 \quad (4.94)$$

and

$$\psi'_{m8.5} = H_{8.5} \quad \text{with} \quad H_{8.5} \equiv - \frac{\sigma_{5-8.5}}{f_0} \int_{p_5}^{p_{8.5}} \omega_d dp \quad (4.95)$$

It follows from (4.92), (4.94) and (4.95) that

$$\psi'_{m5} = \frac{2p_{10} - p_{8.5} - p_5}{2p_{10} - p_2 - p_3} H_{8.5} = 0.43 H_{8.5},$$

$$\psi'_{m3} = 0.43 H_{8.5} \quad \text{and} \quad \psi'_{m8.5} = -0.57 H_{8.5} \quad (4.96)$$

(4.94), (4.95) and (4.96) form the complete set of equations, which are used to correct the computed tendencies of the 'dry' BK3-equations by adding the moist tendencies to them. The heating term $H_{8.5}$ is determined with the computed precipitation from the equations of the 'dry' model. These precipitation computations have been extensively described by EXTER BLOKLAND, DEN (1972).

It has to be noted here that in the case that no release of latent heat is taking place at all, $H_{8.5} = 0$ and $\psi'_{m3} = \psi'_{m8.5} = \psi'_{m5} = D'_{m3} = D'_{m8.5} = D_{m5} = 0$ is the exact solution of the set of equations (4.17), (4.71), (4.72), (4.73), (4.74) and (4.91). With release of latent heat, (4.94), (4.95) and (4.96) can be considered to be a first-order approximation of the solution, which is exact for a specified value of p_x close to 400 mbar.

4.2 *Comparison of the method with the results of section III 3.5*

The results obtained in the previous section will be further worked out and compared with those of III 3.5, which are valid for the centres of young developing short frontal waves.

From (4.17) and (4.96) it follows that

$$D_{m5} = - \frac{2p_{10} - p_{8.5} - p_5}{(2p_{10} - p_2 - p_3)f_0} \nabla^2 H_{8.5} = - \frac{0.43}{f_0} \nabla^2 H_{8.5} \quad (4.97)$$

Combination of (4.71) with (4.94) and of (4.72) with (4.95) gives

$$D'_{m3} = 0 \quad (4.98)$$

and

$$D'_{m8.5} = - \frac{1}{f_0} \nabla^2 H_{8.5} \quad (4.99)$$

Substitutions of (4.97), (4.98) and (4.99) into (4.82), (4.84) and (4.87) give

$$\omega_{m3} = \frac{0.22 \times 10^4}{f_0} \nabla^2 H_{8.5}, \quad (4.100)$$

$$\omega_{m5} = \frac{1.08 \times 10^4}{f_0} \nabla^2 H_{8.5}, \quad (4.101)$$

and

$$\omega_{m8.5} = \frac{0.85 \times 10^4}{f_0} \nabla^2 H_{8.5} \quad (4.102)$$

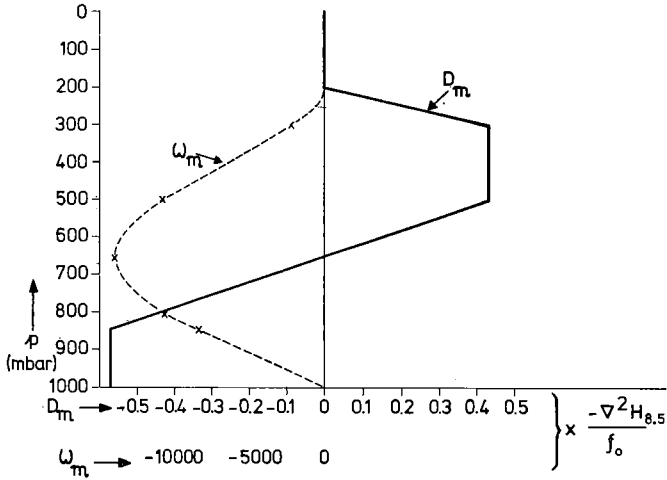


Fig. 18 The profiles of the 'moist' parts of the divergence D and the vertical velocity ω as functions of p used in the BK3-model.

Units: D_m in s^{-1} and ω_m in $m^{-1}kg s^{-3}$.

Formulas (4.75)–(4.79) and (4.97)–(4.99) show that the divergence D_m is completely determined as a function of pressure p and $\nabla^2 H_{8.5}$. Combination of (4.97)–(4.102) with (4.80)–(4.90) determines the profile of ω_m as a function of p and $\nabla^2 H_{8.5}$. Figure 18, which has been taken from the report of HEIJBOER and EXTER BLOKLAND, DEN (1974), shows the profiles of D_m and ω_m . A level of non-divergence clearly exists between 500 and 850 mbar, which can be found by setting $D_m = 0$ in (4.78) and using the results of (4.97) and (4.99). This level is found at 652 mbar. At this level ω_m becomes

$$\omega_{m6.52} = \frac{1.41 \times 10^4}{f_0} \nabla^2 H_{8.5} \quad (4.103)$$

In section III 3.5 the level of non-divergence of D_m was found at 600 mbar for the two-parameter model.

To compare the numerical values of the moist D_m and ω_m with those of table 12 in III 3.5, it is assumed that the dry parts of ω , namely ω_d 's, are the same in both cases and equal those of the reference atmosphere. Then according to (3.70), (4.67) and (4.95), $H_{8.5}$ equals

$$\begin{aligned}
 H_{8.5} &= \frac{\sigma_{5-8.5}}{f_o^2} \int_{p_5}^{p_{8.5}} \left[\int_p^{p_{10}} (A - A^2) dp \right] dp \cdot \text{RVA} \\
 &= (1 - A_{8.5}) (1 - \beta L^*/U_5) L^* \cdot \text{RVA}
 \end{aligned} \tag{4.104}$$

Assuming that the streamfunction ψ at 500 mbar has the form of the sine-wave according to (3.15), then, using (3.16) and $A_{8.5} = 0.43$ according to table 2, the Laplacian of $H_{8.5}$ can be written as

$$\nabla^2 H_{8.5} = -0.57(1 - \beta L^*/U_5) \text{RVA} \tag{4.105}$$

Taking $\beta L^*/U_5 = 0.0258$ as in (4.70), $\nabla^2 H_{8.5}$ becomes

$$\nabla^2 H_{8.5} = -0.56 \text{RVA} \tag{4.106}$$

This result can be used to express $f_o D_m$ and $f_o \omega_m$ as functions of the advection of relative vorticity at 500 mbar. The computations have been carried out for pressure levels with intervals of 100 mbar after the substitution of (4.106) into (4.97) and (4.99), and using those results in the formulas for D_m and ω_m given by (4.75)–(4.90). The results are given in table 21.

pressure level (mbar)	$D_m^1 = f_o D_m / \text{RVA}$ according to table 12 of III 3.5	$f_o D_m / \text{RVA}$ used in the BK3-model	$\omega_m^1 = f_o \omega_m / \text{RVA}$ according to table 12 of III 3.5 ($10^4 \text{m}^{-1} \text{kg s}^{-2}$)	$f_o \omega_m / \text{RVA}$ used in the BK3-model ($10^4 \text{m}^{-1} \text{kg s}^{-2}$)
200	+0.64	0	0	0
300	+0.48	+0.24	-0.56	-0.12
400	+0.32	+0.24	-0.96	-0.36
500	+0.16	+0.24	-1.20	-0.60
600	0	+0.08	-1.28	-0.76
700	-0.16	-0.08	-1.20	-0.77
800	-0.32	-0.24	-0.96	-0.61
900	-0.48	-0.31	-0.56	-0.31
1000	-0.64	-0.31	0	0

Table 21 Comparison of the 'moist' D_m^1 and ω_m^1 according to the method in 4.1 with those in III 3.5 valid for the centres of young developing short frontal waves.

This table clearly shows that, assuming the RVA has the same value in both cases, the absolute values of D_m as well as of ω_m computed according to the method followed in this section are underestimated with respect to the values of III 3.5 except for the

divergences at 500 and 600 mbar. However, for the computations in the BK3-model not the moist D_m 's or ω 's themselves are used, but the moist tendencies of the streamfunction at 300, 500 and 850 mbar. Therefore, they will be compared with the moist tendencies of the two-parameter model in section III 3.5.

For that purpose the tendency of ψ as given in III 3.5 is split up into a dry and a moist part as $\dot{\psi} = \dot{\psi}_d + \dot{\psi}_m$. Then, according to (3.49) it can be shown that

$$\begin{aligned}\dot{\psi}_{m8.5} &= A_{8.5}\dot{\psi}_{m5} + C_{8.5}^*\dot{\psi}_m^*, & \dot{\psi}_{m3} &= A_3\dot{\psi}_{m5} + C_3^*\dot{\psi}_m^*, \\ \dot{\psi}'_{m8.5} &= (1 - A_{8.5})\dot{\psi}'_{m5} - C_{8.5}^*\dot{\psi}_m^* & \text{and} & \dot{\psi}'_{m3} = (A_3 - 1)\dot{\psi}'_{m5} + C_3^*\dot{\psi}_m^*\end{aligned}\quad (4.107)$$

$\dot{\psi}_5$ and $\dot{\psi}^*$ of the two-parameter model are defined by equations (3.55) and (3.57). (3.57) was derived from (3.34) after the application of the Laplacian operator. Without the Laplacian it reads

$$-K_4\dot{\psi}_5 + \frac{K_4}{K_1}[\dot{\psi}^* + J(\psi_5, \psi^*)] + \int_{p_5}^{p_{8.5}} \left(\frac{\sigma \cdot \omega}{f_0} + \frac{R \cdot Q}{c_p \cdot f_0 \cdot p} \right) dp = 0 \quad (4.108)$$

Without release of latent heat ($Q = 0$), (3.55) and (4.108) read

$$\begin{aligned}\nabla^2\dot{\psi}_{d5} + J(\psi_5, \nabla^2\psi_5 + f) &= -K_2[\nabla^2\dot{\psi}_d^* + J(\psi^*, \nabla^2\psi^*)] \\ &\quad - K_3J(\psi^*, \nabla^2\psi^*)\end{aligned}\quad (4.109)$$

and

$$-K_4\dot{\psi}_{d5} + \frac{K_4}{K_1}[\dot{\psi}_d^* + J(\psi_5, \psi^*)] = - \int_{p_5}^{p_{8.5}} \frac{\sigma \cdot \omega_d}{f_0} dp \quad (4.110)$$

With release of latent heat and using (3.62) the equations (3.55) and (4.108) can be expressed as

$$\begin{aligned}\nabla^2\dot{\psi}_{d5} + \nabla^2\dot{\psi}_{m5} + J(\psi_5, \nabla^2\psi_5 + f) &= -K_2[\nabla^2\dot{\psi}_d^* + \nabla^2\dot{\psi}_m^* + J(\psi^*, f)] \\ &\quad - K_3J(\psi^*, \nabla^2\psi^*)\end{aligned}\quad (4.111)$$

and

$$-K_4(\dot{\psi}_{d5} + \dot{\psi}_{m5}) + \frac{K_4}{K_1}[\dot{\psi}_d^* + \dot{\psi}_m^* + J(\psi_5, \psi^*)] = 0 \quad (4.112)$$

Subtraction of (4.109) from (4.111) and of (4.110) from (4.112) yields

$$\nabla^2\dot{\psi}_{m5} = -K_2\nabla^2\dot{\psi}_m^* \quad (4.113)$$

and

$$-K_4\psi_{m5} + \frac{K_4}{K_1}\psi_m^* = \int_{p_5}^{p_{8.5}} \frac{\sigma \cdot \omega_d}{f_o} dp \quad (4.114)$$

In accordance with the condition that $\psi_{m5} = \psi_m^* = 0$ at the boundary of the computational area, it follows from (4.113) that

$$\psi_{m5} = -K_2\psi_m^* \quad (4.115)$$

Now it follows from (4.114) and (4.115) that

$$\begin{aligned} \psi_{m5} &= -\frac{K_1K_2}{K_4(K_1K_2 + 1)} \int_{p_5}^{p_{8.5}} \frac{\sigma \cdot \omega_d}{f_o} dp \quad \text{and} \\ \psi_m^* &= \frac{K_1}{K_4(K_1K_2 + 1)} \int_{p_5}^{p_{8.5}} \frac{\sigma \cdot \omega_d}{f_o} dp \end{aligned} \quad (4.116)$$

Substitution of these expressions for ψ_{m5} and ψ_m^* into (4.107) using the definition of C^* in (3.48) and of K_1 and K_4 in (3.54) leads to

$$\psi'_{m8.5} = -\int_{p_5}^{p_{8.5}} \frac{\sigma \cdot \omega_d}{f_o} dp \quad \text{and} \quad \psi'_{m3} = -\frac{A_3 - 1}{K_4} \int_{p_5}^{p_{8.5}} \frac{\sigma \cdot \omega_d}{f_o} dp \quad (4.117)$$

In accordance with III 3.5 the following values are used: $A_3 = 1.32$, $K_1 = 0.8$, $K_2 = 0.2/0.84$ and $K_4 = 0.56$. Then it follows from (4.117) that $\psi'_{m8.5} = H_{8.5}$, $\psi'_{m3} = 0.57H_{8.5}$ and from (4.116) that $\psi_{m5} = 0.29H_{8.5}$. The tendencies $\psi_{m8.5}$ and ψ_{m3} become $\psi_{m8.5} = \psi_{m5} - \psi'_{m8.5} = -0.71H_{8.5}$ and $\psi_{m3} = \psi_{m5} + \psi'_{m3} = 0.86H_{8.5}$. These values can be compared with those of (4.96) used in the BK3-model. So for the BK3-model at 300 mbar there is a reduction of $\sim 50\%$ for ψ_{m3} and at 500 mbar an increase of $\sim 50\%$ for ψ_{m5} . At 850 mbar the absolute value of $\psi_{m8.5}$ has been decreased by $\sim 20\%$. So the difference is smallest at the lowest level.

The computed values for the two-parameter model in III.3.5 and those of (4.96) for the BK3-model are given in table 22.

4.3 Further discussion on the assumptions

In section 4.1 two assumptions were made, which led to a simplification of the equations. The first assumption implied a dry atmosphere above 500 mbar, provided it was also dry below that level. It can happen, of course, in the atmosphere that condensation takes place above 500 mbar and not below that level. Such situations occur in cases of occluding fronts, which are mostly connected with the mature or decaying stages of cyclones, but not with the early development stage. The development stage, which is of most interest for this treatise, is the one in which condensation almost always takes place in the whole layer from 500 to 850 mbar and sometimes also in the layer from 300 to 500 mbar. The formulas (4.94), (4.95) and (4.96) were derived under the assumption of condensation in the layer from \bar{p}_x , which is close to 400 mbar, to 500 mbar. To investigate the consequence of this assumption, two other cases are considered here, namely case 1 with release of latent heat in the whole layer from 300 to 500 mbar, and case 2 with no condensation at all in that layer.

Case 1

Equations (4.92) and (4.95) remain valid, but (4.94) becomes

$$\psi'_{m3} = H_3 \quad \text{with} \quad H_3 \equiv -\frac{\sigma_{3-5}}{f_0} \int_{p_3}^{p_5} \omega_d dp \quad (4.118)$$

Now the same procedure as in the previous section is applied to express H_3 as a function of the RVA at 500 mbar. Then according to (3.70) and (4.66)

$$H_3 = \frac{\sigma_{3-5}}{f_0^2} \int_{p_3}^{p_5} \left[\int_p^{p_{10}} (A - A^2) dp \right] dp \cdot \text{RVA} = (A_3 - 1) (1 - \beta L^*/U_5) L^* \cdot \text{RVA} \quad (4.119)$$

Combination of (4.119) with (4.104) gives

$$H_3 = \frac{A_3 - 1}{1 - A_{8.5}} H_{8.5} = 0.57 H_{8.5} \quad \text{for} \quad A_3 = 1.32 \quad \text{and} \quad A_{8.5} = 0.44 \quad (4.120)$$

So

$$\psi'_{m3} = 0.57 H_{8.5} \quad (4.121)$$

The results of (4.95) and (4.120) are substituted into (4.92) leading to

$$\dot{\psi}_{m5} = 0.32H_{8.5} \quad (4.122)$$

It follows from (4.95), (4.121) and (4.122) that

$$\dot{\psi}_{m3} = \dot{\psi}_{m5} + \dot{\psi}'_{m3} = 0.89H_{8.5} \quad \text{and} \quad \dot{\psi}_{m8.5} = \dot{\psi}_{m5} - \dot{\psi}'_{m8.5} = -0.68H_{8.5} \quad (4.123)$$

A comparison with the previous results is given in table 22.

Case 2

Equations (4.92) and (4.95) remain unchanged, but (5.73) becomes

$$\dot{\psi}'_{m3} = \frac{\sigma_{3-5}}{f_0} \int_{p_3}^{p_5} \omega_m dp \quad (4.124)$$

To express the tendency $\dot{\psi}'_{m3}$ as a function of $H_{8.5}$ is a little more complicated in this case. For that purpose (4.85), (4.71) and (4.17) are used. After substitution of these formulas into (4.124) one gets

$$\dot{\psi}'_{m3} = \frac{\sigma_{3-5}}{f_0^2} \frac{p_5 - p_3}{6} [3(p_5 - p_2)\nabla^2\dot{\psi}_{m5} + (2p_5 + p_3 - 3p_2)\nabla^2\dot{\psi}'_{m3}] \quad (4.125)$$

To eliminate the Laplacian operators it is assumed that the tendencies $\dot{\psi}_{m5}$ and $\dot{\psi}'_{m3}$ have the form of a sine-wave with the same wavelengths in the x - and y -direction of the chosen coordinate system for the streamfunction at 500 mbar, so that $\nabla^2\dot{\psi}_{m5} = -(\mu_x^2 + \mu_y^2)\dot{\psi}_{m5}$ and $\nabla^2\dot{\psi}'_{m3} = -(\mu_x^2 + \mu_y^2)\dot{\psi}'_{m3}$. Now with the aid of (4.66) and using the numerical values of (4.70), (4.125) becomes

$$\begin{aligned} \dot{\psi}'_{m3} &= \frac{(A_3 - 1)(1 - \beta L^*/U_5)}{\int_{p_3}^{p_5} \int_p^{p_{10}} (A - A^2) dp} \frac{p_5 - p_3}{6} [-3(p_5 - p_2)\dot{\psi}_{m5} - (2p_5 + p_3 - 3p_2)\dot{\psi}'_{m3}] \\ &= -0.59\dot{\psi}_{m5} - 0.46\dot{\psi}'_{m3} \end{aligned} \quad (4.126)$$

The results of (4.126) and (4.92) can be combined with (4.95), so that

$$\dot{\psi}_{m5} = 0.47H_{8.5} \quad \text{and} \quad \dot{\psi}'_{m3} = -0.19H_{8.5} \quad (4.127)$$

Then it follows that

$$\dot{\psi}_{m3} = \dot{\psi}_{m5} + \dot{\psi}'_{m3} = 0.28H_{8.5} \quad \text{and} \quad \dot{\psi}_{m8.5} = \dot{\psi}_{m5} - \dot{\psi}'_{m8.5} = -0.53H_{8.5} \quad (4.128)$$

The results obtained in this section are summarized in table 22.

	I	II	III	IV
moist tendencies	results of III 3.5	condensation in whole layer 300—500 mbar	method in BK3-model of 4.1	no condensation in layer 300—500 mbar
$\dot{\psi}_{m3}$	+0.87 $H_{8.5}$	+0.89 $H_{8.5}$	+0.43 $H_{8.5}$	+0.28 $H_{8.5}$
$\dot{\psi}_{m5}$	+0.29 $H_{8.5}$	+0.32 $H_{8.5}$	+0.43 $H_{8.5}$	+0.47 $H_{8.5}$
$\dot{\psi}_{m8.5}$	-0.71 $H_{8.5}$	-0.68 $H_{8.5}$	-0.57 $H_{8.5}$	-0.53 $H_{8.5}$

Table 22 Comparison of several methods for the incorporation of the release of latent heat.

- I: Results of the two-parameter model of III 3.5. They are valid for the centre at sea level of a young developing short frontal wave.
- II: Condensation in the whole column 300—850 mbar. The dry part of ω , ω_d equals that of the reference atmosphere.
- III: Method used in the BK3-model described in 4.1. No assumptions have been made about the patterns of the streamfunctions or tendencies. The assumption of partial condensation in the column 300—500 mbar has been made.
- IV: Condensation only in the column 500—850 mbar. The moist tendencies $\dot{\psi}_{m5}$ and $\dot{\psi}'_{m3}$ have the form of a sine-wave.

The moist tendencies of methods I, II, III and IV can be compared with one another assuming that $H_{8.5}$ has the same value in each case. Table 22 shows that method II agrees best with the results of III 3.5. (It is noted here that the divergence- and ω -values of the two-parameter model in that section have been compared with three case-studies). The differences between the four methods are smallest at 850 mbar and greatest at 300 mbar. Comparing II with III and III with IV, it can be seen that with a decreasing amount of release of latent heat above 500 mbar the absolute values of the moist tendencies at 300 and 850 mbar decrease also. However, at 500 mbar the values of the tendencies increase.

5 Final prognostic equations for polar stereographic projection

5.1 The equations of the dry model

The basic equations used are those as discussed in Chapter II. They are summarized below.

Vorticity equation (2.23):

$$m_1^2 \nabla^2 \psi + \frac{m_1^2 f_o}{f_1} J(\psi, m_1^2 \nabla^2 \psi) + m_1^2 J(\psi, f) + \frac{f_1^2}{f_o} D = 0$$

Continuity equation (2.21):

$$\frac{\partial \omega}{\partial p} + D = 0$$

Thermodynamic equation (2.24) without heating term:

$$\frac{\partial \dot{\psi}}{\partial p} + \frac{m_1^2 f_o}{f_1} J\left(\psi, \frac{\partial \psi}{\partial p}\right) + \frac{\sigma}{f_o} \omega = 0$$

Boundary conditions (2.8):

$$\omega = 0 \quad \text{for} \quad p = 0 \quad \text{and} \quad p = 1000 \text{ mbar.}$$

With the aid of the above equations the prognostic equations can be formulated in a similar way as was done in 2. with the equations in β -plane approximation. They are given below and are analogous to (4.9), (4.10), (4.11), (4.12), (4.13), (4.14), (4.15), (4.23), (4.24) and (4.25). The subscripts d referring to the dry equations are omitted here.

$$m_1^2 \nabla^2 \psi_3 + \frac{m_1^2 f_o}{f_1} J(\psi_3, m_1^2 \nabla^2 \psi_3) + m_1^2 J(\psi_3, f) + \frac{f_1^2}{f_o} D_3 = 0 \quad (4.129)$$

$$m_1^2 \nabla^2 \psi_5 + \frac{m_1^2 f_o}{f_1} J(\psi_5, m_1^2 \nabla^2 \psi_5) + m_1^2 J(\psi_5, f) + \frac{f_1^2}{f_o} D_5 = 0 \quad (4.130)$$

$$m_1^2 \nabla^2 \psi_{8.5} + \frac{m_1^2 f_o}{f_1} J(\psi_{8.5}, m_1^2 \nabla^2 \psi_{8.5}) + m_1^2 J(\psi_{8.5}, f) + \frac{f_1^2}{f_o} D_{8.5} = 0 \quad (4.131)$$

$$\int_0^{p_{10}} D \, dp = 0 \quad (4.132)$$

$$\int_{p_3}^{p_5} \left[\frac{\partial \dot{\psi}}{\partial p} + \frac{m_1^2 f_o}{f_1} J\left(\psi, \frac{\partial \psi}{\partial p}\right) + \frac{\sigma_{3-5}}{f_o} \omega \right] dp + \varepsilon_3 = 0 \quad (4.133)$$

$$\int_{p_5}^{p_{8.5}} \left[\frac{\partial \psi}{\partial p} + \frac{m_1^2 f_o}{f_1} J \left(\psi, \frac{\partial \psi}{\partial p} \right) + \frac{\sigma_{5-8.5}}{f_o} \omega \right] dp + \varepsilon_{8.5} = 0 \quad (4.134)$$

$$\omega = - \int_0^p D dp = \int_p^{p_{10}} D dp \quad (4.135)$$

$$\varepsilon_3 = (A_3 - 1) \psi_3^* - \frac{\sigma_{3-5}}{f_1^2} \left[\int_{p_3}^{p_5} \int_p^{p_{10}} (A \cdot K - A^2) dp \right] dp \cdot \frac{m_1^2 f_o}{f_1} J(\psi_5, m_1^2 \nabla^2 \psi_5) \quad (4.136)$$

$$\varepsilon_{8.5} = (1 - A_{8.5}) \psi_5^* - \frac{\sigma_{5-8.5}}{f_1^2} \int_{p_5}^{p_{8.5}} \left[\int_p^{p_{10}} (A \cdot K - A^2) dp \right] dp \cdot \frac{m_1^2 f_o}{f_1} (\psi_5, m_1^2 \nabla^2 \psi_5) \quad (4.137)$$

$$m_1^2 \nabla^2 \psi_5^* = - \frac{m_1^2 f_o}{f_1} J(\psi_5, m_1^2 \nabla^2 \psi_5) - m_1^2 J(\psi_5, f) \quad (4.138)$$

The integrations of the equations (4.132), (4.133) and (4.134), the elimination of the divergences in (4.129), (4.130), (4.131) and the integrated equations (4.132), (4.133) and (4.134) are carried out in the same way as was done in the sections 3.2 and 3.3. So the equations of the dry BK3-model, valid for polar stereographic projection, become

$$\nabla^2 \psi_5^* = - \frac{f_o}{f_1} J_1 - J_2, \quad (4.139)$$

$$\begin{aligned} \nabla^2 \psi_{8.5}' - \frac{f_1^2}{m_1^2 f_o^2} (a_{00} \psi_{8.5}' - a_{01} \psi_3') &= - \frac{f_o}{f_1} [(1 - a_{04}) J_1 - J_3] \\ - \frac{f_1}{f_o} (a_{00} J_7 + a_{01} J_8) - J_2 + J_4 - \frac{f_1^2 a_{05}}{m_1^2 f_o^2} \psi_5^* & \end{aligned} \quad (4.140)$$

$$\begin{aligned} \nabla^2 \psi_3' - \frac{f_1^2}{m_1^2 f_o^2} (a_{10} \psi_3' - a_{11} \psi_{8.5}') &= \frac{f_o}{f_1} [(1 + a_{14}) J_1 - J_5] \\ + \frac{f_1}{f_o} (a_{10} J_8 + a_{11} J_7) - J_6 + J_2 - \frac{f_1^2 a_{15}}{m_1^2 f_o^2} \psi_5^* & \end{aligned} \quad (4.141)$$

$$\nabla^2 \psi_5 = -\frac{f_o}{f_1} J_1 - J_2 - \frac{f_1}{f_o} (a_0 J_7 + a_1 J_8) + \frac{f_1^2}{m_1^2 f_o^2} (a_0 \psi'_{8.5} - a_1 \psi'_3), \quad (4.142)$$

with

$$\begin{aligned} J_1 &\equiv J(\psi_5, m_1^2 \nabla^2 \psi_5), & J_2 &\equiv J(\psi_5, f), & J_3 &\equiv J(\psi_{8.5}, m_1^2 \nabla^2 \psi_{8.5}), \\ J_4 &\equiv J(\psi_{8.5}, f), & J_5 &\equiv J(\psi_3, m_1^2 \nabla^2 \psi_3), & J_6 &\equiv J(\psi_3, f), & J_7 &\equiv J(\psi_5, \psi_{8.5}) \text{ and} \\ J_8 &\equiv J(\psi_5, \psi_3) \end{aligned} \quad (4.143)$$

The coefficients $a_0, a_1, a_{00}, a_{01}, a_{10}, a_{11}, a_{04}, a_{05}, a_{14}$ and a_{15} are given by (4.61)–(4.65).

5.2 *The corrections due to the inclusion of release of latent heat*

The prognostic ‘moist’ equations valid for stereographic projection can be formulated in a similar way as (4.16)–(4.22). Equations (4.16)–(4.18) are given below, whereas (4.19)–(4.22) remain unchanged.

$$m_1^2 \nabla^2 \dot{\psi}_{m3} + \frac{f_1^2}{f_o} D_{m3} = 0 \quad (4.144)$$

$$m_1^2 \nabla^2 \dot{\psi}_{m5} + \frac{f_1^2}{f_o} D_{m5} = 0 \quad (4.145)$$

$$m_1^2 \nabla^2 \dot{\psi}_{m8.5} + \frac{f_1^2}{f_o} D_{m8.5} = 0 \quad (4.146)$$

For the derivation of the moist corrections from the above formulated equations exactly the same procedure is followed as in 4.1, leading to the same formulas for the corrections of the tendencies, which for convenience are given below.

$$\begin{aligned} \dot{\psi}'_{m3} &= 0, & \dot{\psi}'_{m8.5} &= H_{8.5}, & \dot{\psi}'_{m5} &= 0.43H_{8.5}, & \dot{\psi}'_{m3} &= 0.43H_{8.5}, \\ \dot{\psi}_{m8.5} &= -0.57H_{8.5} \end{aligned}$$

with

$$H_{8.5} \equiv -\frac{\sigma_{5-8.5}}{f_o} \int_{p_5}^{p_{8.5}} \omega_d dp \quad (4.147)$$

6 Description of the computational procedures

6.1 Computational grid

A rectangular grid has been defined on a plane going through the parallel of 60°N. With the aid of a stereographic projection the earth's surface is projected from the south pole on this plane. The x - and y -axis of the coordinate system are parallel to the longitude circles of 30°W and 120°W, respectively. The grid point distance d is equal to 375 km at 60°N. The discrete coordinates of the grid points in the x - and y -direction are denoted by i and j with $x = d(i - 1)$ and $y = d(j - 1)$, so that according to the stereographic projection formula (2.15) i and j are related to the latitude φ and the longitude λ (positive in the east-direction) as

$$d(i - i' - 1) = a \cdot m \cdot \cos \lambda \quad \text{and} \quad d(j - j' - 1) = a \cdot m \cdot \sin \lambda, \quad (4.148)$$

with

$$x = x_s + d \cdot i' \quad \text{and} \quad y = y_s + d \cdot j'.$$

x_s and y_s are the coordinates of the stereographic projection along 30°W and 120°W, respectively. i' and j' are the number of grid point distances along the x_s - and y_s -axis to the north pole with $i' = 4.5$ and $j' = 16.5$. The value of the earth's radius a has been taken as $a = 6371229$ m. The coordinates i and j vary from $i = 1$ to $i = 25$ and from $j = 1$ to $j = 32$. The thus defined grid covers Europe, the North Atlantic Ocean and North America. It is partly given in figure 7.

The coordinates i and j of the computational grid are related to the latitude φ according to

$$\sin \varphi = (1 - h)/(1 + h)$$

with

$$h \equiv \frac{d^2[(i - i' - 1)^2 + (j - j' - 1)^2]}{a^2(1 + \sin 60^\circ)^2} \quad (4.149)$$

Using this formula it is possible to compute the Coriolis parameter f_1 and the map scale factor m_1 for each grid point at latitude $\varphi = \varphi_1$.

6.2 Finite difference approximations

The Laplacian of a quantity Q has been approximated with the wellknown second-order scheme

$$\nabla^2_{i,j}(Q) = (Q_{i+1,j} + Q_{i-1,j} + Q_{i,j+1} + Q_{i,j-1} - 4Q_{i,j})/d^2, \quad (4.150)$$

with $Q_{i,j}$ the value of Q at the grid point with coordinates i and j .

For the time integrations the second-order leap-frog scheme has been applied, namely

$$\frac{\partial}{\partial t}_{i,j,n}(Q) = (Q_{i,j,n+1} - Q_{i,j,n-1})/(2\Delta t), \quad (4.151)$$

with $Q_{i,j,n}$ the value of Q at the grid point (i, j) and at the discrete time n . n is related to the time t as $n = t/\Delta t$.

For the Jacobian three difference schemes have been applied, namely the one by ARAKAWA (1966), a fourth-order scheme developed by OPSTEEGH at the Royal Netherlands Meteorological Institute, and the simple second-order scheme. These three schemes are described below.

The Jacobian J of two quantities f and g can be expressed in three mathematically identical ways as

$$\begin{aligned} J(f, g) &\equiv \frac{\partial f}{\partial x} \frac{\partial g}{\partial y} - \frac{\partial f}{\partial y} \frac{\partial g}{\partial x} \equiv \frac{\partial}{\partial x} \left(f \frac{\partial g}{\partial y} \right) - \frac{\partial}{\partial y} \left(f \frac{\partial g}{\partial x} \right) \equiv \frac{\partial}{\partial y} \left(g \frac{\partial f}{\partial x} \right) \\ &\quad - \frac{\partial}{\partial x} \left(g \frac{\partial f}{\partial y} \right) \end{aligned} \quad (4.152)$$

The finite difference approximations of these three expressions for the Jacobian at the grid point with coordinates i and j are denoted by JJ_a , JJ_b and JJ_c respectively. See also figure 19 for the locations of the grid points.

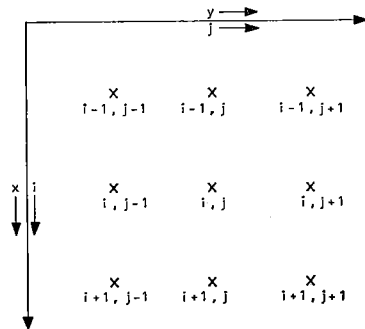


Fig. 19 Locations of the grid points used for the finite difference approximations.

$$JJ_a \equiv [(f_{i+1,j} - f_{i-1,j})(g_{i,j+1} - g_{i,j-1}) - (f_{i,j+1} - f_{i,j-1})(g_{i+1,j} - g_{i-1,j})]/(4d^2) \quad (4.153)$$

$$JJ_b \equiv [f_{i+1,j}(g_{i+1,j+1} - g_{i+1,j-1}) - f_{i-1,j}(g_{i-1,j+1} - g_{i-1,j-1}) - f_{i,j+1}(g_{i+1,j+1} - g_{i-1,j+1}) + f_{i,j-1}(g_{i+1,j-1} - g_{i-1,j-1})]/(4d^2) \quad (4.154)$$

$$JJ_c \equiv [g_{i,j+1}(f_{i+1,j+1} - f_{i-1,j+1}) - g_{i,j-1}(f_{i+1,j-1} - f_{i-1,j-1}) - g_{i+1,j}(f_{i+1,j+1} - f_{i+1,j-1}) + g_{i-1,j}(f_{i-1,j+1} - f_{i-1,j-1})]/(4d^2) \quad (4.155)$$

The finite difference scheme by ARAKAWA reads

$$JJ_{i,j} = (JJ_a + JJ_b + JJ_c)/3 \quad (4.156)$$

This scheme had been applied to several experiments with the dry version of the BK3-model and also to the operational version till the end of 1973.

The fourth-order scheme of the Jacobian is given by

$$JJ_{i,j} = \left\{ \begin{aligned} & [\frac{4}{3}(f_{i+1,j} - f_{i-1,j}) - \frac{1}{6}(f_{i+2,j} - f_{i-2,j})] \\ & \cdot [\frac{4}{3}(g_{i,j+1} - g_{i,j-1}) - \frac{1}{6}(g_{i,j+2} - g_{i,j-2})] \\ & - [\frac{4}{3}(f_{i,j+1} - f_{i,j-1}) - \frac{1}{6}(f_{i,j+2} - f_{i,j-2})] \\ & \cdot [\frac{4}{3}(g_{i+1,j} - g_{i-1,j}) - \frac{1}{6}(g_{i+2,j} - g_{i-2,j})] \end{aligned} \right\} / (4d^2) \quad (4.157)$$

The scheme cannot be applied to the grid points of the rows and columns next to the boundary of the computational grid, so that at these points the simple second-order approximation given by (4.153) is used. This fourth-order scheme has been used in experimental dry and moist versions of the BK3-model and also in the operational version from the beginning of 1974.

6.3 *Lateral boundary conditions and smoothing procedures*

Due to the finite area of the computational grid, lateral boundary conditions are necessary to perform the calculations.

During the integrations the four tendencies ψ_5^* , ψ_3' , $\psi_{8.5}'$ and ψ_5' occurring in equations (4.139)–(4.142) are kept equal to zero at the outer two rows and columns of grid points. After each time step a linear interpolation is made for ψ_5 , ψ_3' and $\psi_{8.5}'$ at the rows and columns of grid points next to the boundaries, namely

$$\begin{aligned}
\psi_{i,j} &= (\psi_{i,j-1} + \psi_{i,j+1})/2 \quad \text{for } i = 3, \dots, 23 \quad \text{and } j = 2, 31, \\
\psi_{2,2} &= (\psi_{1,1} + \psi_{3,3})/2, \quad \psi_{24,2} = (\psi_{25,1} + \psi_{23,3})/2, \\
\psi_{i,j} &= (\psi_{i-1,j} + \psi_{i+1,j})/2 \quad \text{for } i = 2, 24 \quad \text{and } j = 3, \dots, 30, \\
\psi_{2,31} &= (\psi_{1,32} + \psi_{3,30})/2, \quad \psi_{24,31} = (\psi_{25,32} + \psi_{23,30})/2
\end{aligned} \tag{4.158}$$

This interpolation proved to be an efficient way to suppress computational instability near the boundaries of the grid. This instability is possible due to the fact that the boundaries are partly located in meteorologically active areas, so that too strong gradients in the patterns of the streamfunctions can be caused by keeping the values constant. It is clear that the linear interpolation (4.158) acts as the most simple smoothing operator.

However, the use of (4.158) near the boundaries of the grid is not a sufficient condition to prevent all kinds of instability. For instance, non-linear instability can arise in the interior of the area during the integration process. To suppress this unwanted phenomenon, the smoothing operator devised by SHUMAN (1957) is applied to the streamfunctions. The way in which it is applied is outlined in the next section.

The SHUMAN-operator related to the streamfunction ψ in the x -direction of the grid has the following form

$$\begin{aligned}
\tilde{\psi}_{i,j} &\equiv \psi_{i,j} - A_{s0}\psi_{i,j} + A_{s1}(\psi_{i+1,j} + \psi_{i-1,j}) - A_{s2}(\psi_{i+2,j} + \psi_{i-2,j}) \\
&\quad + A_{s3}(\psi_{i+3,j} + \psi_{i-3,j})
\end{aligned}$$

with

$$A_{s0} = 0.27236, \quad A_{s1} = 0.22049, \quad A_{s2} = 0.11318 \quad \text{and} \quad A_{s3} = 0.02886 \tag{4.159}$$

The properties of this smoothing operator can be most easily clarified with the aid of a simple sinusoidal wave. If $\psi_{i,j} = A \cos(\mu_x d \cdot i) \cos(\mu_y d \cdot j)$, after the use of (4.159) in the x - and y -direction, ψ has been changed into

$$\tilde{\tilde{\psi}}_{i,j} \equiv R\psi_{i,j} \tag{4.160}$$

with

$$\begin{aligned}
R &= [1 - A_{s0} + 2A_{s1} \cos(\mu_x d) - 2A_{s2} \cos(2\mu_x d) + 2A_{s3} \cos(3\mu_x d)] \\
&\quad \cdot [1 - A_{s0} + 2A_{s1} \cos(\mu_y d) - 2A_{s2} \cos(2\mu_y d) + 2A_{s3} \cos(3\mu_y d)]
\end{aligned}$$

where d is the distance between two grid points, $\mu_x \equiv 2\pi/L_x$ and $\mu_y \equiv 2\pi/L_y$.

The response function R is given in table 23 for several values of L_x/d and ratios $L_x/L_y = 0$ and 1 and for one, three and thirty times of repeated application. The table clearly shows the features of this operator. Waves with wavelengths larger than four and smaller than eight grid distances are amplified with a maximum at $L_x \approx 6d$.

All other waves are damped with an absolute minimum at $L_x = 2d$ and a relative minimum at $L_x \approx 12d$. In table 23 these features are most pronounced for the case when smoothing is repeated thirty times.

It is clear that the use of SHUMAN's smoothing operator is an effective way to suppress non-linear instability (discovered by Phillips (1959)), which results in an unlimited accumulation of noise in the wavelengths equal to $2d$, $3d$ and $4d$.

L_x/d	$L_x/L_y = 0$			$L_x/L_y = 1$		
	1×	3×	30×	1×	3×	30×
2	0.003	0.000	0.000	0.000	0.000	0.000
3	0.678	0.312	0.000	0.460	0.097	0.000
4	0.954	0.868	0.243	0.910	0.754	0.059
5	1.000	1.001	1.010	1.001	1.002	1.020
6	1.004	1.011	1.113	1.007	1.022	1.239
7	1.001	1.003	1.029	1.002	1.006	1.059
8	0.999	0.996	0.960	0.997	0.992	0.992
9	0.997	0.992	0.922	0.995	0.984	0.850
10	0.997	0.990	0.903	0.993	0.980	0.816
11	0.996	0.989	0.897	0.992	0.978	0.804
12	0.996	0.989	0.897	0.992	0.978	0.804
13	0.997	0.990	0.900	0.993	0.979	0.810
14	0.997	0.990	0.905	0.993	0.980	0.819
15	0.997	0.991	0.911	0.994	0.981	0.829
20	0.998	0.994	0.937	0.996	0.987	0.879
∞	1	1	1	1	1	1

Table 23 Response function of SHUMAN's smoothing operator for several repeated applications on a sinusoidal wave in the x - and y -direction of the coordinate system.

6.4 Computational scheme

The computer program of the BK3-model starts with the objective analyses of the geopotential heights of the 300, 500 and 850 mbar surfaces. The practical application of this analysis program, which is based on the procedures developed by CRESSMAN (1959), was developed by BOUMAN (1969).

The three height fields consist of 3×800 values of the geopotential. These fields are transformed into streamfunctions according to

$$\begin{aligned} \psi_3 &= g \cdot z_3/f_0, & \psi_5 &= g \cdot z_5/f_0, & \psi_{8.5} &= g \cdot z_{8.5}/f_0, & \psi'_3 &= \psi_3 - \psi_5, \\ \psi'_{8.5} &= \psi_5 - \psi_{8.5} & \text{with } f_0 &= 10^{-4} \text{s}^{-1} \end{aligned} \quad (4.161)$$

The subscripts 3, 5 and 8.5 refer to 300, 500 and 850 mbar respectively.

With the aid of (4.149) and (2.15) the fields of the Coriolis-parameter f and the quadratic map scale factor m^2 are computed for each grid point. The three vorticities $m_1^2 \nabla^2 \psi_3$, $m_1^2 \nabla^2 \psi_5$ and $m_1^2 \nabla^2 \psi_{8.5}$ and the Jacobians $J_1 - J_8$ defined in (4.143) are computed using the difference approximations given in 6.2. The barotropic tendency $\dot{\psi}_5^*$ can be solved now from (4.139) after the approximation of the Laplacian of $\dot{\psi}_5^*$ according to (4.150). The approximate solution is obtained with the aid of an over-relaxation method according to the extrapolation method of LIEBMANN, and using the lateral boundary condition $\dot{\psi}_5^* = 0$. Now the forcing functions of the set of Helmholtz-equations (4.140) and (4.141) are completely known. After the approximation of the Laplacians of $\dot{\psi}_3'$ and $\dot{\psi}_{8.5}'$ by finite differences according to (4.150), these tendencies are simultaneously solved from this set of Helmholtz-equations, using the same technique as for the solution of (4.139). These tendencies are substituted into (4.142), so that the forcing function of that equation is known and the tendency $\dot{\psi}_5$ can be solved.

Now the time integrations are performed for the streamfunctions ψ_3' , ψ_5 and $\psi_{8.5}'$, using a forward time step of $\frac{1}{2}\Delta t$ at $t = 0$, a central time step of Δt at $t = \frac{1}{2}\Delta t$ and for other values of t central steps of $2\Delta t$, using (4.151). In most experiments, a time step of $\Delta t = 3600$ s could be taken, but in some cases it was necessary to take steps of 1800 s, in order to prevent linear instability.

After each time step Δt the corrections due to the release of latent heat are applied to the streamfunctions ψ_3' , ψ_5 and $\psi_{8.5}'$, if the moist version of the model is used. According to (4.147), the streamfunctions ψ_3' , ψ_5 and $\psi_{8.5}'$ are corrected with 0 , $0.43H_{8.5}\Delta t$ and $H_{8.5}\Delta t$, respectively. The quantity $H_{8.5}\Delta t$ is directly related to the release of latent heat derived from the precipitation computations with the aid of the equations (4.139)–(4.142) of the dry model over the period t to $t + \Delta t$.

To prevent non-linear instability, SHUMAN's smoothing operator is used various times, depending on the total number of scans needed to solve the Poisson-equation (4.139) and the set of Helmholtz-equations (4.140) and (4.141). If the number of scans, needed to solve the equations, is greater than the one needed at $t = 0$ for either the Poisson-equation or the Helmholtz-equations, then the streamfunctions ψ_3' , ψ_5 and $\psi_{8.5}'$ are smoothed by the Shuman-operator. This smoothing is performed three times in the x - and y -direction of the computational grid.

After each time step the linear interpolations (4.158) are carried out near the boundaries of the grid.

CHAPTER V

A SURVEY OF THE PERFORMANCE OF
THE DRY AND MOIST VERSIONS OF THE
BK3-MODEL**1 Some remarks on the performance of the dry versions of the BK3-model with and without the correction terms in the integrated forms of the thermodynamic equation**

Some experiments were carried out for the 25-3-71, 00 GMT situation with the dry version of the BK3-model. Two versions were used, namely the model with the correction terms ε_3 and $\varepsilon_{8.5}$, which have been defined by (4.136) and (4.137), and the model without these terms. As can be seen in section IV 3.3, such a version with $\varepsilon_3 = \varepsilon_{8.5} = 0$ can be obtained by setting $a_{04} = a_{05} = a_{14} = a_{15} = 0$ in the equations (4.140), (4.141) and (4.142) of the model.

The experiments were performed with five different values of the static stability parameters σ_{3-5} and $\sigma_{5-8.5}$ by using five values of L^* in (4.66) and (4.67). The values varied from low ones, belonging to a saturated adiabatic lapse rate, to the relatively high values of the upper part of the ICAO standard atmosphere. The results of these experiments were described by Heijboer (1972). A short summary is given here.

With respect to the influence of static stability, the models with and without the correction terms showed the same qualitative behaviour, i.e. with increasing values of the static stability, less baroclinic development, decreasing values of the horizontal divergence at 300, 500 and 850 mbar and also decreasing values for ω at 500 mbar resulted. The production of areal mean kinetic energy and areal mean squared vorticity at 500 mbar also decreased.

These results are not surprising, as they are predicted by the stability theory of III 4. As shown in (3.91), this theory predicts that for unstable waves the development of the perturbation is inversely proportional to the root of the static stability.

More interesting are the differences caused by the inclusion of the correction terms ε_3 and $\varepsilon_{8.5}$ in the equations of the model. Comparison of the two versions using the same static stability showed that in general the inclusion of the correction terms in the model had led to a smaller baroclinic development in the prognoses. A further subjective inspection revealed that the long waves with wavelengths of about 4000 km in the thickness fields z_3' and $z_{8.5}'$ were damped compared with those predicted by the model without the correction terms. Using the values σ_{3-5} and $\sigma_{5-8.5}$ given in

(4.70), the predicted sea level pressures in the centres of the highs proved to be more realistic with the correction terms included. Without these terms the predicted pressures were generally too high.

It should be noted here that the pressure at sea level is not directly forecast by the model. This field is estimated with the aid of the predicted height field of 500 mbar and the thickness field of 500–850 mbar according to

$$p_{\text{surface}} = 1.25(z_5 - 1.25z'_{8.5} - 31) + 1000 \quad (5.1)$$

where z_5 is the geopotential height of 500 mbar in gpdam, $z'_{8.5} \equiv z_5 - z_{8.5}$ the thickness of the thermal field 500–850 mbar in gpdam, and p_{surface} the pressure at sea level in mbar. This formula can be derived with the aid of an empirical linear relation, which exists between the thicknesses of 500–850 mbar and of 500–1000 mbar, if the lapse rate is assumed to be saturated-adiabatic. This relation reads $z'_{10} = 1.25z'_{8.5} + 31$ with z'_{10} and $z'_{8.5}$ in gpdam. Over sea, the approximation (5.1) is fairly accurate, but over land, in cases of extreme deviations from the assumed vertical temperature profile in the boundary layer below 850 mbar, the result may be unacceptable.

Further experiments were carried out on 10 other cases with different weather situations varying from west circulations to blocking circulations, using one version of the model with and one without the correction terms, both with the low values of the static stability belonging to a saturated adiabatic lapse rate. In all these cases the model with the correction terms proved to be more stable for the long waves and to give better pressure predictions for the highs at sea level. In one case the model without correction terms had even become computationally unstable. This kind of instability could not be removed by a reduction of the time steps used in the integrations.

The effect of the correction terms on the behaviour of the long as well as the short waves is further elucidated in section 3. It should be noted here that stabilization of the long waves can also be obtained by an increase of the static stability of the model by using values higher than those of saturated adiabatic lapse rates and in accordance with the mean value of the static stability of the ICAO standard atmosphere. However, such values are not realistic for frontal systems as has been discussed in III 3.3.

The dry version of the model including the correction terms and using the coefficients computed in IV 3.4 was operational from 28-2-'72, 12 GMT till 3-11-'75, 00 GMT. The performance of this model with respect to forecasts of the geostrophic wind at 850 mbar for periods of 12 and 24 hours ahead has been described by HEIJBOER (1973). The verification was done for a period of one year, and it proved that the forecasts of both windspeed and wind direction up to 24 hours ahead were as good as the persistence forecasts up to 12 hours ahead.

2 The performance of the moist version of the BK3-model

Experiments with the inclusion of latent heat have been described by HEIJBOER and EXTER BLOKLAND, DEN (1974). The used version of the model contained the correction terms and the coefficients as calculated in IV 3.4. The results were compared with those of the operational dry version of the model. A summary of these experiments is given below.

A number of cases were selected during the winter season '72-'73. All cases showed explosive development at sea level (deepening of 20 mbar or more in 24 hours). During the summer and the autumn of 1973 the moist version was run parallel to the operational dry version. The reason for selecting the summer season was to control the performance of the moist version for the period when, due to the relatively high air temperature, the amount of moisture is high, while on the other hand the circulation is in general less intense. The experiments showed that the moist model was able to predict explosive development of frontal depressions in contrast with the dry version, which for all the selected cases could not properly predict the development at sea level.

A model suitable for operational purposes, however, should not only predict existing developments correctly, but should also predict no development if there is none in reality. In general, this proved to be the case, and only in a few cases false explosive development on the synoptic scale had been forecast. However, the moist model showed an unwanted phenomenon, which prevented the model from becoming operational. It proved that in general the forecast pressure pattern at sea level was too noisy. The noise usually consisted of waves with wavelengths of three or four grid distances ($\sim 1000 - \sim 1500$ km). In cases of developing frontal waves it sometimes appeared that the model predicted such an unrealistic disturbance in the cold front behind the original one.

This feature of the model can be reasonably explained as follows: If there is an initially small disturbance with a wavelength equal to three or four grid distances, which is equivalent barotropic like the reference atmosphere, then the dry version of the model will hold this disturbance equivalent barotropic, due to the influence of the correction terms (see also the next section), so that the wave shows no baroclinic development. In section III 2.1 it has been shown that in the reference atmosphere vertical velocities occur, which are upward in areas with advection of positive relative vorticity ($RVA > 0$) at 500 mbar. If in this area the humidity of the air is high enough, precipitation with release of latent heat is possible. Accordingly, a baroclinic part due to the release of latent heat will be added to the equivalent barotropic tendency of the streamfunction $\psi'_{8.5}$ of the thickness field (see for instance section IV 4.1, where this moist part is given by (4.95)). Now the disturbance becomes baroclinic and obtains a structure like that of a simple baroclinic wave, which is described in the next section. It is shown in that section that for such waves the correction terms will

favour a further amplification of the baroclinic part of the wave in the thickness field. This enhanced baroclinicity will be accompanied with an increased upward vertical velocity, increased release of latent heat etc. Thus the disturbance has become baroclinically unstable. If the small disturbance is already baroclinic in the initial stage, one may expect that the moist version will always be more unstable than the dry version of the model, due to the possibility of release of latent heat.

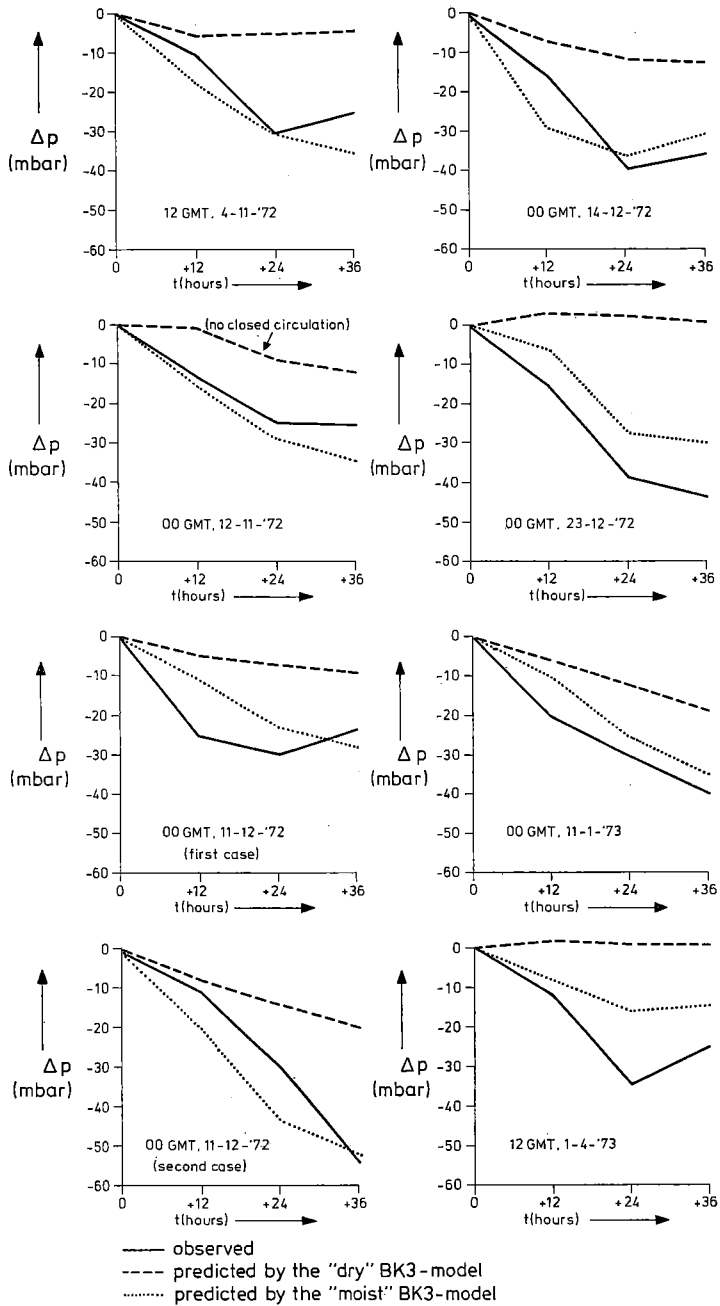
Small-scale noise can be present in the objective analyses, but can also be generated by the 'aliasing' process caused by the use of finite difference equations in the model. This noise could be suppressed by the application of SHUMAN's smoothing operator, but in practice it proved that this smoothing was only sufficient for the dry version of the model and not for the moist version.

The considerations given above lead to the conclusion that a real dissipation mechanism has to be included in the model. Recent experiments with the inclusion of horizontal eddy diffusion terms together with the use of SHUMAN's smoothing operator proved to yield the desired dissipation of the small waves.

The experiments with the moist version of the model support the conclusions from the stability analysis of the quasi-geostrophic equations given in section III.4, namely, that short frontal waves can only be unstable if latent heat is released in the disturbance. This is illustrated in figure 20, which has been taken from the report of HELBOER and EXTER BLOKLAND, DEN (1974). The predicted and observed pressure changes of the surface low centres are given for the eight selected cases discussed in that report. The figure clearly shows that the dry version of the model can hardly predict the explosive deepening of the surface lows, this in contrast with the moist version.

Finally, one case has been chosen to illustrate the capability of the moist model to predict explosive cyclogenesis at sea level. It is noted here that this case is one of the best prognoses of the moist model. Figure 21a shows the initial surface pressure on 23-12-'72, 00 GMT. The analysis of the situation 24 hours later is given in figure 21b. Figure 21c shows the prognosis of the dry model without any production of vorticity for the low centered at 50°N and 40°W. Figure 21d shows that the low had been forecast very well by the moist model. The initial analysis of 500 mbar, the analysis of 500 mbar 24 hours later, the prognosis of the dry model valid for the same time and also that of the moist model are given in the figures 22a, 22b, 22c and 22d, respectively. It can be seen that there is no great difference between the forecasts by the dry and moist models of which the latter is slightly better for this case. This

Fig. 20 Comparison between the observed pressure tendencies (extracted from the handmade analyses by the Weather Service of the Royal Netherlands Meteorological Institute) and the forecast tendencies of the estimated surface pressure by (5.1) with the dry and the moist version of the BK3-model.



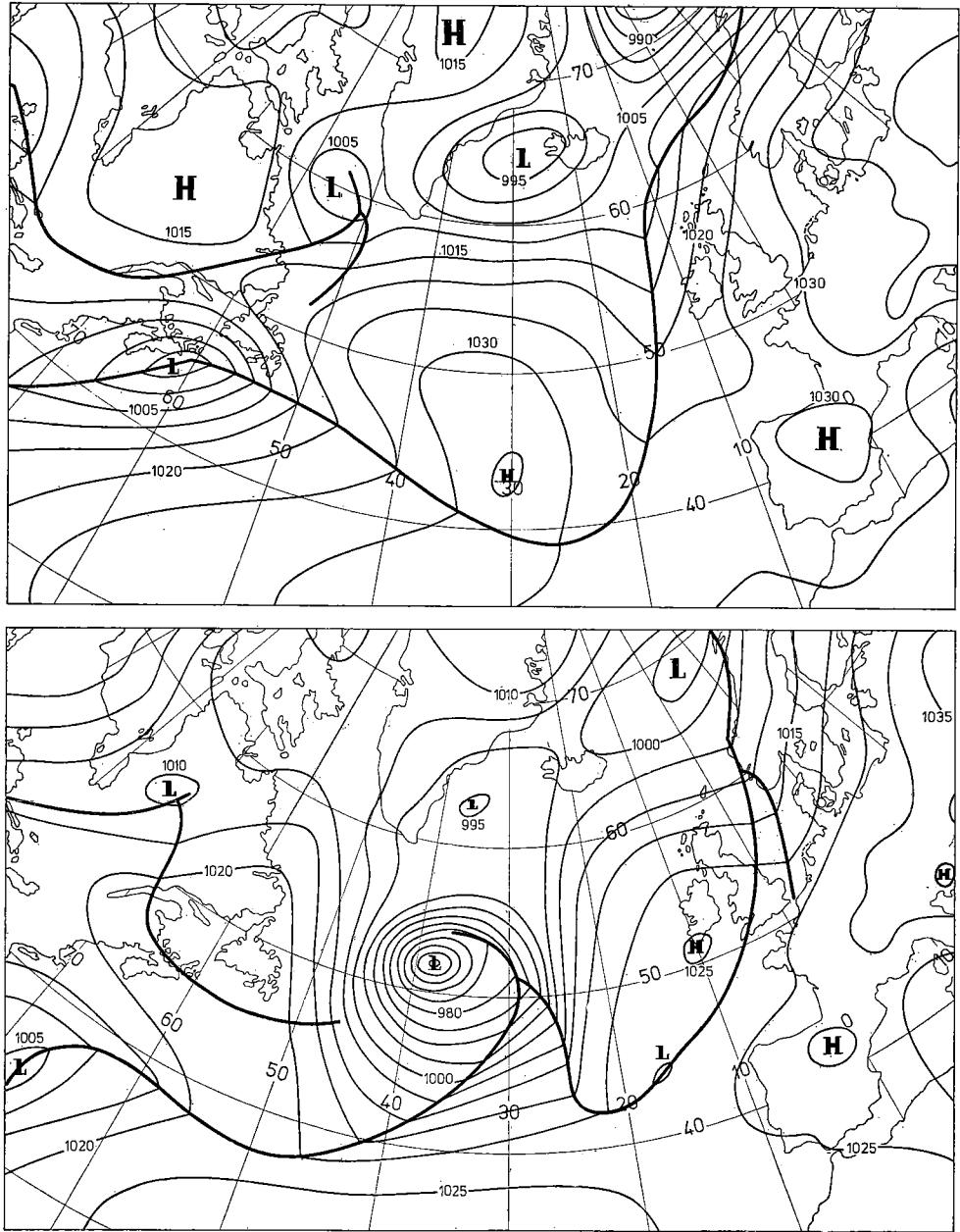
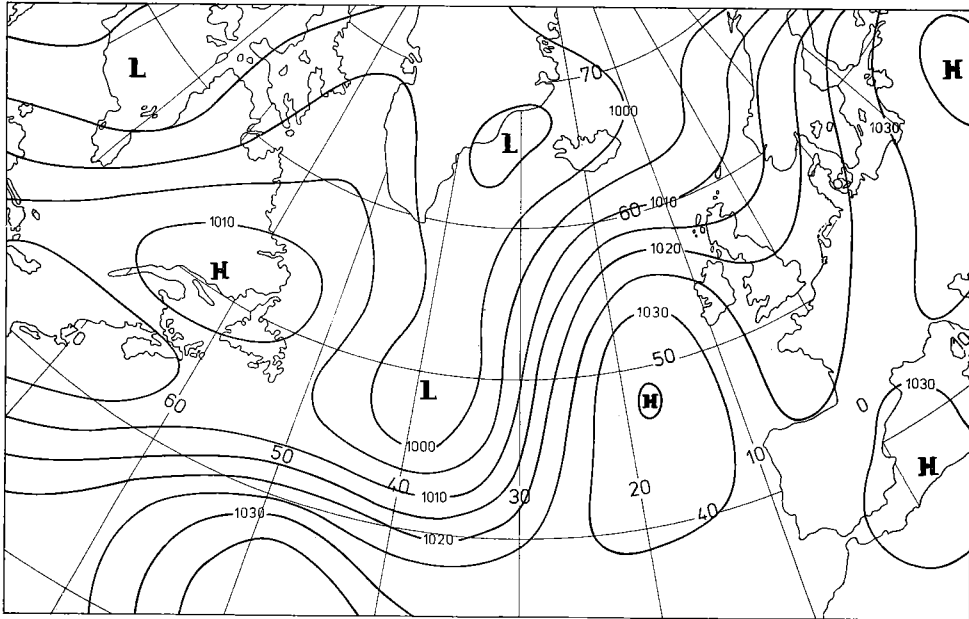
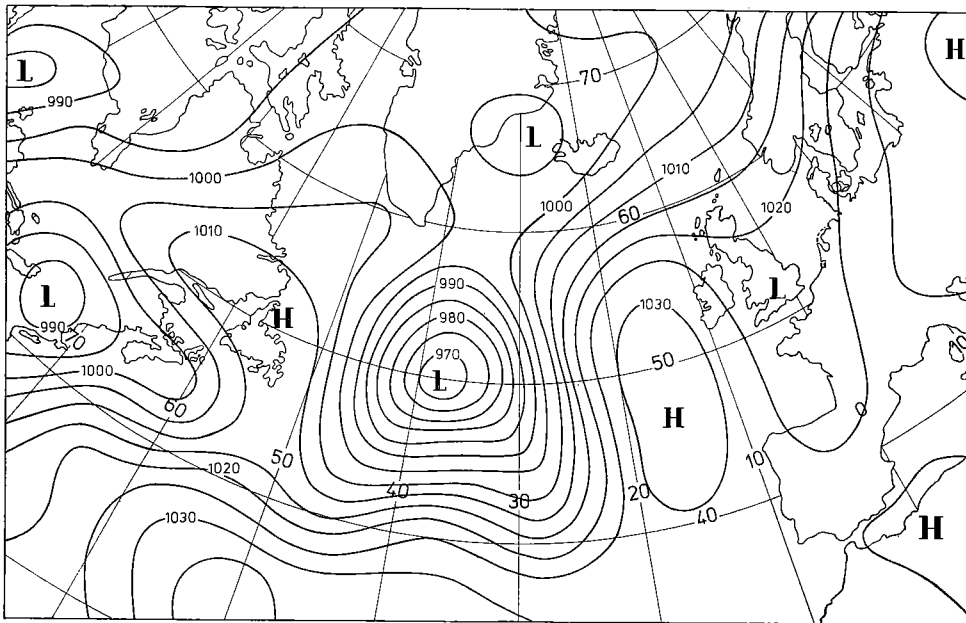


Fig. 21 Comparison between the forecast estimated surface pressure with the dry and the moist version of the BK3-model.
 a. Surface pressure analysis, valid for 24-12-72, 00 GMT.



c



d

- b. Surface pressure analysis, valid for 25-12-'72, 00 GMT.
 c. Surface +24 prognosis with the dry BK3-model, valid for 25-12-'72, 00 GMT.
 d. Surface +24 prognosis with the moist BK3-model, valid for 25-12-'72, 00 GMT.

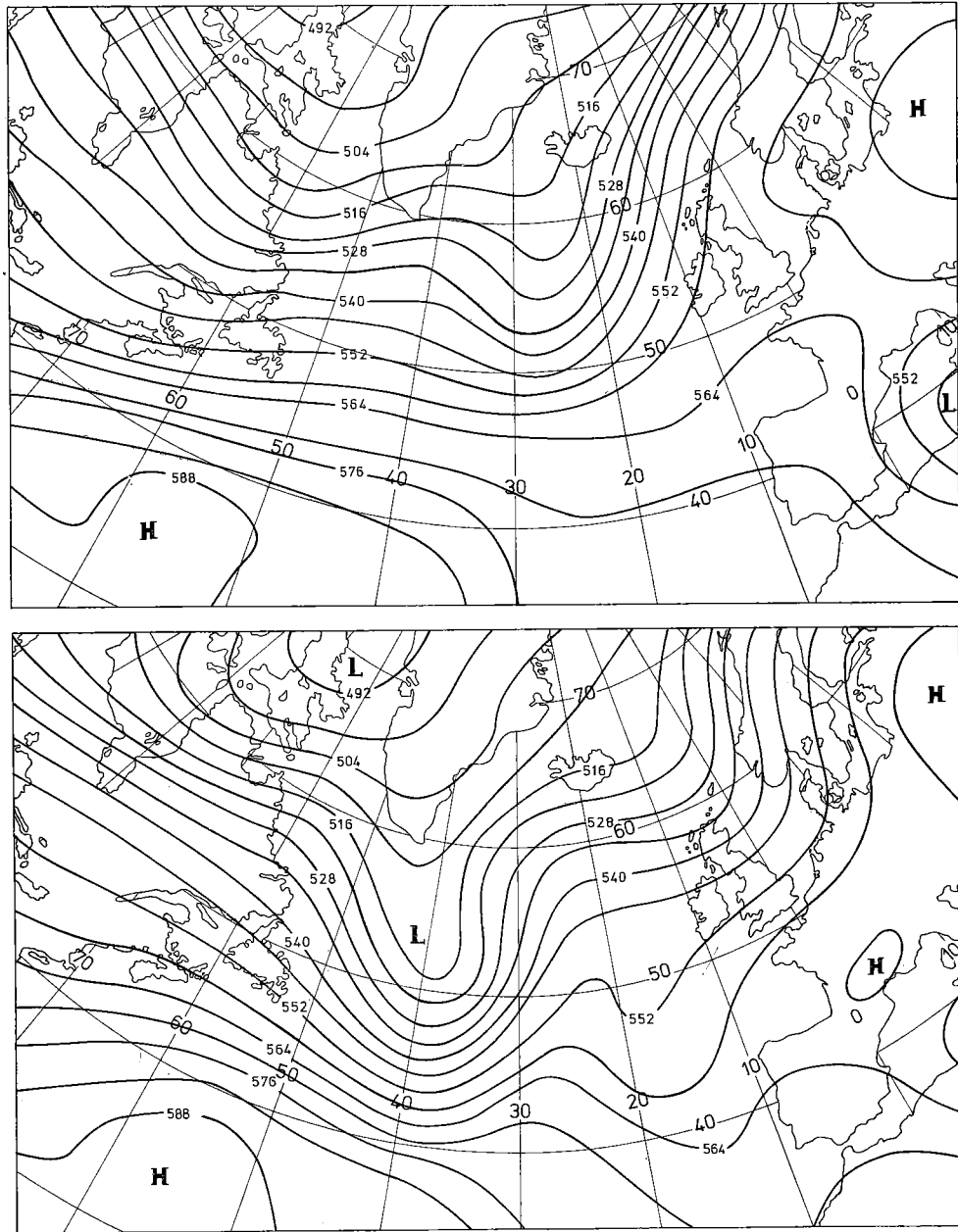
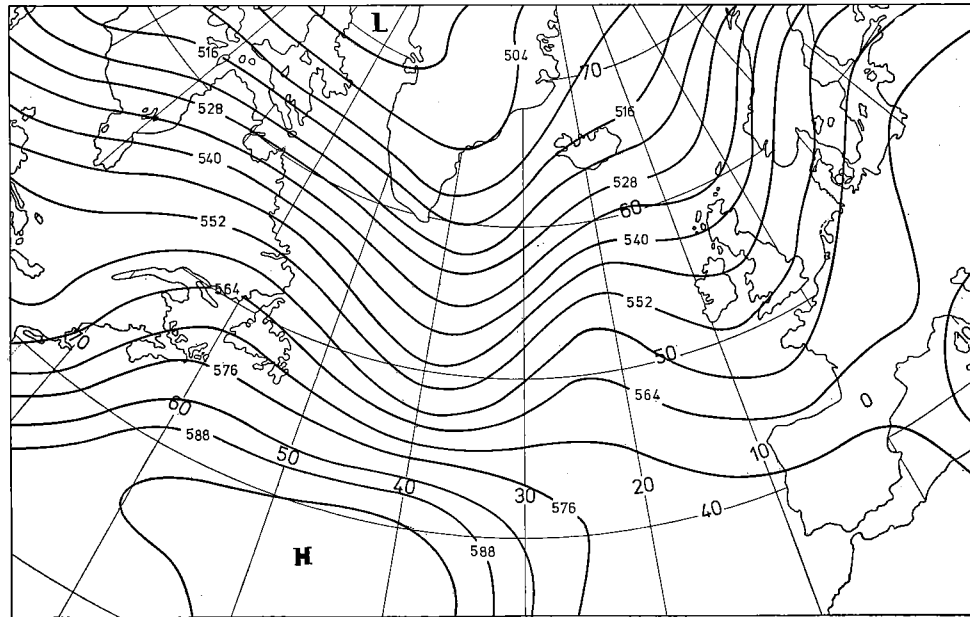
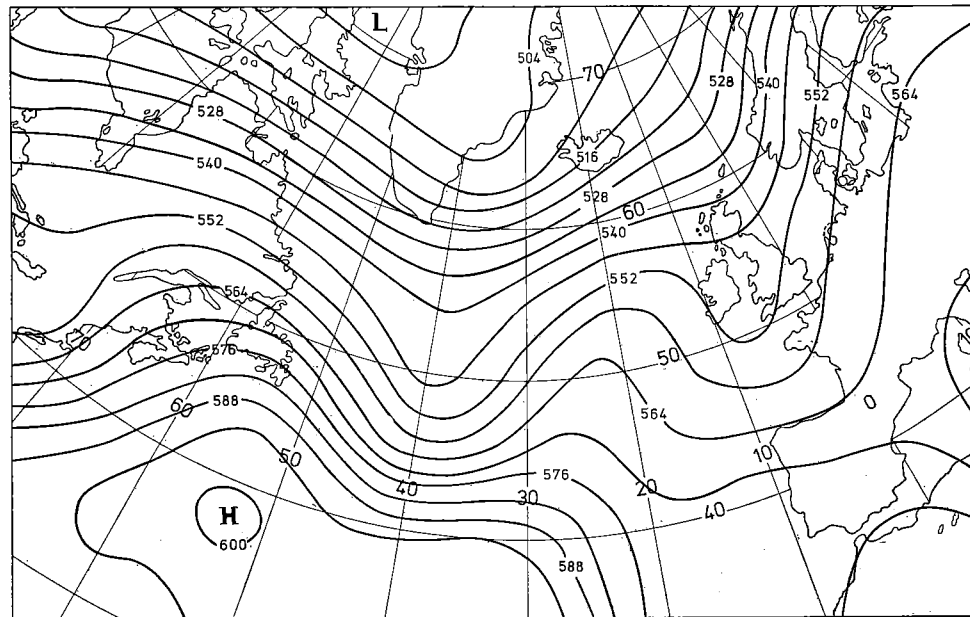


Fig. 22 Comparison between the forecast height (gpdam) of the topography of 500 mbar with the dry and the moist BK3-model.
 a. 500 mbar analysis, valid for 24-12-'72, 00 GMT.



c



d

b. 500 mbar analysis, valid for 25-12-'72, 00 GMT.

c. 500 mbar +24 prognosis with the dry BK3-model, valid for 25-12-'72, 00 GMT.

d. 500 mbar +24 prognosis with the moist BK3-model, valid for 25-12-'72, 00 GMT.

feature proved to be generally true for the prognoses of 500 mbar. The greatest differences between the dry and moist versions of the models are found at sea level.

One of the cases in the above-mentioned report, namely the gale of 13-11-'72, has also been investigated by EMMRICH (1975). He came to the conclusion that the release of latent heat had been very important for the development of that depression.

3 Some further theoretical considerations with respect to the correction terms in the BK3-model

The character and the influence of the correction terms ε_3 and $\varepsilon_{8.5}$ on the behaviour of the BK3-model will be investigated with the aid of simple streamfunctions. For that purpose the streamfunction at 500 mbar is supposed to satisfy:

$$\psi_5 = -U_5 \cdot y + F_5 \cos(\mu_y \cdot y) \sin[\mu_x(x - \varphi_5)] + E \quad (5.2)$$

F_5 and φ_5 both depend on time t . At $t = t_0$, $\varphi_5 = 0$. U_5 and E are constant.

The advection of relative vorticity (RVA) at 500 mbar then becomes

$$\text{RVA} \equiv -J(\psi_5, \nabla^2 \psi_5) = U_5 F_5 \mu_x (\mu_x^2 + \mu_y^2) \cos(\mu_y \cdot y) \cos[\mu_x(x - \varphi_5)] \quad (5.3)$$

When (5.2) is substituted into (4.25) the solution ψ_5^* is

$$\psi_5^* = -\mu_x U_5 F_5 (1 - \beta L^*/U_5) \cos(\mu_y \cdot y) \cos[\mu_x(x - \varphi_5)]$$

With this expression for ψ_5^* , ε_3 and $\varepsilon_{8.5}$ become according to (5.3), (4.23) and (4.24):

$$\begin{aligned} \varepsilon_3 = & -U_5 F_5 \frac{\mu_x}{L^*} \left\{ (A_3 - 1) (1 - \beta L^*/U_5) L^* \right. \\ & \left. - \frac{\sigma_{3-5}}{f_0^2} \int_{p_3}^{p_5} \left[\int_p^{p_{10}} (A - A^2) dp \right] dp \right\} \cdot \cos(\mu_y \cdot y) \cos[\mu_x(x - \varphi_5)] \quad (5.4) \end{aligned}$$

and

$$\begin{aligned} \varepsilon_{8.5} = & -U_5 F_5 \frac{\mu_x}{L^*} \left\{ (1 - A_{8.5}) (1 - \beta L^*/U_5) L^* \right. \\ & \left. - \frac{\sigma_{5-8.5}}{f_0^2} \int_{p_5}^{p_{8.5}} \left[\int_p^{p_{10}} (A - A^2) dp \right] dp \right\} \cdot \cos(\mu_y \cdot y) \cos[\mu_x(x - \varphi_5)] \quad (5.5) \end{aligned}$$

If for the specifications of σ_{3-5} and $\sigma_{5-8.5}$ in (4.66) and (4.67) the value of L^* (denoted by L_s^*) is taken according to the values of IV 3.4, namely $(L_x)_s = 1550$ km and $(L_x)_s/(L_y)_s = 0.48$, while in (5.4) and (5.5) L^* may be varying, one gets after substitution of (4.66) and (4.67) into respectively (5.4) and (5.5):

$$\begin{aligned} \varepsilon_3 = & -\mu_x U_5 F_5 (A_3 - 1) (1 - L_s^*/L^*) [1 - (L^* + L_s^*)\beta/U_5] \\ & \cdot \cos(\mu_y \cdot y) \cos[\mu_x(x - \varphi_5)] \end{aligned} \quad (5.6)$$

and

$$\begin{aligned} \varepsilon_{8.5} = & -\mu_x U_5 F_5 (1 - A_{8.5}) (1 - L_s^*/L^*) [1 - (L^* + L_s^*)\beta/U_5] \\ & \cdot \cos(\mu_y \cdot y) \cos[\mu_x(x - \varphi_5)] \end{aligned} \quad (5.7)$$

Considering the integrated thermodynamic equations (4.13) and (4.14), it is clear that the correction terms ε_3 and $\varepsilon_{8.5}$ act as fictitious heat sources or sinks depending on the sign of these terms. Calling this heat Q_{fict} one can write the terms in accordance with equation (2.14)

$$\varepsilon_3 = \int_{p_3}^{p_5} \frac{R \cdot Q_{\text{fict}}}{c_p f_{\sigma} p} dp \quad \text{and} \quad \varepsilon_{8.5} = \int_{p_5}^{p_{8.5}} \frac{R \cdot Q_{\text{fict}}}{c_p f_{\sigma} p} dp \quad (5.8)$$

This introduction of an artificial heat source or sink has no physical meaning, but as has been outlined in III 3.3, it is a possible way to account for the equivalent barotropic character of the long waves, if one takes the low values of the static stability according to saturated adiabatic lapse rates. Yet, it is interesting to investigate where the heat thus introduced is positive (sources) or negative (sinks), and for what wavelengths these sources or sinks are of importance. It follows from (5.6) and (5.7) that there are two wavelengths, denoted by $(L_x)_1$ and $(L_x)_2$, for which both ε_3 and $\varepsilon_{8.5}$ are zero, namely

$$(L_x)_1 = (L_x)_s \quad \text{and} \quad (L_x)_2 = [4\pi^2 \{1 + (L_x)_s^2/(L_y)_s^2\} U_5/\beta - (L_x)_s^2]^{\frac{1}{2}} \quad (5.9)$$

It follows from (5.9) that for $(L_x)_s = 1550$ km and for the ratio $(L_x)_s/(L_y)_s = 0.48$, $(L_x)_1 = 1550$ km and $(L_x)_2 = 9520$ km. This means that one can expect maximum absolute values for ε_3 and $\varepsilon_{8.5}$ for the long waves with wavelengths somewhere between 1550 and 9520 km. Comparison of (5.2) with (5.6) and (5.7) shows that for waves with wavelengths between 1550 and 9520 km and with the ratio $L_x/L_y = 0.48$, ε_3 and $\varepsilon_{8.5}$ are negative downstream of the ridge and positive upstream of it. For waves with $L_x/L_y = 0.48$ and with wavelengths smaller than 1550 km or larger than 9520 km the

results are opposite. It follows immediately from (5.8) that the results obtained for ε_3 and $\varepsilon_{8.5}$ are also valid for Q_{fict} .

The influence of the correction terms on the behaviour of the model at a certain time $t = t_0$ can be examined by the investigation of the differences between the tendencies $\dot{\psi}'_3, \dot{\psi}'_5$ and $\dot{\psi}'_{8.5}$ of the model with and without the correction terms in the forcing function assuming that both versions of the model use the same streamfunctions ψ'_3, ψ'_5 and $\psi'_{8.5}$ at $t = t_0$. These differences are denoted as follows:

$$(\dot{\psi}'_3)_{\text{dif}} \equiv (\dot{\psi}'_3)_{\text{inc}} - (\dot{\psi}'_3)_{\text{not}}, \quad (\dot{\psi}'_5)_{\text{dif}} \equiv (\dot{\psi}'_5)_{\text{inc}} - (\dot{\psi}'_5)_{\text{not}}$$

and

$$(\dot{\psi}'_{8.5})_{\text{dif}} \equiv (\dot{\psi}'_{8.5})_{\text{inc}} - (\dot{\psi}'_{8.5})_{\text{not}} \quad (5.10)$$

The subscripts 'inc' and 'not' refer to the quantities with the correction terms included and not included, respectively. The equations for the differences between the tendencies are obtained by subtracting (4.58) with $a_{04} = a_{05} = 0$ from the original equation (4.58), by subtracting (4.59) with $a_{14} = a_{15} = 0$ from the original (4.59) and by subtracting (4.60) with $(\dot{\psi}'_5)_{\text{not}}$ from (4.60) with $(\dot{\psi}'_5)_{\text{inc}}$. So one gets at $t = t_0$,

$$(\nabla^2 - a_{00}) (\dot{\psi}'_{8.5})_{\text{dif}} + a_{01} (\dot{\psi}'_3)_{\text{dif}} = a_{04} J(\psi_5, \nabla^2 \psi_5) - a_{05} \dot{\psi}'_5^*, \quad (5.11)$$

$$(\nabla^2 - a_{10}) (\dot{\psi}'_3)_{\text{dif}} + a_{11} (\dot{\psi}'_{8.5})_{\text{dif}} = a_{14} J(\psi_5, \nabla^2 \psi_5) - a_{15} \dot{\psi}'_5^* \quad (5.12)$$

and

$$\nabla^2 (\dot{\psi}'_5)_{\text{dif}} = a_0 (\dot{\psi}'_{8.5})_{\text{dif}} - a_1 (\dot{\psi}'_3)_{\text{dif}} \quad (5.13)$$

With the aid of the definitions of ε_3 and of $\varepsilon_{8.5}$ in (4.23) and (4.24) and using the definitions of the coefficients in (4.62)–(4.65), one obtains after lengthy but straightforward calculations:

$$(\nabla^2 - a_{00}) (\dot{\psi}'_{8.5})_{\text{dif}} + a_{01} (\dot{\psi}'_3)_{\text{dif}} = +a_{01} \varepsilon_3 - a_{00} \varepsilon_{8.5} \quad (5.14)$$

and

$$(\nabla^2 - a_{10}) (\dot{\psi}'_3)_{\text{dif}} + a_{11} (\dot{\psi}'_{8.5})_{\text{dif}} = -a_{10} \varepsilon_3 + a_{11} \varepsilon_{8.5} \quad (5.15)$$

Using the results of (5.6) and (5.7), the equations (5.14) and (5.15) can also be expressed as

$$(\nabla^2 - a_{00}) (\dot{\psi}'_{8.5})_{\text{dif}} + a_{01} (\dot{\psi}'_3)_{\text{dif}} = a_{05} G \quad (5.16)$$

and

$$(\nabla^2 - a_{10})(\psi'_3)_{\text{dif}} + a_{11}(\psi'_{8.5})_{\text{dif}} = a_{15}G \quad (5.17)$$

with

$$G \equiv U_5 F_5 \mu_x (1 - L_s^*/L^*) [1 - (L^* + L_s^*)\beta/U_5] \cos(\mu_y \cdot y) \cos[\mu_x(x - \varphi_5)] \quad (5.18)$$

Equations (5.13), (5.16) and (5.17) possess the following solutions for $(\psi'_{8.5})_{\text{dif}}$, $(\psi'_3)_{\text{dif}}$ and $(\psi'_5)_{\text{dif}}$.

$$(\psi'_{8.5})_{\text{dif}} = -S_{8.5} U_5 F_5 \mu_x \cos(\mu_y \cdot y) \cos[\mu_x(x - \varphi_5)], \quad (5.19)$$

$$(\psi'_3)_{\text{dif}} = -S_3 U_5 F_5 \mu_x \cos(\mu_y \cdot y) \cos[\mu_x(x - \varphi_5)] \quad (5.20)$$

and

$$(\psi'_5)_{\text{dif}} = -S_5 U_5 F_5 \mu_x \cos(\mu_y \cdot y) \cos[\mu_x(x - \varphi_5)] \quad (5.21)$$

with

$$S_{8.5} \equiv - \frac{(1 - L_s^*/L^*) [1 - (L^* + L_s^*)\beta/U_5] [a_{01}a_{15} + a_{05}(\mu_x^2 + \mu_y^2 + a_{10})]}{a_{01}a_{11} - (\mu_x^2 + \mu_y^2 + a_{00})(\mu_x^2 + \mu_y^2 + a_{10})} \quad (5.22)$$

$$S_3 \equiv - \frac{(1 - L_s^*/L^*) [1 - (L^* + L_s^*)\beta/U_5] [a_{05}a_{11} + a_{15}(\mu_x^2 + \mu_y^2 + a_{00})]}{a_{01}a_{11} - (\mu_x^2 + \mu_y^2 + a_{00})(\mu_x^2 + \mu_y^2 + a_{10})} \quad (5.23)$$

and

$$S_5 \equiv - \frac{-a_0 S_{8.5} + a_1 S_3}{\mu_x^2 + \mu_y^2} \quad (5.24)$$

Up to now the results have been obtained with the assumption that ψ_5 satisfies (5.2), but without any restriction to the streamfunctions ψ_3 and $\psi_{8.5}$ of the thickness fields 300–500 and 500–850 mbar. For the further investigations it is assumed that ψ_3 and $\psi_{8.5}$ also consist of sinusoidal waves. In agreement with the structure of the reference atmosphere, which was specified in III 2.1 by correlating the heights z of each pressure level with the heights of the 500 mbar level at the same grid points, the two thickness fields will each consist of two parts, namely an equivalent barotropic part like the reference atmosphere and a baroclinic departure, which is uncorrelated with the wave at 500 mbar. Therefore, it is supposed that the two thickness fields have the following forms:

$$\psi_3 = (A_3 - 1)\psi_5 + \frac{g \cdot B_3}{f_0} + F_3 \cos(\mu_y \cdot y) \cos[\mu_x(x - \varphi_3)] \quad (5.25)$$

and

$$\psi'_{8.5} = (1 - A_{8.5})\psi_5 - \frac{g \cdot B_{8.5}}{f_0} + F'_{8.5} \cos(\mu_y \cdot y) \cos[\mu_x(x - \phi'_{8.5})] \quad (5.26)$$

with F'_3 , $F'_{8.5}$, ϕ'_3 and $\phi'_{8.5}$ dependent on t and $\phi'_3 = \phi'_{8.5} = 0$ at $t = t_0$.

Differentiation of (5.2), (5.25) and (5.26) with respect to t at $t = t_0$ yields:

$$\begin{aligned} (\dot{\psi}_5)_{t=t_0} &= (\dot{F}_5)_{t=t_0} \cos(\mu_y \cdot y) \sin(\mu_x \cdot x) \\ &\quad - \mu_x F_5(\dot{\phi}_5)_{t=t_0} \cos(\mu_y \cdot y) \cos(\mu_x \cdot x), \end{aligned} \quad (5.27)$$

$$\begin{aligned} (\dot{\psi}'_3)_{t=t_0} &= [(A_3 - 1)(\dot{F}_5)_{t=t_0} + \mu_x F'_3(\dot{\phi}'_3)_{t=t_0}] \cos(\mu_y \cdot y) \sin(\mu_x \cdot x) \\ &\quad + [(\dot{F}'_3)_{t=t_0} - (A_3 - 1)\mu_x F_5(\dot{\phi}_5)_{t=t_0}] \cos(\mu_y \cdot y) \cos(\mu_x \cdot x) \end{aligned} \quad (5.28)$$

and

$$\begin{aligned} (\dot{\psi}'_{8.5})_{t=t_0} &= [(1 - A_{8.5})(\dot{F}_5)_{t=t_0} + \mu_x F'_{8.5}(\dot{\phi}'_{8.5})_{t=t_0}] \cos(\mu_y \cdot y) \sin(\mu_x \cdot x) \\ &\quad + [(\dot{F}'_{8.5})_{t=t_0} - (1 - A_{8.5})\mu_x F_5(\dot{\phi}_5)_{t=t_0}] \cos(\mu_y \cdot y) \cos(\mu_x \cdot x) \end{aligned} \quad (5.29)$$

The tendencies given by (5.27), (5.28) and (5.29) can be interpreted in terms of changes of amplitudes and of phases at $t = t_0$ as follows:

\dot{F}_5 , $(A_3 - 1)\dot{F}_5$ and $(1 - A_{8.5})\dot{F}_5$ are the changes of the amplitudes of the wave at 500 mbar and of the equivalent barotropic parts of the streamfunctions ψ'_3 and $\psi'_{8.5}$ of the two thickness fields 300–500 and 500–850 mbar.

$\dot{\phi}_5$ is the change of phase of the wave at 500 mbar and of the equivalent barotropic parts of ψ'_3 and $\psi'_{8.5}$ and can be considered as the wave velocity of the equivalent barotropic part of the wave at $t = t_0$.

\dot{F}'_3 and $\dot{F}'_{8.5}$ are the changes of the amplitudes of the baroclinic parts of the waves of ψ'_3 and $\psi'_{8.5}$.

$\dot{\phi}'_3$ and $\dot{\phi}'_{8.5}$ are the changes of the phases of the baroclinic parts of the waves of ψ'_3 and $\psi'_{8.5}$ and can be considered as the wave velocities of those parts at $t = t_0$.

The sinusoidal wave given by (5.2), (5.25) and (5.26) is used as initial condition for the two versions of the BK3-model with and without the correction terms. Two cases will be considered, namely the case of the reference atmosphere with $F'_3 = F'_{8.5} = 0$ at $t = t_0$ and the more general baroclinic case with $F'_3 \neq 0$ and $F'_{8.5} \neq 0$. The computed tendencies at $t = t_0$ following from the two versions of the BK3-model can be interpreted in terms of changes of amplitudes and of phases after comparison with formulas

(5.27), (5.28) and (5.29). This interpretation leads to a better insight in the behaviour of the model with regard to the development and the velocity of the wave at $t = t_0$.

The case of the reference atmosphere

In this case $F'_3 = 0$ and $F'_{8.5} = 0$ at $t = t_0$ in (5.25) and (5.26). After substitution of (5.25) and (5.26) into equations (4.58), (4.59) and (4.60) of the BK3-model it follows without any restriction to ψ_5 that

$$\psi'_3 = (A_3 - 1)\psi_5, \quad \psi'_{8.5} = (1 - A_{8.5})\psi_5 \quad \text{and} \quad \psi_5 = \psi_5^* \quad (5.30)$$

This result can be derived by substituting (5.30) into (4.58), (4.59) and (4.60). After the substitution of (4.64) for a_{05} and a_{04} into (4.58) and of (4.65) for a_{15} and a_{14} into (4.59), these equations are transformed into (4.57). Using the definitions of a'_1 and of a'_0 in (4.42), of b'_1 and b'_0 in (4.43), the formulas for a_0 and for a_1 in (4.61) and those for σ_{3-5} and $\sigma_{5-8.5}$ in (4.66) and (4.67), it is found that

$$a_0(1 - A_{8.5}) - a_1(A_3 - 1) = 0 \quad (5.31)$$

Making use of this result (4.60) also becomes identical to (4.57). Due to the lateral boundary condition $\psi'_3 = \psi'_{8.5} = \psi_5 = \psi_5^* = 0$ (5.30) is the unique solution.

By differentiating (5.25) and (5.26) (with $F'_3 = F'_{8.5} = 0$) with respect to t it follows immediately that the tendencies contained in (5.30) equal those of the reference atmosphere. This result is not surprising, because the model with the correction terms ε_3 and $\varepsilon_{8.5}$ included has been designed in such a way that if the initial condition is the reference atmosphere, it remains so once and for all.

Now it is again assumed that ψ_5 satisfies (5.2) at $t = t_0$. After substitution of this sine-wave into (4.57) ψ_5^* becomes

$$\psi_5^* = -U_5 F_5 R_5 \mu_x \cos(\mu_y \cdot y) \cos(\mu_x \cdot x) \quad (5.32)$$

with

$$R_5 \equiv 1 - \beta \cdot L^*/U_5 \quad (5.33)$$

and $L^* \equiv 1/(\mu_x^2 + \mu_y^2)$ as mentioned in relation with (4.27). Then according to (5.30) the tendencies for the reference atmosphere are

$$(\psi_5)_{\text{inc}} = -U_5 F_5 R_5 \mu_x \cos(\mu_y \cdot y) \cos(\mu_x \cdot x), \quad (5.34)$$

$$(\psi'_3)_{\text{inc}} = -U_5 F_5 R_3 \mu_x \cos(\mu_y \cdot y) \cos(\mu_x \cdot x) \quad (5.35)$$

and

$$(\dot{\psi}'_{8.5})_{\text{inc}} = -U_5 F_5 R_{8.5} \mu_x \cos(\mu_y \cdot y) \cos(\mu_x \cdot x) \quad (5.36)$$

with

$$R_3 \equiv (A_3 - 1)R_5 \quad (5.37)$$

and

$$R_{8.5} \equiv (1 - A_{8.5})R_5 \quad (5.38)$$

The subscript 'inc' refers to the correction terms included. Noting that $F'_3 = F'_{8.5} = 0$, it follows after the comparison of (5.34)–(5.36) with (5.27)–(5.29) that

$$(\dot{\phi}'_5)_{t=t_0} = U_5 R_5 = U_5 - \beta \cdot L^* \quad (5.39)$$

and

$$(\dot{F}'_5)_{t=t_0} = (\dot{F}'_3)_{t=t_0} = (\dot{F}'_{8.5})_{t=t_0} = 0 \quad (5.40)$$

(5.39) shows that the wave at 500 mbar and the equivalent barotropic parts of ψ'_3 and $\psi'_{8.5}$ move with the Rossby-Haurwitz speed at $t = t_0$. (5.40) shows that the baroclinic parts, which are not present at $t = t_0$, do not appear either. In exactly the same manner it can be shown that (5.39) and (5.40) are valid for all times t . For several values of L_x with $L_x/L_y = 0.48$ and $U_5 = 31 \text{ ms}^{-1}$ the Rossby-Haurwitz speed (relative with regard to U_5) in (5.39) has been computed and is given in figure 23.

Now the tendencies at $t = t_0$ for the BK3-model without the correction terms are computed. For that purpose the results of (5.34), (5.35), (5.36), (5.19), (5.20) and (5.21) are substituted into (5.10) so that

$$(\dot{\psi}'_5)_{\text{not}} = -U_5 F_5 (R_5 - S_5) \mu_x \cos(\mu_y \cdot y) \cos(\mu_x \cdot x), \quad (5.41)$$

$$(\dot{\psi}'_3)_{\text{not}} = -U_5 F_5 (R_3 - S_3) \mu_x \cos(\mu_y \cdot y) \cos(\mu_x \cdot x) \quad (5.42)$$

Fig. 23 Changes of phase (relative with respect to U_5) and of amplitude at $t = t_0$ of an equivalent barotropic sine-wave according to the reference atmosphere with $L_x/L_y = 0.48$ for the BK3-model with the correction terms included and with these terms not included.

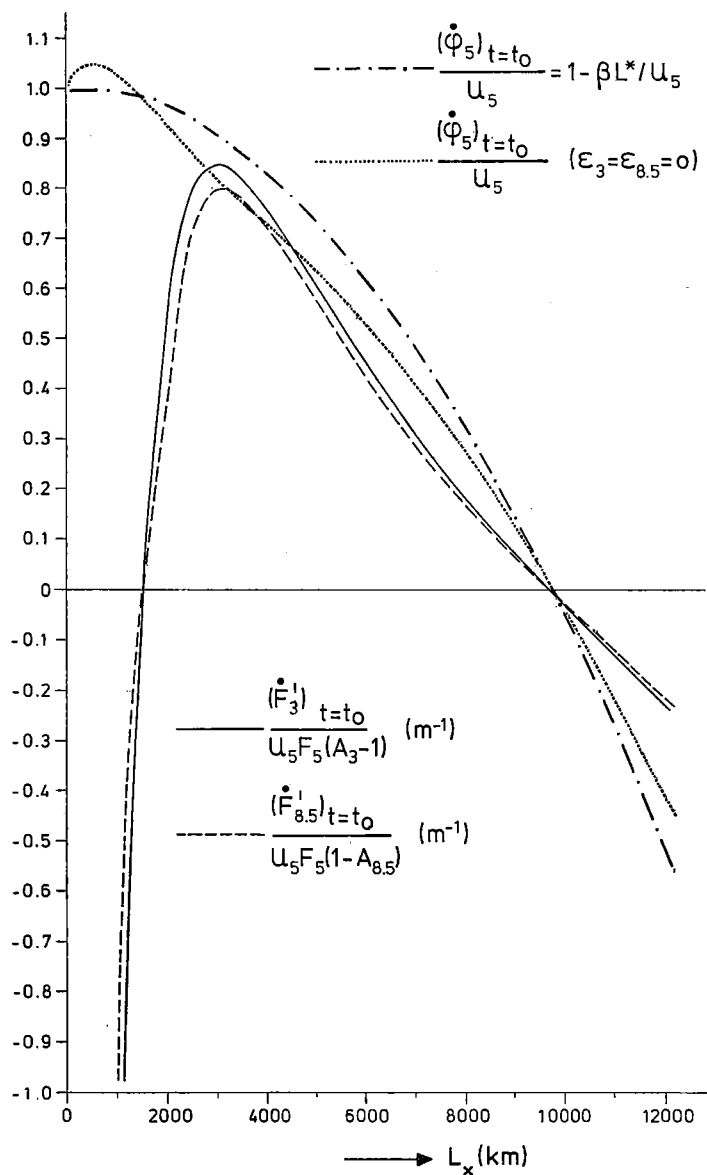
For the BK3-model with the correction terms:

----- Relative velocity (equal to the relative Rossby-Haurwitz speed) of the sine-wave of 500 mbar and of the thicknesses 300–500 and 500–850 mbar.

The amplitudes of the wave of 500 mbar and of the baroclinic parts of the waves of the thickness fields 300–500 and 500–850 mbar (not present at $t = t_0$) do not change at $t = t_0$.

For the BK3-model without the correction terms:

..... Relative velocity (relative with respect to U_5) of the sine-wave of 500 mbar and of



the equivalent barotropic parts of the thicknesses 300—500 and 500—850 mbar.

The amplitude of the wave of 500 mbar does not change at $t = t_0$ ($(\dot{F}_5)_{t=t_0} = 0$).

- Change of the amplitude (relative with respect to $U_5 F_5 (A_3 - 1)$) of the baroclinic part of the thickness 300—500 mbar.
- - - Change of the amplitude (relative with respect to $U_5 F_5 (1 - A_{8.5})$) of the baroclinic part of the thickness 500—850 mbar.

and

$$(\dot{\psi}'_{8.5})_{\text{not}} = -U_5 F_5 (R_{8.5} - S_{8.5}) \mu_x \cos(\mu_y \cdot y) \cos(\mu_x \cdot x) \quad (5.43)$$

Comparison of (5.41)–(5.43) with (5.27)–(5.29) yields

$$(\dot{\phi}'_5)_{t=t_0} = (R_5 - S_5) U_5 \quad \text{and} \quad (\dot{F}'_5)_{t=t_0} = 0, \quad (5.44)$$

$$(\dot{F}'_3)_{t=t_0} = \mu_x F_5 U_5 [S_3 - (A_3 - 1) S_5] \quad (5.45)$$

and

$$(\dot{F}'_{8.5})_{t=t_0} = \mu_x F_5 U_5 [S_{8.5} - (1 - A_{8.5}) S_5] \quad (5.46)$$

(5.44) shows that for the BK3-model without the correction terms the velocity of the wave at 500 mbar and of the equivalent barotropic parts of ψ'_3 and $\psi'_{8.5}$ move with a velocity which is in general not equal to the velocity obtained for the BK3-model with the correction terms included, as can be seen by comparing (5.44) with (5.39). The formulas (5.45) and (5.46) show that the changes of the amplitudes of the baroclinic parts of ψ'_3 and $\psi'_{8.5}$ are in general not equal to zero. The quantities $(\dot{\phi}'_5)_{t=t_0}/U_5$, $(\dot{F}'_3)_{t=t_0}/[U_5 F_5 (A_3 - 1)]$ and $(\dot{F}'_{8.5})_{t=t_0}/[U_5 F_5 (1 - A_{8.5})]$ have been computed for several values of L_x , using the chosen ratio $L_x/L_y = 0.48$, $U_5 = 31 \text{ ms}^{-1}$ and the values of the coefficients in IV 3.4. The results are given in figure 23. Consideration of (5.22), (5.23) and (5.24) in relation to (5.9) shows that for the wavelengths 1550 and 9520 km $S_{8.5} = S_3 = S_5 = 0$. Consequently in that case $(\dot{\phi}'_5)_{t=t_0}$ in (5.44) equals $(\dot{\phi}'_5)_{t=t_0}$ in (5.39) and $(\dot{F}'_3)_{t=t_0} = (\dot{F}'_{8.5})_{t=t_0} = 0$. Figure 23 shows that for the waves with wavelengths between 1550 and 9520 km the velocity of the waves at 500 mbar and of the equivalent barotropic parts of ψ'_3 and $\psi'_{8.5}$ for the model without the correction terms are somewhat smaller than the Rossby-Haurwitz speed obtained for the model with ε_3 and $\varepsilon_{8.5}$ included. It also appears that for the model without the correction terms the tendencies of the amplitudes of the baroclinic departures from the reference atmosphere at $t = t_0$, \dot{F}'_3 and $\dot{F}'_{8.5}$ are positive for the wavelengths between 1550 and 9520 km, with a maximum at about 3000 km. Outside this interval the tendencies are negative.

Starting with the reference atmosphere as initial condition at $t = t_0$, it can be discussed with the aid of (5.39), (5.40), (5.44), (5.45) and (5.46) and figure 23 what happens a short time later. With the correction terms included, the sine-waves of the 500 mbar level and of the two thickness fields 300–500 and 500–850 mbar remain to move with the Rossby-Haurwitz speed and show no baroclinic development, due to $(\dot{F}'_3)_{t=t_0} = (\dot{F}'_{8.5})_{t=t_0} = 0$. Without the correction terms, however, \dot{F}'_3 and $\dot{F}'_{8.5}$ are positive for the waves with wavelengths between 1550 and 9520 km, so that the baroclinic parts of the two thickness fields (lagging 90° with respect to the wave at 500 mbar)

begin to develop, and a short time after t_0 the wave gets a structure allowing further baroclinic development. For the other wavelengths the effect is opposite, due to $\dot{F}'_3 < 0$ and $\dot{F}'_{8.5} < 0$.

So for the long waves having wavelengths between 1550 and 9520 km the model without the correction terms must be more baroclinically unstable than the version with the correction terms included and for the other waves the effects is opposite.

It will be shown that this conclusion is also valid for the more general case of a baroclinic sine-wave with $F'_3 \neq 0$ and $F'_{8.5} \neq 0$ at $t = t_0$.

The case of a baroclinic sinusoidal wave

(5.2), (5.25) and (5.26) with $\varphi_5 = \varphi'_3 = \varphi'_{8.5} = 0$ and $F'_3 \neq 0$ and $F'_{8.5} \neq 0$ are the initial conditions of the wave at $t = t_0$ and can be substituted into the BK3-equations (4.57)–(4.60) with the correction terms included. Then the tendencies for $t = t_0$ can be computed and are denoted by $(\dot{\psi}'_5)_{inc}$, $(\dot{\psi}'_3)_{inc}$ and $(\dot{\psi}'_{8.5})_{inc}$. These tendencies are rather complicated and are not further specified. According to (5.27), (5.28) and (5.29) these tendencies can be expressed in terms of changes of amplitudes and of phases at $t = t_0$. These changes are denoted by $(\dot{F}'_5)_{inc}$, $(\dot{F}'_3)_{inc}$, $(\dot{F}'_{8.5})_{inc}$, $(\dot{\phi}'_5)_{inc}$, $(\dot{\phi}'_3)_{inc}$ and $(\dot{\phi}'_{8.5})_{inc}$. Similarly it is possible to compute the tendencies for $t = t_0$ if the correction terms are not included. These tendencies are denoted by $(\dot{\psi}'_5)_{not}$, $(\dot{\psi}'_3)_{not}$ and $(\dot{\psi}'_{8.5})_{not}$, and they can also be expressed in terms of changes of amplitudes and of phases at $t = t_0$ using (5.27), (5.28) and (5.29). These changes are denoted by $(\dot{F}'_5)_{not}$, $(\dot{F}'_3)_{not}$, $(\dot{F}'_{8.5})_{not}$, $(\dot{\phi}'_5)_{not}$, $(\dot{\phi}'_3)_{not}$ and $(\dot{\phi}'_{8.5})_{not}$. The influence of the correction terms is revealed by the difference between the tendencies $(\dot{\psi})_{inc}$ and $(\dot{\psi})_{not}$ denoted by $(\dot{\psi})_{dif}$. So it follows from the considerations given above that at $t = t_0$:

$$(\dot{\psi}'_5)_{dif} = (\dot{F}'_5)_{dif} \cos(\mu_y \cdot y) \sin(\mu_x \cdot x) - \mu_x F'_5 (\dot{\phi}'_5)_{dif} \cos(\mu_y \cdot y) \cos(\mu_x \cdot x), \quad (5.47)$$

$$\begin{aligned} (\dot{\psi}'_3)_{dif} = & [(A_3 - 1) (\dot{F}'_3)_{dif} + \mu_x F'_3 (\dot{\phi}'_3)_{dif}] \cos(\mu_y \cdot y) \sin(\mu_x \cdot x) \\ & + [(\dot{F}'_3)_{dif} - (A_3 - 1) \mu_x F'_3 (\dot{\phi}'_3)_{dif}] \cos(\mu_y \cdot y) \cos(\mu_x \cdot x), \end{aligned} \quad (5.48)$$

and

$$\begin{aligned} (\dot{\psi}'_{8.5})_{dif} = & [(1 - A_{8.5}) (\dot{F}'_5)_{dif} + \mu_x F'_{8.5} (\dot{\phi}'_{8.5})_{dif}] \cos(\mu_y \cdot y) \sin(\mu_x \cdot x) \\ & + [(\dot{F}'_{8.5})_{dif} - (1 - A_{8.5}) \mu_x F'_{8.5} (\dot{\phi}'_{8.5})_{dif}] \cos(\mu_y \cdot y) \cos(\mu_x \cdot x) \end{aligned} \quad (5.49)$$

with

$$\begin{aligned} (\dot{F}'_5)_{dif} &\equiv (\dot{F}'_5)_{inc} - (\dot{F}'_5)_{not}, & (\dot{F}'_3)_{dif} &\equiv (\dot{F}'_3)_{inc} - (\dot{F}'_3)_{not}, \\ (\dot{F}'_{8.5})_{dif} &\equiv (\dot{F}'_{8.5})_{inc} - (\dot{F}'_{8.5})_{not}, & (\dot{\phi}'_5)_{dif} &\equiv (\dot{\phi}'_5)_{inc} - (\dot{\phi}'_5)_{not}, \\ (\dot{\phi}'_3)_{dif} &\equiv (\dot{\phi}'_3)_{inc} - (\dot{\phi}'_3)_{not} & \text{and} & (\dot{\phi}'_{8.5})_{dif} \equiv (\dot{\phi}'_{8.5})_{inc} - (\dot{\phi}'_{8.5})_{not} \end{aligned} \quad (5.50)$$

For the sine-wave in (5.2) as initial condition at $t = t_0$ for the equations of the BK3-model the three tendencies $(\dot{\psi}_5)_{\text{dif}}$, $(\dot{\psi}'_3)_{\text{dif}}$ and $(\dot{\psi}'_{8.5})_{\text{dif}}$ have already been computed and these are given in (5.21), (5.20) and (5.19), respectively. So after equating $(\dot{\psi}_5)_{\text{dif}}$ in (5.21) with $(\dot{\psi}'_5)_{\text{dif}}$ in (5.47) it follows that

$$(\dot{\phi}_5)_{\text{dif}} = S_5 U_5 \quad \text{and} \quad (\dot{F}'_5)_{\text{dif}} = 0 \quad (5.51)$$

Similarly one can deduce that

$$(\dot{\phi}'_3)_{\text{dif}} = 0 \quad \text{and} \quad (\dot{F}'_3)_{\text{dif}} = -\mu_x U_5 F_5 [S_3 - (A_3 - 1)S_5], \quad (5.52)$$

$$(\dot{\phi}'_{8.5})_{\text{dif}} = 0 \quad \text{and} \quad (\dot{F}'_{8.5})_{\text{dif}} = -\mu_x U_5 F_5 [S_{8.5} - (1 - A_{8.5})S_5] \quad (5.53)$$

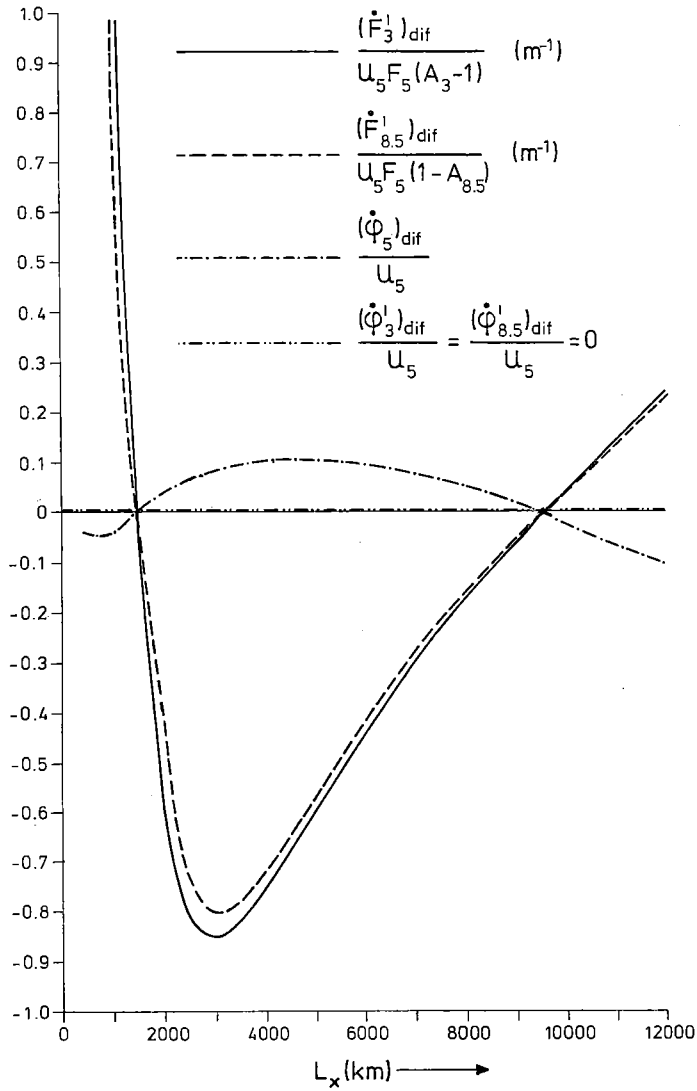
Formulas (5.51), (5.52) and (5.53) give the expressions for the differences between the changes of the phases and of the amplitudes at $t = t_0$ of the baroclinic sinusoidal wave caused by the inclusion of the correction terms in the BK3-model.

The quantities $(\dot{\phi}_5)_{\text{dif}}/U_5$, $(\dot{F}'_3)_{\text{dif}}/[U_5 F_5 (A_3 - 1)]$ and $(\dot{F}'_{8.5})_{\text{dif}}/[U_5 F_5 (1 - A_{8.5})]$ have been computed for several values of L_x , using the chosen ratio $L_x/L_y = 0.48$, $U_5 = 31 \text{ ms}^{-1}$ and the values of the coefficients in IV 3.4. The results are given in figure 24. This figure shows that the tendencies $(\dot{F}'_3)_{\text{dif}}$ and $(\dot{F}'_{8.5})_{\text{dif}}$ of the amplitudes of the baroclinic departures from the reference atmosphere are negative for waves having wavelengths between 1550 and 9520 km and positive for the other wavelengths. The minimum is found at ~ 3000 km. This means that for these wavelengths, due to the correction terms, the baroclinic parts of the two thickness fields 300–500 and 500–850 mbar are damped and the wave gets a structure which allows less baroclinic development. So the following conclusions can be drawn:

For the waves with wavelengths between 1550 and 9520 km the model with the correction terms included is more stable with regard to baroclinic development than the model without these terms. For the other wavelengths the effect is opposite. Thus for the short baroclinic waves with wavelengths < 1550 km the influence of the correction terms will be an amplification of the amplitudes of the waves describing the baroclinic parts of the thermal fields.

Fig. 24 Difference between the BK3-model with the correction terms included and with those terms not included with respect to the behaviour at $t = t_0$ of the simple baroclinic sine-wave with $L_x/L_y = 0.48$ according to (5.2), (5.25) and (5.26).

- Change of the amplitude (relative with respect to $U_5 F_5 (A_3 - 1)$) of the baroclinic part of the thickness of 300–500 mbar as function of the wavelength L_x .
 - - - - - Change of the amplitude (relative with respect to $U_5 F_5 (1 - A_{8.5})$) of the baroclinic part of the thickness of 500–850 mbar as function of the wavelength L_x .
-



The amplitudes of the waves of 500 mbar and of the equivalent barotropic parts (according to the reference atmosphere) of the thicknesses of 300—500 mbar and 500—850 mbar do not change at $t = t_0$.

----- Phase changes at $t = t_0$ of the wave of 500 mbar and the equivalent barotropic parts (according to the reference atmosphere) of the thicknesses of 300—500 and 500—850 mbar as functions of the wavelength L_x .

----- Phase changes (equal to zero) of the baroclinic parts of the thicknesses of 300—500 and 500—850 mbar as functions of the wavelength L_x .

Figure 24 also shows that for the waves with wavelengths between 1550 and 9520 km the correction terms do cause a slight increase of the wave velocity at $t = t_0$ for the wave at 500 mbar and also for the equivalent barotropic parts of the thickness fields. The maximum is found for $L_x \approx 4000\text{--}5000$ km and amounts to $\sim 10\%$ of U_5 .

The conclusions obtained for the simple baroclinic wave as initial condition agree with the conclusions valid for the reference atmosphere.

Clearly, the conclusions drawn here for the reference atmosphere as well as for the simple baroclinic wave as initial conditions for the equations of the BK3-model are only valid for $t = t_0$. After that point of time, due to the non-linearity of the equations, higher order components will arise in the tendencies of the model, and the wave gets a structure which is more complicated than the simple sinusoidal wave given by (5.2), (5.25) and (5.26). So a comparison of the tendencies obtained from the equations of the model with those in (5.27), (5.28) and (5.29) is no longer possible. Despite this limitation it appears that the conclusions valid for $t = t_0$ do agree with the behaviour of the model in practice. Compared with the model without the correction terms, the model with these terms included tends to favour the short waves and has a tendency to damp the long waves (wavelengths $\sim 3000\text{--}\sim 4000$ km), especially their thickness fields. It appears that the model with the correction terms has a tendency to make the long waves more and more equivalent barotropic during the prediction time. In the daily routine this effect proved to be not serious for most cases, because the long waves are already to a high degree equivalent barotropic at $t = t_0$. The development of the short baroclinic waves with wavelengths < 1550 km is favoured by the model with the correction terms included, compared with that of the version without these terms. This could even lead to instability for these waves. However, in practice SHUMAN's smoothing operator is applied at specified times during the time-integrations of the equations. See also IV 6.4. This smoothing has a strong damping influence on the shortest waves with wavelengths of two to three grid distances ($\sim 750\text{--}\sim 1000$ km) as can be seen from table 23. In most cases this smoothing proved to be sufficient to keep the shortest waves stable in the dry version of the model. However, in some cases it could be seen that the amplitudes of the waves with wavelengths of three to four grid distances ($\sim 1000\text{--}\sim 1500$ km) became too large. Concerning the ultra-long waves it can be remarked that the model is not suitable to describe them well, since if they would have a structure like that of the reference atmosphere, they would move with the Rossby-Haurwitz speed, which is a bad approximation for the velocity of these waves. In general they can be considered stationary for prediction times up to 36 hours ahead.

LIST OF SYMBOLS

A	p -dependable parameter in the definition of the reference atmosphere as given in (3.1)
$A_2, A_3, A_5, A_6,$ $A_7, A_{8.5}, A_{10}$	Values of A at 200, 300, 500, 600, 700, 850 and 1000 mbar respectively ($A_5 = 1$ according to the definition of A)
A'	A/A_6
A'_u, A'_l	A' for $p = p_u$ and $p = p_l$
$A_{s0}, A_{s1}, A_{s2}, A_{s3}$	Constants given in (4.159)
a	Radius of earth (= 6371229 m)
$a_0, a_1, a_{00},$ a_{01}, a_{10}, a_{11}	Coefficients in the equations of the BK3-model defined in (4.61), (4.62) and 4.63)
a_{04}, a_{05}	Coefficients, defined in (4.64), in the dry version of the BK3-model resulting from the correction terms ε_3 and $\varepsilon_{8.5}$
a_{14}, a_{15}	Coefficients, defined in (4.65), in the dry version of the BK3-model resulting from the correction terms ε_3 and $\varepsilon_{8.5}$
$a_0^*, a_1^*, a_{00}^*,$ $a_{01}^*, a_{10}^*, a_{11}^*$	Parts of the coefficients, defined in (4.69), in the dry version of the BK3-model not dependent on the static stability parameters
a'_0, a'_1	Coefficients, defined in relation with (4.42), dependent on the parameter A of the reference atmosphere
α	$\lambda(p_l - p_u)$, dimensionless parameter used in the stability analysis of the quasi-geostrophic equations indicating the stability of the flow
α^*	Quantity given in relation with (4.38)
B	p -dependable parameter in the definition of the reference atmosphere as given in (3.1)
$B_3, B_5, B_7,$ $B_{8.5}, B_{10}$	Values of B at 300, 500, 700, 850 and 1000 mbar respectively ($B_5 = 0$ according to the definition of the reference atmosphere)
b'_0, b'_1	Coefficients defined in relation with (4.43) dependent on the parameter A of the reference atmosphere
β	$\left(\frac{df}{dy}\right)_{\varphi = 45^\circ}$, Rossby parameter
β^*	Quantity defined in relation with (4.43)
C_1, C_2	Functions defined in (3.46) and dependent on A and B respectively
$C_3, C_{8.5}$	Functions given in relation with (4.44) and (4.45)
C^*	Function dependent on A defined in (3.48)
$C_{3}^*, C_{8.5}^*$	Values of C^* at 300 and 850 mbar respectively
c	Phase velocity (may be real or complex)
c_i	Complex part of c
c_r	Real part of c
c_p	Specific heat of dry air at constant pressure

c_v	Specific heat of dry air at constant volume
c'_0	Coefficient defined in relation with (4.49)
$(c'_{5})_{inc}, (c'_{3})_{inc},$ $(c'_{8.5})_{inc}$	Phase velocities at $t = t_0$ of the sinusoidal wave at 500 mbar defined in (5.2) and the sinusoidal waves of the thickness fields 300-500 and 500-850 mbar for a wave satisfying the reference atmosphere when the correction terms are included in the equations of the BK3-model
$(c'_{5})_{not}, (c'_{3})_{not},$ $(c'_{8.5})_{not}$	Phase velocities at $t = t_0$ of the sinusoidal wave at 500 mbar defined in (5.2) and the sinusoidal waves of the thickness fields 300-500 and 500-850 mbar for a wave satisfying the reference atmosphere when the correction terms are not included in the equations of the BK3-model
D	Horizontal divergence of the wind vector
D_h, D_i, D_j	Divergences at the three pressure levels p_h, p_i and p_j , respectively
D_{hi}	$D_h - D_i$
D_{ij}	$D_i - D_j$
$D_3, D_5, D_{8.5}$	Values of D at 300, 500 and 850 mbar, respectively
D_d	Dry part of D
D_m	Moist part of D
$D_{d3}, D_{d5}, D_{d8.5}$	Values of D_d at 300, 500 and 850 mbar, respectively
$D_{m3}, D_{m5}, D_{m8.5}$	Values of D_m at 300, 500 and 850 mbar, respectively
D'_{m3}	$D_{m3} - D_{m5}$
$D'_{m8.5}$	$D_{m5} - D_{m8.5}$
D'	$f_0 D / RVA$
D'_d	$f_0 D_d / RVA$, function of A , defined in (3.70)
D'_m	$f_0 D_m / RVA$, function of A and C^* , defined in (3.71)
D'_1, D'_2	Functions describing the D -profil defined in relation with (3.123)
d	Grid point distance (375 km at 60°N)
d'_0, d'_1	Coefficients defined in relation with (4.48) dependent on the parameter A
A	$a_0 b_1 - a_1 b_0$, quantity defined in (4.68)
Δp	Increment of pressure
Δt	Increment of time
Δy	Increment along the y -axis
Δz	Height difference between two isohypses of a level of constant pressure
δ	Phase shift in the vertical of the perturbation T' of the thermal field
E	Constant given in relation with (3.15) and (5.2)
$E_3, E_{8.5}$	Functions dependent on p given in relation with (4.44) and (4.45)
ε_3	Correction term, defined in (3.41), used in the thermodynamic equation integrated from 300 to 500 mbar

$\epsilon_{8.5}$	Correction term, defined in (3.42), used in the thermodynamic equation integrated from 500 to 850 mbar
F	$A \cdot K - A^2$
F_h, F_i, F_j	Functions defining the profile of D in the dry version of the BK3-model given in (4.31), (4.32) and (4.33)
F_p	Function, defined in (3.99), describing the structure of the perturbation ψ^* in the vertical
F_r	Real part of F_p
F_i	Complex part of F_p
F_5	Value of F_p at 500 mbar
F'	Amplitude dependent on t defined in relation with (5.2)
$F_3, F_{8.5}$	F_p/F_5 , given in (3.107)
$\dot{F}_3, \dot{F}_{8.5}$	Amplitudes dependent on t , defined in relation with (5.25) and (5.26)
$\dot{F}_5, \dot{F}'_3, \dot{F}'_{8.5}$	Tendencies of F_5, F_3 and $F_{8.5}$
$(\dot{F}_5)_{inc}, (\dot{F}'_3)_{inc}, (\dot{F}'_{8.5})_{inc}$	Tendencies \dot{F}_5, \dot{F}'_3 and $\dot{F}'_{8.5}$, obtained for the BK3-model with the correction terms included
$(\dot{F}_5)_{not}, (\dot{F}'_3)_{not}, (\dot{F}'_{8.5})_{not}$	Tendencies \dot{F}_5, \dot{F}'_3 and $\dot{F}'_{8.5}$ obtained for the BK3-model with the correction terms not included
$(\dot{F}_5)_{dif}, (\dot{F}'_3)_{dif}, (\dot{F}'_{8.5})_{dif}$	$(\dot{F}_5)_{inc} - (\dot{F}_5)_{not}$ $(\dot{F}'_3)_{inc} - (\dot{F}'_3)_{not}$ $(\dot{F}'_{8.5})_{inc} - (\dot{F}'_{8.5})_{not}$
f	$2\Omega \sin \varphi$, Coriolis parameter
f_0	Value of f at 45°N
f_1	Value of f at latitude $\varphi = \varphi_1$
$f(\alpha)$	$1 + 4\alpha^{-2} - 4\alpha^{-1}\coth(\alpha)$, function of the dimensionless parameter used in the stability analysis of the quasi-geostrophic equations
G	$\pm \alpha f(\alpha)^{\frac{1}{2}}$, defined in relation with (3.96)
G'	Quantity defined in (5.18)
g	$\pm [-g(\alpha)]^{\frac{1}{2}}$, defined in relation with (3.114)
$g(\alpha)$	Acceleration of gravity
γ	$\alpha^2 f(\alpha)$, defined in (3.92)
H_3	Phase shift in the vertical of the perturbation ψ'
$H_{8.5}$	Heating function due to the release of latent heat in the layer 300-500 mbar, defined in (4.118)
h	Heating function due to the release of latent heat in the layer 500-850 mbar, defined in (4.95)
I	Quantity used in (4.149)
i	Maximum value of positive RVA given in relation with (3.21)
i	$(-1)^{\frac{1}{2}}$, used in (3.77) and (3.78)
i	Discrete coordinate in the x -direction (parallel to 30°W) of the computational grid defined in IV.6.1

i	Discrete coordinate in the x_s -direction of polar stereographic projection (parallel to 30°W)
J	Jacobian defined in (2.11)
$J_1, J_2, J_3, J_4,$ J_5, J_6, J_7, J_8	Jacobians used in the forcing functions in the equations of the dry version of the BK3-model, defined in (4.143)
$JJ_{i,j}$	Finite difference approximation of the Jacobian for the grid point with coordinates i and j given in (4.157)
JJ_a, JJ_b, JJ_c	Finite difference approximations of the Jacobian defined in (4.153), (4.154) and (4.155), respectively
j	Discrete coordinate in the y -direction (parallel to 120°W) of the computational grid defined in IV.6.1
j^*	Discrete coordinate in the y_s -direction of polar stereographic projection (parallel to 120°W)
K	$(\int_0^{p_0} A^2 dp) / (\int_0^{p_0} A dp)$, constant of the reference atmosphere
K_1, K_2, K_3, K_4	Constants used in the two-parameter model, defined in (3.54)
L	Heat of condensation of water vapor
L_x	Wavelength in the x -direction (west to east)
L_y	Wavelength in the y -direction (south to north)
$(L_x)_s$	Chosen value of L_x in V.3
$(L_y)_s$	Chosen value of L_y in V.3
$(L_x)_1, (L_x)_2$	Values of L_x for which ε_3 and $\varepsilon_{8,5}$ are zero
L_1, L_2	Distances between the points of maximum RVA-values of the RVA-areas of a wave train numbered with $n - 1$, n and $n + 1$
L^*	$1/(\mu_x^2 + \mu_y^2)$
L_s^*	Chosen value of L^* in V.3
L_1^*, L_2^*	Values of L^* for which $\sigma = \sigma_{r.a.}$
λ	Longitude $[\sigma(\mu_x^2 + \mu_y^2)]^{1/2} / f_0$, parameter used in the stability analysis of the quasi-geostrophic equations, defined in relation with (3.81)
λ_0	Longitude of the origin of the coordinate system defined in (2.1)
m	$(1 + \sin 60^\circ) / (1 + \sin \varphi)$, map scale factor of polar stereographic projection
m_1	Map scale factor at latitude $\varphi = \varphi_1$
μ_x	$2\pi / L_x$, wavenumber in the x -direction (west to east)
μ_y	$2\pi / L_y$, wavenumber in the y -direction (south to north)
n	Total number of waves around the latitude circle 45°N
P_0, P_1, P_2	Functions dependent on x , y and t given in relation with (3.127)
p	Pressure
p_h, p_i, p_j	Pressures of the chosen levels for D_h , D_i and D_j , respectively
p_u	Pressure of the upper level
p_l	Pressure of the lowest level

p_m	$\frac{1}{2}(p_u + p_l)$, pressure of the middle level
\tilde{p}_u	Upper level of the layer in which latent heat is released
\tilde{p}_l	Lowest level of the layer in which latent heat is released
p_x	Pressure of a level between 300 and 500 mbar
\tilde{p}_x	Pressure of a specified level between 300 and 500 mbar
$p_2, p_3, p_5, p_7,$ $p_{8.5}, p_{10}$	Pressures of 200, 300, 500, 700, 850 and 1000 mbar, respectively
p_{surface}	Pressure at sea level
Q	Amount of heat supply per unit time and mass
Q_{fict}	Fictitious Q as defined in (5.8)
q	Specific humidity
q_s	Saturation specific humidity
R	Gas constant for dry air
	Response function given in relation with (4.160)
RVA	$-J(\psi_5, \nabla^2 \psi_5)$, advection of relative vorticity at 500 mbar
RVA_s	Advection of relative vorticity at the steering level
$ \text{RVA}_s _{\text{max}}$	Maximum absolute value of RVA_s
R_3	Quantity defined in (5.37)
R_5	Quantity defined in (5.33)
$R_{8.5}$	Quantity defined in (5.38)
Ro	Rosby number
ρ	Density of air
S_3	Quantity defined in (5.23)
S_5	Quantity defined in (5.24)
$S_{8.5}$	Quantity defined in (5.22)
Σ	Summation
σ	Static stability dependent on p
σ_5	Value of σ at 500 mbar
σ_{3-5}	Mean value of the static stability for the layer 300-500 mbar
$\sigma_{5-8.5}$	Mean value of the static stability for the layer 500-850 mbar
$\sigma_{\text{r.a.}}$	Static stability of the reference atmosphere
$\sigma_{\text{s.ad.}}$	Static stability of a saturated adiabatic lapse rate
$\tilde{\sigma}$	Effective static stability parameter used in (3.94)
$\tilde{\sigma}_m$	Mean value of $\tilde{\sigma}$ for the layer bounded by p_u and p_l
T	Absolute temperature
T_p	Value of T at the pressure level p
T'	Thermal field of the perturbation ψ'
t	Time
t_0	Fixed moment of time
U	Geostrophic windspeed of the basic flow in the x -direction directed from west to east

U_u	Value of U at the upper boundary p_u
U_1	Value of U at lowest boundary p_1
U_m	Value of U at the middle level p_m
U_5, U_6	Values of U at 500 and 600 mbar
u	Component of the horizontal wind in the x -direction (west to east)
u_0	Component of the horizontal quasi-geostrophic wind in the x -direction (from west to east) at 45°N
u_1	Component of the horizontal quasi-geostrophic wind in the x_s -direction at latitude $\varphi = \varphi_1$
V	Velocity of an air particle
v	Component of the horizontal wind in the y -direction (south to north)
v_0	Component of the horizontal quasi-geostrophic wind in the y -direction (from south to north) at 45°N
v_1	Component of the horizontal quasi-geostrophic wind in the y_s -direction at latitude $\varphi = \varphi_1$
w	$\frac{dz}{dt}$, vertical velocity
x	Coordinate along 45°N from west to east
x_s	Coordinate of polar stereographic projection, parallel to 30°W
x_{s1}	x_s at latitude φ_1
y	Coordinate perpendicular to the latitude of 45°N
y_s	Coordinate of polar stereographic projection parallel to 120°W
y_{s1}	y_s at latitude φ_1
z	Geopotential height of a pressure level
$z_1, z_2, z_3, z_5,$ $z_7, z_{8.5}, z_{10}$	Values of z of 100, 200, 300, 500, 700, 850 and 1000 mbar, respectively
$z_3', z_{8.5}', z_{10}'$	Thicknesses of the layers 300-500, 500-850 and 500-1000 mbar, respectively
z^*	Height departure from the reference atmosphere
z_5^*	Height amplitude of the sinusoidal wave according to (3.15) given by (3.21)
ζ	Relative vorticity defined in (2.9)
Φ	Geopotential
φ	Latitude
φ_0	45°N
φ_1	Chosen value of φ
φ_5	Phase of the sinusoidal wave defined in (5.2)
φ_3'	Phase of the baroclinic part of the streamfunction of the thickness field 300-500 mbar defined in (5.25)
$\varphi_{8.5}'$	Phase of the baroclinic part of the streamfunction of the thickness

field 500-850 mbar defined in (5.26)

$\phi_5, \phi_3, \phi_{8.5}$	Tendencies of ϕ_5, ϕ_3 and $\phi_{8.5}$
$(\phi_5)_{inc}, (\phi_3)_{inc}, (\phi_{8.5})_{inc}$	ϕ_5, ϕ_3 and $\phi_{8.5}$ derived from the BK3-model with the correction terms included
$(\phi_5)_{not}, (\phi_3)_{not}, (\phi_{8.5})_{not}$	ϕ_5, ϕ_3 and $\phi_{8.5}$ derived from the BK3-model with the correction terms not included
$(\phi_5)_{dif}, (\phi_3)_{dif}, (\phi_{8.5})_{dif}$	$(\phi_5)_{inc} - (\phi_5)_{not}$ $(\phi_3)_{inc} - (\phi_3)_{not}$ $(\phi_{8.5})_{inc} - (\phi_{8.5})_{not}$
ψ	$g \cdot z/f_0$, quasi-geostrophic streamfunction
$\psi_3, \psi_5, \psi_{8.5}$	Quasi-geostrophic streamfunctions at 300, 500 and 850 mbar, respectively
$\psi'_3, \psi'_{8.5}$	Streamfunctions of the thickness fields 300-500 and 500-850 mbar
$\psi_{i,j}$	Value of ψ at the grid point with the coordinates i and j
$\tilde{\psi}_{i,j}$	Value of $\psi_{i,j}$ after the application of SHUMAN's smoothing operator in the x - or y -direction
ψ'	Streamfunction of the perturbation
ψ'_m	Value of ψ' at the middle level p_m
ψ_m^*	Amplitude of the perturbation ψ' at the middle level p_m
ψ_1^*, ψ_2^*	Coefficients dependent on t defined in relation with (3.82)
ψ_5^*	Amplitude of the sinusoidal wave defined in (3.15)
ψ_d	Dry part of the tendency of ψ
ψ_m	Moist part of the tendency of ψ
$\psi_{d3}, \psi_{d5}, \psi_{d8.5}$	Values of ψ_d at 300, 500 and 850 mbar, respectively
$\psi_{m3}, \psi_{m5}, \psi_{m8.5}$	Values of ψ_m at 300, 500 and 850 mbar, respectively
ψ'_{m3}	$\psi_{m3} - \psi_{m5}$
$\psi'_{m8.5}$	$\psi_{m5} - \psi_{m8.5}$
$(\psi_5)_{inc}, (\psi_3)_{inc}, (\psi_{8.5})_{inc}$	Tendencies of ψ_5, ψ_3 and $\psi_{8.5}$ for the BK3-model with the correction terms included (used in V.3)
$(\psi_5)_{not}, (\psi_3)_{not}, (\psi_{8.5})_{not}$	Tendencies of ψ_5, ψ_3 and $\psi_{8.5}$ for the BK3-model with the correction terms not included (used in V.3)
$(\psi_5)_{dif}, (\psi_3)_{dif}, (\psi_{8.5})_{dif}$	$(\psi_5)_{inc} - (\psi_5)_{not}$ $(\psi_3)_{inc} - (\psi_3)_{not}$ $(\psi_{8.5})_{inc} - (\psi_{8.5})_{not}$
ψ_5^*	Barotropic tendency of ψ_5 defined in (4.25)
ψ^*	Streamfunction of the baroclinic departure from the reference atmosphere used in the two-parameter model in III.3.5
	Amplitude of the wave defined in (3.77) dependent on p
ψ_{10}^*	Value of the baroclinic departure ψ^* at 1000 mbar
ψ_m^*	Moist tendency of ψ^*
ψ_d^*	Dry tendency of ψ^*

Ω	Absolute value of the angular velocity of the earth
ω	$\frac{dp}{dt}$, vertical velocity in the pressure coordinate system
ω_d	Dry part of ω
ω_m	Moist part of ω
$\omega_{m3}, \omega_{m5},$ $\omega_{m8.5}, \omega_{m10}$	ω_m at 300, 500, 850 and 1000 mbar, respectively
ω^*	Amplitude of the wave of the ω -field defined in (3.78)
ω'	$f_o\omega/RVA$
ω'_d	$\int_p^{p_{10}} D'_d dp$, defined in (3.70)
ω'_m	$\int_p^{p_{10}} D'_m dp$, defined in (3.71)
ω'_1, ω'_2	Functions describing the ω -profile defined in relation with (3.124)
∇^2	$\frac{\partial^2}{\partial x^2} + \frac{\partial^2}{\partial y^2}$, Laplacian operator
$\frac{\partial}{\partial t}$	partial derivative with respect to t

Due to the vast amount of symbols some inconsistency, especially with regard to the symbols marked with ' and *, was inevitable.

SUMMARY

This treatise explains in detail the design of a three-level quasi-geostrophic model. This model is suitable for short-range weather predictions up to 36 hours ahead.

In the model developing short frontal waves are especially emphasized. The inclusion of the release of latent heat proved to be absolutely necessary to describe the development of short frontal waves properly.

The model includes a 'dry' and a 'moist' version, which differ with regard to the incorporation of released latent heat. The dry version was operational from 28-2-'72, 12 GMT till 3-11-'75, 00 GMT. The noise in the forecast streamfunction prevented the moist version from becoming operational during that period.

The design of the baroclinic model named BK3 is based on the experience that barotropic forecasts of the pattern of the streamfunction at 500 mbar with the aid of the vorticity equation do lead to fairly good predictions at least up to 36 hours ahead. With this empirical knowledge the dry version of the model has been designed according to the following principle:

'If the atmosphere is equivalent barotropic at a certain time $t = t_0$, the model must keep the atmosphere exactly equivalent barotropic during the forecast period'.

In this treatise this has been achieved by the incorporation of so-called correction terms in the integrated thermodynamic equations for 300–500 mbar and for 500–850 mbar. These correction terms are approximately zero for values of the static stability computed from saturated adiabatic lapse rates with saturated potential temperatures from 10° to 14°C. This means that for short frontal waves having such values of the static stability, the original thermodynamic equations remain unaltered.

A general review of the investigations leading to the construction of the baroclinic model is given in the introduction in Chapter I.

After that the equations of motion, the continuity equation, the equation of state and the first law of thermodynamics have been simplified with the aid of a scale-analysis given by PHILLIPS (1963). The simplifications lead to so-called quasi-geostrophic equations in β -plane approximation, which are given in Chapter II.

The scale-analysis also shows that one has to account for the release of latent heat if the precipitation is ≥ 1 mm/hour. The vertical velocity at the surface of the earth induced by smoothed mountains is also important. The influence of the surface friction is of minor importance.

The basic equations for the BK3-model, which are valid for polar stereographic projection, have been derived in a similar way with the aid of a scale-analysis as the equations in β -plane approximation. In these equations the horizontal wind components are approximated by the geostrophic wind, while the relative vorticity is also

based on these wind components, with the neglect of the derivatives of the Coriolis-parameter.

Chapter III deals with theoretical investigations with special emphasis on developing short frontal waves.

In this chapter an equivalent barotropic reference atmosphere is defined. It is evident that the horizontal divergence D and the vertical velocity ω become functions of pressure p and of the advection of the relative vorticity at 500 mbar (RVA). For 25-3-'71, 00 GMT, the profiles of D and ω are further specified as functions of p just as the RVA. It is assumed that the numerical values for that date are fairly representative of polar jetstream conditions over the Atlantic and Western Europe as is also indicated by the computations of the static stability at 500 mbar, the mean value of which agrees with that of the ICAO standard atmosphere.

It follows from a comparison of height and thermal fields of the reference atmosphere with those of the real atmosphere that the behaviour of the long waves (wavelengths of about 4000 km) agrees best with that of the reference atmosphere, since such waves are in general to a certain degree equivalent barotropic. The short frontal waves (wavelengths from 1000–2500 km), however, are baroclinic and therefore the relation between these waves and the reference atmosphere is further investigated.

Concerning the integrated thermodynamic equations from 300 to 500 and from 500 to 850 mbar, it is evident that it is not possible to describe the behaviour of equivalent barotropic long waves correctly if the low values of the static stability belonging to saturated adiabatic lapse rates are used. This is only possible for values of the static stability in accordance with the values of the ICAO standard atmosphere around 500 mbar. This problem has been solved with the aid of correction terms, which are zero for the 'saturated adiabatic values' of the static stability.

To evaluate the integrals of ω in the integrated thermodynamic equations, a knowledge of the vertical profile of the horizontal divergence is necessary. For the long waves showing equivalent barotropic behaviour the divergence profile of the reference atmosphere can be taken. However, with respect to the baroclinic short waves the profiles of the divergence have to be further investigated. This is done with the aid of a simple two-parameter model taking into account the release of latent heat. It is clear that for the centre of a perturbation at sea level the profile of the divergence must consist of two parts, namely the one of the reference atmosphere and in addition a linear part due to the incorporation of the release of latent heat. The values of ω , computed from these two parts of the divergence, are of the same order of magnitude. The divergence- and ω -computations have been compared with three case studies, and a fair agreement is shown.

Further theoretical investigations have been carried out with the aid of a stability analysis of the linearized quasi-geostrophic equations. Two kind of wave solutions are of interest, namely the most unstable wave and a stable wave with a structure like

the one of the reference atmosphere with a level of non-divergence at 500 mbar. The wavelength of the most unstable wave only agrees with the wavelengths of the short frontal waves if release of latent heat is taken into account. It also appears that three parameters are sufficient to describe the spatial structure of the most unstable wave completely, i.e. one parameter for the basic flow and two parameters for the baroclinic perturbation.

Regarding the construction of a baroclinic model, the investigations of Chapter III lead to the following five conclusions:

1. At least three levels are necessary.
2. The values of the static stability have to be in accordance with those of saturated adiabatic lapse rates.
3. Correction terms have to be included in the integrated thermodynamic equations to preserve the equivalent barotropic character of the long waves.
4. Release of latent heat is necessary to make the short frontal waves unstable.
5. A profile of the dry part of the horizontal divergence has to be taken in accordance with that of the equivalent barotropic reference atmosphere and likewise a linear profile for the moist part of the divergence.

Chapter IV deals with the design of the baroclinic model. To develop the prognostic equations the vorticity equation is applied to the levels 300, 500 and 850 mbar, the continuity equation is integrated along the vertical over the whole atmospheric column from 0 to 1000 mbar, and the thermodynamic equation is integrated from 300 to 500 mbar and from 500 to 850 mbar. It appears that the tendencies of the streamfunctions, the horizontal divergence D and the vertical velocity ω occur linearly in the equations. Consequently, it is possible to split up the equations into a moist and a dry part. According to the conclusions obtained in Chapter III, the divergence profile of the reference atmosphere is used to perform the integrations of ω in the set of 'dry' equations. For the integrals of ω in the set of 'moist' equations a linear profile of D is used. After the integrations of the equations for the dry part of the model six equations remain with six unknown quantities, namely the tendencies of the streamfunctions at 300, 500 and 850 mbar and three horizontal divergences, which were chosen at three characteristic levels. The equations for the dry part of the BK3-model are obtained after the elimination of these three divergences. A similar procedure is followed for the set of moist equations, and after the integrations six equations remain containing three moist tendencies and three moist divergences at 300, 500 and 850 mbar, respectively. However, the heating function Q in these equations (which represents the release of latent heat between 500 and 850 mbar) consists of two parts of which the part depending on the moist component of ω is unknown. This difficulty can be solved with the aid of the assumption that an ascending moist air parcel has to follow a saturated adiabatic lapse rate. Since it has been assumed that the static stability parameters in the model also equal those computed from

such lapse rates, this offers the possibility to eliminate the 'moist' part of the heating function. After the introduction of an assumption concerning a partial release of latent heat in the layer from 300 to 500 mbar, and release of latent heat in the whole layer from 500 to 850 mbar, the elimination can be carried out and a set of three very simple equations for the three moist tendencies at 300, 500 and 850 mbar results.

The final prognostic equations of the dry part and the moist part of the BK3-model are formulated in the β -plane approximation, as well as for the polar stereographic projection with the surface of the earth being projected from the south pole on a plane going through the parallel of 60°N .

The values of the static stability parameters as well as those of the coefficients in the equations of the operational dry version of the BK3-model are based on the values determined for the reference atmosphere and on the values for the areas of advection of positive vorticity at 500 mbar for 25-3-'71, 00 GMT. However, it is in principle possible to extend the method for the computation of the coefficients by using the values obtained from the objective analyses at $t = 0$ for each individual case. Up to now such an extension has not been elaborated.

For the computational model the equations valid for the polar stereographic projection are used. The computational grid has been defined on the plane going through 60°N on which a rectangular grid has been fixed with the x - and the y -axis parallel to the longitudecircles of 30°W and 120°W , respectively. The grid consists of 800 grid points and covers Europe, the North Atlantic and North America. The equations of the computational model are replaced by finite difference equations. The Laplacian of each quantity is approximated with a second-order scheme, while for the Jacobians three schemes have been used, namely the most simple second-order scheme, the scheme of ARAWAKA and a fourth-order scheme developed by OFSTEGH of the Royal Netherlands Meteorological Institute. For the time integrations the leap-frog scheme is applied. As lateral boundary conditions, the tendencies of the streamfunctions at 300, 500 and 850 mbar are kept equal to zero during the time integrations.

To suppress computational instability near the boundaries of the grid, which is due to the fact that the boundaries are partly located in meteorologically active areas, the values of the streamfunctions of the rows and columns next to the boundary are found by a linear interpolation between the values on the boundary (which are kept constant) and those on the nearest inside rows and columns. This is done after each time step. The non-linear instability is prevented by the use of SHUMAN's smoothing operator applied to the streamfunctions at 300, 500 and 850 mbar. It appeared that smoothing must be performed if the number of scans needed to solve either the Poisson- or Helmholtz-equations at time t is greater than the number needed at $t = 0$.

Chapter V gives a survey of the performance of the dry and the moist versions of the BK3-model.

Experiments carried out with the dry version of the model showed that with increasing values of the static stability there was less baroclinic development. These results were valid for the version without the correction terms as well as for the version with the correction terms included.

Concerning the influence of the correction terms it appeared that the model with those terms included showed less baroclinic development, especially in the thickness fields of the long waves (wavelengths of about 4000 km). The predicted pressures in the centres of the high pressure systems at sea level proved to be more realistic if the correction terms were included, while without those terms the predicted pressure values were in general too high.

The experiments carried out with the moist version of the model showed that explosive developments at sea level of the frontal waves (deepening of 20 mbar or more in 24 hours) could be predicted. These results support the conclusions drawn from the stability analysis in Chapter III, namely that short frontal waves can only be unstable if latent heat is released.

The influence of the correction terms on the behaviour of the dry version has been further investigated with the aid of two kinds of sinusoidal waves, namely a wave satisfying the reference atmosphere and a baroclinic wave. The results obtained for these waves agree with the performance of the dry version of the model in use. It appears that for the waves with wavelengths between 1550 km and 9520 km the model with the correction terms included is more baroclinically stable than the model without these terms. For the other wavelengths the effect is opposite.

REFERENCES

- ARAKAWA, A. (1966). Computational design for long-term numerical integrations of the equations of atmospheric motion. *J.computational phys.*, pp. 119-143.
- BENGTSSON, L. and MOEN, L. (1971). An operational system for numerical weather prediction. In: *Satellite and computer applications to synoptic meteorology*. WMO-No. 283.
- BENWELL, G. R. R. et al. (1971). The Bushby-Timpson 10-level model on a fine mesh. *Scient. pap. Met. Off.* No. 32, London.
- BOUMAN, D. J. (1969). Objectieve analyse. In: *Beschrijving van programma's voor de EL-X8*. Scientific report of the Royal Netherlands Meteorological Institute. W.R. 69-3, pp. 37-50.
- BOUMAN, D. J. and SCHMIDT, F. H. (1962). Het numeriek voorspellen van stromingspatronen in de atmosfeer. Scientific report of the Royal Netherlands Meteorological Institute. W.R. 62-5.
- BRUNT, D. (1939). *Physical and dynamical meteorology*. Cambridge Univ. Press.
- BURGER, A. P. (1958). Scale consideration of planetary motions of the atmosphere. *Tellus*, 10, pp. 195-205.
- CHARNEY, J. G. (1947). The dynamics of long waves in a baroclinic westerly current. *J. met.*, 4, pp. 135-162.
- CHARNEY, J. G. (1948). On the scale of atmospheric motion. *Geof. publ. Oslo*, 17, (2).
- CRESSMAN, G. P. (1959). An operational objective analysis system. *Monthly weather rev.*, 87, pp. 367-374.
- CRESSMAN, G. P. (1961). A diagnostic study of mid-tropospheric development. *Monthly weather rev.*, 89, pp. 74-82.
- DANARD, M. B. (1964). On the influence of released latent heat on cyclone development. *J. appl. met.*, 3, pp. 27-37.
- DANARD, M.B. (1966). On the contribution of released latent heat to changes in available potential energy. *J. appl. met.*, 5, pp. 81-84.
- DANARD, M. B. (1966). Further studies with a quasi-geostrophic numerical model incorporating effects of released latent heat. *J. appl. met.*, 5, pp. 388-395.
- DANARD, M. B. (1966). A quasi-geostrophic numerical model incorporating effects of release of latent heat. *J. appl. met.*, 5, pp. 85-93.
- DODDS, I. (1971). A comparison of depressions of Europe and the North-East Atlantic. *Weather*, 26, pp. 210-216.
- DUSHAN, J. D. (1973). An investigation of the Sutcliffe development theory. NASA Contractor Report CR-2192.
- EADY, E. T. (1949). Long waves and cyclone waves. *Tellus*, 1 (3), pp. 33-52.
- EMMRICH, P. (1975). Entwicklung und Aufbau des Niedersachsen-Orkans vom 13. November 1972. *Ber. D. Wetterd.*, Nr. 135 (Bd. 17), pp. 3-34.
- EXTER BLOKLAND, A. W. den (1972). Experimenten met het numeriek opstellen van neerslagverwachtingen (with English summary). Scientific report of the Royal Netherlands Meteorological Institute. W.R. 72-8.
- GALEN, J. van (1969). Baroklien 3-parameter model. In: *Beschrijving van programma's voor de EL-X8*. Scientific Report of the Royal Netherlands Meteorological Institute. W.R. 69-3, pp. 73-90.
- GATES, W. L. (1961). Static stability measures in the atmosphere. *J. Met.*, 18, pp. 526-533.
- HALTNER, G. J. (1971). *Numerical weather prediction*. Wiley, New York enz.
- HALTNER, G. J. and MARTIN, F. L. (1957). *Dynamical and physical meteorology*. McGraw Hill Book Co.
- HEIJBOER, L. C. (1972). Experimenten met nieuwe versies van het Bk3-programma. Published in the series 'Verslagen' of the Royal Netherlands Meteorological Institute. V-246.

- HEIJBOER, L. C. (1973). Windverwachtingen voor 12 en 24 uur vooruit op 850 mbar door het BK3-model en de relatie tussen de geostrofische wind op 850 mbar en de gemeten wind van de meetpaal Katwijk (with English summary). Scientific report of the Royal Netherlands Meteorological Institute. W.R. 73-1.
- HEIJBOER, L. C. and EXTER BLOKLAND, A. W. den (1974). The inclusion of latent heat in a three-level model with filtered equations and its influence upon the development of depressions. Scientific report of the Royal Netherlands Meteorological Institute. W.R. 74-11.
- HOLTON, J. R. (1972). An introduction to dynamic meteorology. Acad. Press, New York enz.
- PALMÉN, E. H. (1958). Vertical circulation and release of kinetic energy during the development of hurricane hazel into an extratropical storm. *Tellus*, 10, pp. 1-23.
- PALMÉN, E. and HOLOPAINEN, E. O. (1962). Divergence, vertical velocity and conversion between potential and kinetic energy in an extratropical disturbance. *Geophysica*. Helsinki. 8, pp. 89-113.
- PALMÉN, E. and NEWTON, C. W. (1969). Atmospheric circulation systems. *Int. Geoph. Series*, Vol. 13.
- PETTERSEN, S. (1955). A general survey of factors influencing development at sea level. *J. met.*, 12, pp. 36-42.
- PETTERSEN, S., DUNN, G. E. and MEANS, L. L. (1955). Report of an experiment in forecasting of cyclone development. *J. met.*, 12, pp. 58-67.
- PHILLIPS, N. A. (1957). A map projections system suitable for large-scale numerical weather prediction. 75th anniv. Vol. of *J. Met. Soc. Japan*, pp. 262-267.
- PHILLIPS, N. A. (1959). An example of non-linear computational instability. In: *the atmosphere and the sea in motion*, pp. 501-504.
- PHILLIPS, N. A. (1963). Geostrophic motion. *Rev. geophys.*, 1, pp. 123-176.
- ROSSBY, G. C. et al. (1939). Relation between variations of the zonal circulation of the atmosphere and the displacements of the semipermanent centers of action. *J. Marine Res.*, 2, pp. 38-55.
- SHUMAN, F. G. (1957). Numerical methods in weather prediction: II. Smoothing and filtering. *Monthly weather rev.*, 85, pp. 357-361.
- SHUMAN, G. S. and HOVERMALE, J. B. (1968). An operational six-layer primitive equation model. *J. appl. met.*, 7, pp. 525-547.
- SUTCLIFFE, R. C. (1939). Cyclonic and anticyclonic development. *Q. J. R. Met. Soc. London*, 65, pp. 518-524.
- SUTCLIFFE, R. C. (1947). A contribution to the problem of development. *Q. J. R. Met. Soc. London*, 73, pp. 370-383.
- SUTCLIFFE, R. C. and FORSDYKE, A. G. (1950). The theory and use of upper air thickness patterns in forecasting. *Q. J. R. Met. Soc. London*, 76, pp. 189-217.
- THOMPSON, P. D. (1961). Numerical weather analysis and prediction. New York.
- U.S. WEATHER BUREAU, (1951). Tables of precipitable water and other factors for a saturated pseudo-adiabatic atmosphere. Technical paper No. 14, Washington.
- WIIN-NIELSEN, A. (1961). Diagnosis of divergence in a three-parameter numerical prediction model. *Monthly weather rev.*, 89, pp. 67-73.
- WORLD METEOROLOGICAL ORGANIZATION, (1966). International meteorological tables. WMO-No. 188. TP. 94.

Van de reeks MEDEDELINGEN EN VERHANDELINGEN zijn bij het Staatsdrukkerij- en Uitgeverijbedrijf nog verkrijgbaar de volgende nummers:

23, 25, 27, 29b, 30, 31, 34b, 35, 36, 37, 38, 39, 40, 42, 43, 44, 45, 46, 47, 48, 50, 51, 52, 53, 54, 55, 56, 57, 59.

alsmede

60. C. Kramer, J. J. Post en J. P. M. Woudenbergh. Nauwkeurigheid en betrouwbaarheid van temperatuur- en vochtigheidsbepalingen in buitenlucht met behulp van kwikthermometers, 1954. (60 blz. met 11 fig.)	3,60
62. C. Levert. Regens. Een statistische studie. 1954. (246 blz. met 67 fig. en 143 tab.)	10,30
63. P. Groen. On the behaviour of gravity waves in a turbulent medium, with application to the decay and apparent period increase of swell. 1954. (23 blz.)	1,55
64. H. M. de Jong. Theoretical aspects of aeronavigation and its application in aviation meteorology. 1956. (124 blz. met 80 fig., 9 krt. en 3 tab.)	4,60
65. J. G. J. Scholte. On seismic waves in a spherical earth. 1956. (55 blz. met 24 fig.)	5,15
66. G. Verploegh. The equivalent velocities for the Beaufort estimates of the wind force at sea. 1956. (38 blz. met 17 tab.)	1,80
67. G. Verploegh. Klimatologische gegevens van de Nederlandse lichtschepen over de periode 1910—1940.	
Deel I: Stormstatistieken. — Climatological data of the Netherlands light-vessels over the period 1910—1940. P. I: Statistics of gales. 1956. (68 blz. met tabellen)	3,60
Deel II: Luchtdruk en wind; zeevang. — Climatological data of the Netherlands light-vessels over the period 1910—1940. P. II: Air pressure and wind: state of the sea. 1958. (91 blz. met tabellen.)	7,70
Deel III: Temperaturen en hydrometeoren; onweer. — Climatological data of the Netherlands light-vessels over the period 1910—1940. P. III: temperatures and hydrometeors; thunderstorms. 1953. (146 blz. met tabellen.)	8,25
68. F. H. Schmidt. On the diffusion of stack gases in the atmosphere. 1957. (60 blz., 12 fig. en tab.)	5,15
69. H. P. Berlage. Fluctuations of the general atmospheric circulation of more than one year; their nature and prognostic values. 1957	7,70
70. C. Kramer. Berekening van de gemiddelde grootte van de verdamping voor verschillende delen van Nederland volgens de methode van Penman. 1957. (85 blz., fig. en tab.)	7,20
71. H. C. Bijvoet. A new overlay for the determination of the surface wind over sea from surface weather charts. 1957. (35 blz., fig. en tab.)	2,60
72. J. G. J. Scholte. Rayleigh waves in isotropic and anisotropic elastic media. 1958. (43 blz., fig. en tab.)	3,10
73. M. P. H. Weenink. A theory and method of calculation of wind effects on sea levels in a partly-enclosed sea, with special application to the southern coast of the North Sea. 1958. (111 blz. met 28 fig. en tab.)	8,25
74. H. M. de Jong. Geostrophic flow. Geostrophic approximation in the upper air flow with application to aeronavigation and air trajectories. 1959. (100 blz. met 17 fig., 14 krt. en 2 tab.)	5,15
75. S. W. Visser. A new analysis of some features of the 11-year and 27-day cycles in solar activity and their reflection in geophysical phenomena. 1959. (65 blz. met 16 fig. en 12 tab.)	3,60
76. A. R. Ritsema and J. Veldkamp. Fault plane mechanisms of South East Asian earthquakes. 1960. (63 blz. met 26 fig. en 11 tab.)	4,10

77. G. Verploegh. On the annual variation of climatic elements of the Indian Ocean. P. I: text. P. II: charts. 1960. (64 blz., 15 fig., 28 krt.)	6,15
78. J. A. As. Instruments and measuring methods in paleomagnetic research. 1960. (56 blz., 20 fig.)	2,55
79. D. J. Bouman. Consistency of approximations in discontinuous fields of motion in the atmosphere with an introduction to the use of generalized functions or distributions in meteorology. 1961. (94 blz., 6 fig.)	6,70
80. H. Timmerman. The influence of topography and orography on the precipitation patterns in the Netherlands. 1963. (49 blz., 37 fig. en 5 tab.)	6,70
81. A. W. Hanssen & W. J. A. Kuipers: On the relationship between the frequency of rain and various meteorological parameters (with reference to the problem of objective forecasting). 1965. (77 blz., 18 fig. en 12 tab.)	10,25
82. G. A. de Weille: Forecasting crop infection by the potato blight fungus. A fundamental approach to the ecology of a parasite — host relationship. 1964. (144 blz., 37 fig. en 37 tab.)	14,90
83. H. J. de Fluiter, P. H. van de Pol, J. P. M. Woudenberg (redactie) e.a. Fenologisch en faunistisch onderzoek over boomgaardinsekten. Phenological and faunistic investigations on orchard insects. 1964. (226 blz., 84 fig. en 59 tab.)	9,50
84. D. J. Bouman & H. M. de Jong: Generalized theory of adjustment of observations with applications in meteorology. 1964. (89 blz., 8 fig. en 1 tab.)	11,30
85. L. Otto: Results of current observations at the Netherlands lightvessels over the period 1910—1939. P. I: Tidal analysis and the mean residual currents. 1964. (56 blz. en 8 tab.)	6,40
86. F. H. Schmidt: An analysis of dust measurements in three cities in the Netherlands. 1964. (68 blz., 14 fig. en 22 tab.)	5,65
87. Commissie Meteorologische Voorlichting van Straalvliegtuigen: Climatology of Amsterdam Airport (Schiphol). 1966. (145 blz., 6 fig., 10 tab.)	17,00
88. H. P. Berlage: The southern oscillation and world weather. 1966. (152 blz.) 46 fig., 34 tab.)	15,95
89. G. Verploegh: Observation and analysis of the surface wind over the ocean. 1967. (67 blz., 14 tab., 4 krt.)	6,70
90. R. Dorrestein: Wind and wave data of Netherlands lightvessels since 1949. 1967. (123 blz., 22 tab.)	15,95
91. P. J. Rijkooft: The increase of mean wind speed with height in the surface friction layer. 1968. (115 blz., 31 fig., 16 tab.)	15,95
92. C. J. E. Schuurmans: The influence of solar flares on the tropospheric circulation. Statistical indications, tentative explanation and related anomalies of weather and climate in Western Europe. 1969. (123 blz., 40 fig., 19 tab.)	19,00
93. H. M. de Jong: Optimal track selection and 3-dimensional flight planning Theory and practice of the optimization problem in air navigation under space-time varying meteorological conditions. 1974. (140 blz., 41 fig., 14 tabl., 4 fig. in annex) .	55,00
94. S. J. Bijlsma: On minimal-time ship routing.	40,00
95. L. Csikós: On the theory of the electromagnetic seismograph.	
96. L. Otto: Oceanography of the Ria de Arosa (N.W. Spain). 1975. (210 blz., 79 fig., 19 tab., 3 fig. in annex, 5 tab. in annex)	60,00
97. G. A. de Weille: An approach to the possibilities of forecasting downy mildew infection in onion crops. (83 blz., 19 fig., 6 tab.)	17,50